Review

Biomimetic CaCO Mineralization using Designer Molecules and Interfaces

Nico A. J. M. Sommerdijk, and Gijsbertus de With

Chem. Rev., **2008**, 108 (11), 4499-4550 • DOI: 10.1021/cr078259o • Publication Date (Web): 21 October 2008

Biomimetic $CaCO_3$ Mineralization using Designer Molecules and Interfaces

Nico A. J. M. Sommerdijk* and Gijsbertus de With

Soft-matter cryoTEM Research Unit and Laboratory of Materials and Interface Chemistry, Department of Chemical Engineering and Chemistry, Eindhoven University of Technology, P.O. Box 513, 5600 MB Eindhoven, The Netherlands

Received February 18, 2008

Contents

* E-mail: N.Sommerdijk@tue.nl. Telephone: +31 40 247 5870. Fax: + 31 40 244 5619.

1. Introduction

1.1. Inspiration from Nature

In Nature living organisms use a whole range of organic−inorganic hybrid materials for a variety of purposes, including mechanical support, navigation, protection, and defense.[1,2] These materials are generally molded into specifically designed devices with fascinating properties, in which the structure, size, shape, orientation, texture, and assembly of the constituents are precisely controlled. The human efforts in the fields of chemistry and materials science have led to the development of a complementary set of inorganic and hybrid materials that possess properties that cannot be found in natural materials. However, by mimicking the design and synthesis of, e.g., biomaterials, to date no synthetic materials have evolved that show properties which are superior to those found in their natural counterparts. It is evident that the understanding and ultimately the mimicking of the processes involved in biomineralization may provide new approaches to the fabrication of specialized organic−inorganic hybrid materials.[3]

Only recently, researchers have begun to understand the first principles about how the shape and organization of crystals together with the included organic matrix provide the remarkable properties of biominerals.[4] It is evident that control over polymorphism, crystallographic orientation, and crystal organization are paramount in determining the properties of hybrid materials. In addition, the formation of an intimate interaction between the organic and inorganic phases seems a prerequisite to obtain the unique properties observed in biological materials. The application of both soluble and insoluble directing agents has been extensively explored for the formation of a wide range of materials; however, understanding the correlation between the additive used and the observed crystallographic and other properties of the resulting material still remains a challenge.[5−7]

In this review, we will concentrate on the biomimetic synthesis of calcium carbonate, the most abundant biomineral. Calcium carbonate is also a material of considerable industrial interest, and the study of the factors that influence its formation has a long history. The shapes and forms of

10.1021/cr078259o CCC: $71.00
Published on Web 10/21/2008

Nico Sommerdijk is Associate Professor in Interfacial Materials Chemistry in the Department of Chemical Engineering and Chemistry at the Eindhoven University of Technology, The Netherlands. He studied chemistry at the University of Nijmegen and in 1995 received his Ph.D. in the field of supramolecular chemistry (supervisors Prof. B. Zwanenburg and Prof. R. J. M. Nolte). From 1995 to 1997, he did postdoctoral work with Dr. J. D. Wright at the University of Kent (U.K.), and from 1997 to 1999, he worked with Prof. R. J. M. Nolte (University of Nijmegen). He was a visiting fellow with Prof. B.R. Heywood at Keele University, U.K., in 1997. In 1999, he moved to Eindhoven University of Technology to work in the group of Prof. E. W. Meijer, and he was appointed Assistant Professor in 2000. In 2006, he became associated with the Soft Matter CryoTEM Research Unit, and in 2008 he joined the Laboratory of Materials and Interface Chemistry. His research focuses on the study of (macro)-molecular assemblies and their application as templates in biomimetic mineralization studies. His group combines advanced electron microscopic approaches from the field of materials science with the use of cryoelectron microscopy and cryoelectron tomography.

Gijsbertus de With is a Full Professor in materials science in the Department of Chemical Engineering and Chemistry at the Eindhoven University of Technology, The Netherlands. He graduated from Utrecht State University and received his Ph.D. in 1977 from the University of Twente on the "Structure and charge distribution of molecular crystals". In the same year, he joined Philips Research Laboratories, Eindhoven. In 1985, he was appointed Part-time Professor, and in 1996, he became Full Professor at the Eindhoven University of Technology, where he heads the Laboratory of Materials and Interface Chemistry. His research interests include the chemical and mechanical processing as well as the chemomechanical behavior of multiphase materials. Since 2006, he has also been the chairman of the Soft Matter CryoTEM Research Unit, a consortium that brings together the knowledge of (cryo)TEM experts and several soft matter research groups and the latest cryoTEM technology.

calcium carbonate encountered in nature strongly contrast those that are generally formed in a synthetic environment. Consequently, many researchers have engaged in unraveling the mysteries of calcium carbonate biomineralization, either by analyzing biogenic materials or by trying to understand the interactions between organic and inorganic phases in a laboratory environment. Here we review how synthetic (macro)molecules have been used to mimic the three main modes of control applied in $CaCO_3$ biomineralization, i.e. (a) polymorph selection and oriented nucleation by specific interactions between a template or additive and the developing nucleus, (b) growing crystals with a nonequilibrium morphology by restricting their growth to a confined space or by influencing their preferred direction of growth, and (c) generating composite materials through the inclusion of organic (macro)molecules in the growing mineral phase.

In biological systems, polymorph selection as well as oriented nucleation of crystals is accomplished through the interaction of the inorganic ions with specialized biomacromolecules that contain assemblies of charged groups with defined stereochemistry;[8] the precise control suggests that these surfaces are specifically designed for this purpose. Utilizing 2D assemblies as model systems, scientists have been trying to relate the crystal habit and/or polymorph of generated crystals to the structure of the template.[9−11] Alternatively, water-soluble additives[7,12] can be used to influence polymorph selection through interaction with the mineral in, or closely after, the nucleation stage. In other cases, additives are used to modify the *shape* of the crystals by interacting during the growth process. Also, the mineral phase may be shaped by forcing the crystals to grow in a prefixed confined space, often by making use of an amorphous precursor phase. The use of polymeric or self-assembling additives in many cases leads to their inclusion in the mineral phase and to the concomitant modification of the characteristics of the resulting material.

Due to their versatility, activity, and materials properties, polymers in many cases are the additives of choice for the fabrication of new biomimetic composites and hybrid materials. The realization of their potential has led to the development of an enormous activity concentrated on the study of their action in biomimetic mineralization experiments. However, most polymers in solution are present in a random coil conformation or at least contain long macromolecular chains with extensive conformational freedom. This aspect makes it more difficult to point to specific directing interactions between the organic and the inorganic phases that are responsible for the complex morphologies and materials properties arising from the interplay of the two phases. On this basis, combined with the fact that excellent reviews have appeared describing in detail the progress of the field,[13−15] we decided in this review to concentrate on the work performed using what we call *designer molecules and interfaces*. In our definition, these comprise molecules and ensembles thereof, mostly, but not exclusively, synthetic, with a defined molecular structure and conformation that allows the discussion of the role of their functional groups in the interactions with the developing mineral phase. In addition to this, we will limit ourselves to biomimetic studies, which we define as those mineralization studies that are performed in the presence of a directing organic component in aqueous media and close to room temperature.

1.2. The Chemistry of Calcium Carbonate

Calcium carbonate is the most abundant biomineral and occurs in three main crystalline polymorphs (calcite, vaterite, and aragonite; Table 1), in two hydrated crystal forms (calcium carbonate monohydrate and calcium carbonate hexahydrate), and also as amorphous material. The most stable polymorph, calcite, has a rhombohedral crystal-

Table 1. Some Properties of the Anhydrous Crystalline Forms of Calcium Carbonate

phase	space group	lattice constants	density (g/cm^3)	habit[22]	surface energy (J/m^2)	pK_{sp}
calcite	$R\bar{3}c$	$a = b = 4.990$ [Å], $c = 17.061$ [Å], $\alpha = \beta = 90°$, $\gamma = 120°$ [a]	2.71[b]	10·4	0.59 {10·4} unhydrated,[22] 0.16 {10·4} hydrated,[22] 0.23,[c] 0.317−0.395,[d] 0.057,[e] 0.044,[f] 0.048−0.060,[g] 0.055[h]	8.42,[i] 8.48,[j] 8.48[20]
aragonite	*Pmcn*	$a = 4.9598$ [Å], $b = 7.9641$ [Å], $c = 3.737$ [Å], $\alpha = \beta = \gamma = 90°$ [k]	2.93	110, 011, 010	0.69 {011}CO_3 unhydrated,[22] 0.24 {010}Ca, hydrated[22]	8.22,[i] 8.30,[j] 8.34[20]
vaterite	*P*63	$a = b = 4.13$ [Å], $c = 8.48$ [Å], $\alpha = \beta = 90°$, $\gamma = 120°$ [l]	2.66 (calc)	needle, ellipsoid, disklike	0.62 {010}CO_3, unhydrated,[22] 0.22 {010}CO_3, hydrated[22]	7.60,[i] 7.91[20]

[a] Maslen, E. N.; Streltsov, V. A.; Streltsova, N. R.; Ishizawa, N. *Acta Crystallogr., Sect.B: Struct. Sci.* **1995**, *B51*, 929. [b] Weast, R. C., Astle, M. J., Eds. *Handbook of Chemistry and Physics*, 60th ed.; CRC Press: Boca Raton, FL, 1979. [c] Gilman, J. J. *J. Appl. Phys.* **1960**, *31,* 2208. [d] Gupta, Y. P.; Santhanam, A. T. *Acta Metall.* **1969**, *17,* 419. [e] Calhoun, A.; Chiang, E. *J. Vinyl Addit. Technol.* **2006**, *12*, 174. [f] Schmitt, P.; Koerper, E.; Schultz, J.; Papirer, E. *Chromatographia* **1988**, *25,* 786. [g] Balard, H.; Papirer, E. *Prog. Org. Coat.* **1993**, *22,* 1. [h] Keller, D. S.; Luner, P. *Colloid Surf., A* **2000**, *161*, 401. [i] Mann, S. *Biomineralization*; Oxford University Press: 2001. [j] Plummer, L. N.; Wigley, T. M. L.; Prakhurst, D. L. *Am. J. Sci*. **1978**, *278,* 219. [k] Caspi, E. N.; Pokroy, B.; Lee, P. L.; Quintana, J. P.; Zolotoyabko, E. *Acta Crystallogr., Sect. B: Struct. Sci.* **2005**, *B61*, 129. [l] Kamhi, S. R. *Acta Crystallogr.* **1963**, *16*, 770.

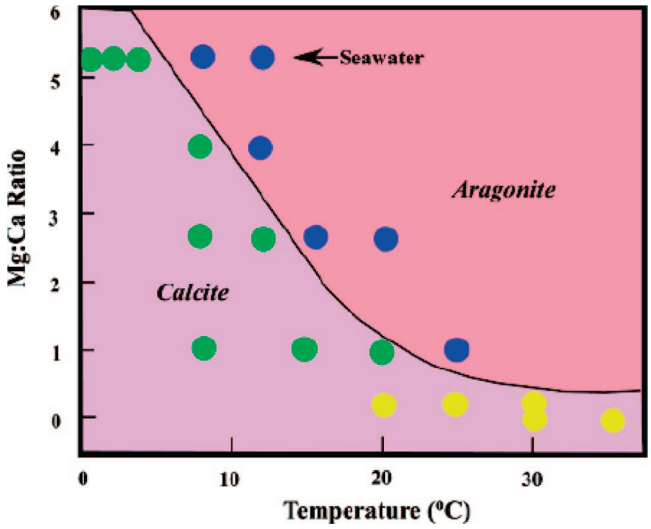

Figure 1. Influence of the Mg/Ca ratio and temperature on the precipitation of different forms of calcium carbonate from seawater. Blue dots are aragonite; yellow dots are calcite; green dots are initially calcite with aragonite overgrowths. (Reprinted with permission from ref 19. Copyright 2003 American Chemical Society.)

lographic unit cell,[16] while the less stable aragonite is orthorhombic and the even less stable vaterite is hexagonal. The morphology of the crystals is predicted by Wull's Rule, which states that the most stable habit is related to the minimum of the sum of the products between crystal surface area and surface energy for the different faces of the crystal.[17] For calcite, this results in rhombohedral crystals expressing their {10·4} faces, aragonite crystallizes as clustered needles growing along the crystallographic *c*-axis, and vaterite forms as hexagonal florets.

Besides its importance as a structural (bio)material, calcium carbonate is also of interest for fundamental studies on template−mineral interactions due to its sensitivity for template effects. When grown in the absence of templates or additives, it appears as rhombohedral crystals of calcite. When grown in an environment containing high concentrations of magnesium ions, e.g. in seawater, a considerable amount of Mg can be incorporated in calcite (up to about 30 mol %, depending on temperature (Figure 1).

The crystallography[18] and the solution chemistry[19,20] of calcium carbonate as well as the chemistry of the carbonic acid system[21] have been extensively described. For nucleation studies, the solubility products (SP) are of particular importance. Although the trends of the SPs for the various compounds as obtained by different researchers are usually the same, their specific values differ (Table 1). Both in a biological and in a synthetic environment, the formation of calcium carbonate can be controlled through the interference of organic molecules and surfaces with the mineral formation process. Consequently, control of crystal growth takes place through the interaction of the organic molecules with the surface of the developing mineral particle. Despite its importance in the process of controlled mineral formation, information on the surface energy of calcium carbonate is limited, both from experimental and theoretical points of view. The most extensive molecular dynamics simulation study was done by de Leeuw and Parker (Table 1).[22] Cleavage studies on single crystal calcite have yielded the surface energies for specific planes,[23] whereas the average overall exposed crystallographic planes were obtained from inverse gas chromatography (IGC) studies. While the results of the simulation and cleavage studies are generally in good agreement, the values from the ICG experiments are usually a factor of 10 lower (see Table 1).

Recently, also molecular simulation studies on the interface of calcium carbonate and water have been done with force fields of varying complexity.[24−26] These studies provide structural as well as energetic details. From the structural point of view, these studies show that there are two conformations of water near the surface. In the first conformation, the oxygen atoms of water are oriented toward the calcium ions of the calcite lattice, while, in the second conformation, the hydrogen atoms of water point toward the oxygen atoms of the calcite lattice. These conformations have a comparable free energy of adsorption of about −2.8 and −2.4 kJ/mol, respectively. An internal barrier of ∼5.6 kJ/mol exists for the transition from the first to the second conformation with a corresponding barrier of ∼5.3 kJ/mol for the reverse transition. Moreover, there is a considerable order of water near the calcite {10·4} surface, namely in four layers at a distance of about 2.2, 3.2, 5.0, and 7.8 Å. While the orientation of the water dipole in the first layer is mainly parallel to the surface, the second is oriented more perpendicular to the surface. The third and fourth layers show no special order. This leads to a large change in entropy, explaining that, although the enthalpy of adsorption for water is quite high, ∼ −45 kJ/mol, the free energy is significantly lower, −2 to −3 kJ/mol.

2. Nucleation and Growth Theory

In order to discuss the effect of organic molecules and surfaces on the nucleation and growth of calcium carbonate,

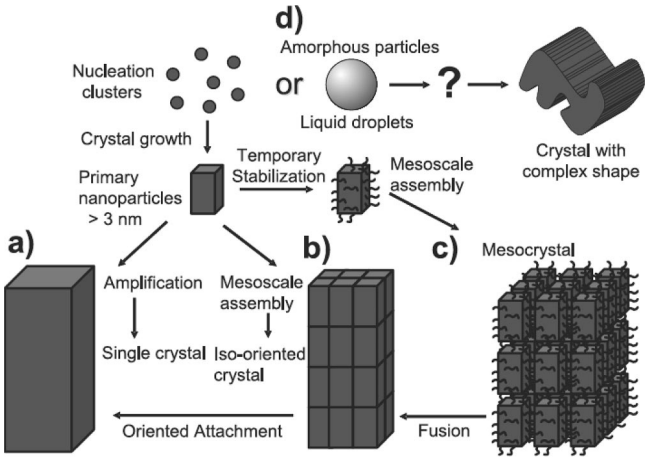

Figure 2. Different pathways of crystallization. Nucleation clusters can develop to form a critical nucleus that develops into a primary nanoparticle. These nanoparticles can develop into a single crystal either by the addition of ions (path a) or by the oriented attachment of multiple particles (path b). When additives adhere to the primary particle surface, mesocrystals can be formed (path c). Alternatively, the assembly of nucleation clusters can lead to the formation of amorphous particles which can crystallize either with or without interaction with an additive to produce different crystal morphologies. (Reproduced from ref 15, Copyright 2007, with kind permission of Springer Science and Business Media.)

it is important to shortly introduce the most important factors involved in the development of minerals, both with and without the presence of control agents.

2.1. Nucleation

The crystallization of inorganic minerals starts from their constituting ions that, based on their ionic complementarity, form small clusters. These clusters undergo a dynamic process of growth and disintegration governed by the counterplay between the increasing surface energy related to the growing surface area ($\sim r^2$) and the reduction of bulk energy related to the formation of a crystal lattice ($\sim r^3$). At the point where the surface energy is counterbalanced by the bulk energy, a critical size is reached. After this, continued growth leads to a reduction of the Gibbs energy of the system as the further decrease of the lattice energy overcompensates the increase in surface energy. In the classical nucleation theory, the resulting primary nanoparticles form the critical crystal nuclei that are the basis of further growth (Figure 2 pathway a).[15]

2.1.1. Homogeneous Nucleation

The ideas about the models of nucleation have evolved over time. Initially, the nucleation model was invoked in which ions (or pairs of ions) nucleate.[27] As this approach is capable of explaining many features of the nucleation process, it is still frequently used.[28,29] However, the model does not include any structural information but only energetic information. Since this model has been reviewed many times, we only provide here the bare essentials, helpful for further discussion, following largely the summary given by Rieke,[30] based on the classic review by Nielsen.[27] A recent review including a discussion of molecular factors involved is given by De Yoreo and Vekilov.[31]

The Gibbs energy of formation of a nucleus of size n is given by the Gibbs energy gained by the formation of a nucleus from the supersaturated solution and the energy lost in the formation of new surface and reads

$$\Delta G = -nkT \ln S + \sigma A \quad (1)$$

where S is the supersaturation, σ the interfacial Gibbs energy for nucleation, and A the surface area. The other symbols have their usual meaning (k Boltzmann's constant, T temperature). The supersaturation S can be determined from the solubility product K_{sp} and the activities a of the species involved,[32] here $a(Ca^{2+})$ and $a(CO_3^{2-})$, via

$$\ln S = \ln[a(Ca^{2+})a(CO_3^{2-})]/K_{sp} \quad (2)$$

The influence of chemical parameters such as the Ca^{2+} ion activity $a(Ca^{2+})$ and partial CO_2 pressure pCO_2 on nucleation is nicely demonstrated by Dickinson et al.[33] These authors varied $a(Ca^{2+})$ and pCO_2 by varying the substrate height in a solution. At low $a(Ca^{2+})$, where the process is thermodynamically controlled (typically below 6 mM), stepped multinucleated rhombohedral calcite crystals were formed, with the amount of calcite being governed by the amount of CO_2. For somewhat higher values of $a(Ca^{2+})$, in a narrow range around 80 mM and dependent on pCO_2, perfect rhombohedral calcite crystals form. In this stage, a balance between kinetic and thermodynamic factors is present, and

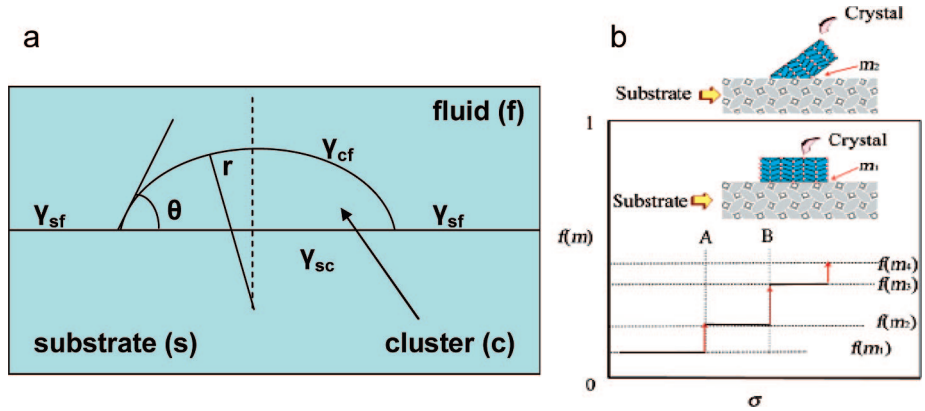

Figure 3. (a) Schematic illustration showing how 3D heterogeneous nucleation depends on the contact angle θ, which is determined by the surface areas and interfacial free energies γ between the three phases. (Reprinted with permission from ref 29. Copyright 2005 American Chemical Society.) (b) Schematic illustration showing the effect of supersaturation-driven interfacial structural mismatch: at increasing supersaturation, at certain values corresponding to the transition from an ordered and structurally matched to a less ordered and structurally mismatched mineral−template interface (represented by A and B), the interfacial correlation factor $f(m)$ increases abruptly ($m_1 > m_2 > m_3 > m_4$). (Reprinted with permission from ref 28. Copyright 2003 American Chemical Society.)

the lowest energy polymorph (calcite) and morphology {10•4} result. At still higher $a(Ca^{2+})$, the kinetic regime commences in which both calcite ($\sim^1/_3$) and vaterite ($\sim^2/_3$) crystals form, with the latter type increasing in number with increasing $a(Ca^{2+})$ and pCO_2.

As mentioned in section 1, an inconsistent energy estimate situation occurs for the estimates of the surface energies from mechanical (cleavage) and physicochemical (liquid probing) experiments. The reason for this discrepancy is not completely clear but must be attributed, at least partially, to adsorption effects on the initial nucleus not taken into account in the independent modeling and experimenting. Attempts have been made to estimate the interface energies via the so-called van Oss−Chaudry−Good approach.[30,34] In that approach, the interface energy is estimated based on additive contributions from dispersion and acid−base interactions. The model is capable of reasonably accurate estimates. However, if unknown adsorption occurs, this approach may be less useful. On the other hand, it is only one of the few, if not the only, quantitative approach capable of delivering estimates for interface energies without undue effort. Sometimes an empirical equation, first introduced by Nielsen,[35] is used which reads

$$\sigma = \alpha^{-2}(11.6 - 1.12 \ln[Ca^{2+}])10^{-21} \text{ J/m}^2 \quad (3)$$

with α being the molecular diameter in meters and $[Ca^{2+}]$ the solubility of the polymorph. The basis for this equation is weak, but it provides at least an order of magnitude estimate.

Using the Hartman−Perdok crystallization model, Aquilano et al.[36] also estimated the various energies involved in the crystallization process of calcite {10•4}. From their analysis, a value of $\gamma_{cv} = 587$ mJ/m^2 resulted (c = crystal, v = vapor). From literature thermodynamic heat of adsorption studies, they used a heat of adsorption of water to calcite of −480 mJ/m^2. Using the Dupré equation, this heat can be equated to $\gamma_{sv} - \beta$, where β is the adsorption energy between water and calcite. Since $\gamma_{sv} = 72$ mJ/m^2 (almost pure water), a value of $\beta = 552$ mJ/m^2 results. This seems to be the first estimate available for β. Using also literature nucleation studies with a value of $\gamma_{cs} = 102$ mJ/m^2 for calcite {10•4}, they obtained $\gamma_{cv} = 582$ mJ/m^2, comparing favorably with their own estimate.

2.1.2. Heterogeneous Nucleation

The interaction of a precritical nucleus with a substrate in most cases lowers the surface Gibbs energy of the particle. This reduces the barrier for the formation of the critical nucleus, favoring the nucleation at the interface (heterogeneous nucleation) over nucleation in bulk solution (homogeneous nucleation). In many cases, the interaction with the surface also favors nucleation on a specific crystal plane, leading to the formation of oriented crystals.

For homogeneous nucleation, the relevant Gibbs energy σ_{hom} equals the nucleus (n)−liquid (l) interface Gibbs energy γ_{nl}, i.e.

$$\sigma_{hom} = \gamma_{nl} \quad (4)$$

For heterogeneous nucleation, the relevant interfacial Gibbs energy σ_{het} is the sum of the Gibbs energies for the nucleus−liquid and nucleus−substrate interfaces minus that for the liquid−substrate interface, i.e.

$$\sigma_{het} = (\gamma_{ns} - \gamma_{ls})(1 - \xi) + \gamma_{nl}\xi \quad (5)$$

where ξ represents the ratio of nucleus−liquid area versus total area. It can be shown that, introducing the contact angle θ (Figure 3),

$$\Delta G^*_{het} = \kappa f(\theta)\Delta G^*_{hom} \quad (6)$$

where the asterisk indicates the critical state. The function $f(\theta)$ depends solely on the shape of the nucleus and the contact angle, while the function κ contains the interface energy γ_{cf} between the growing cluster and the fluid, contains the volume of the growth unit Ω, and is given by $\kappa = 16\gamma_{cf}^3\Omega^2/3(kT)^3$. Alternatively, one may write

$$\Delta G_{het} = \beta v^2\sigma^3/(kT \ln S)^2 \quad (7)$$

with β a shape factor and v the molar density. This leads, via the Arrhenius rate equation with pre-exponential factor A, to an induction time t_{ind} given by

$$\ln t_{ind} = \ln(N^*/A) + \beta v^2\sigma^3/(kT)^3(\ln S)^2 \quad (8)$$

where N^* denotes the number of nuclei formed per unit area (or volume) at time t_{ind}. Using a plot of ln t_{ind} versus 1/(ln S)^2, one can determine the various quantities involved, assuming values for β and ξ.

It is important to note that a number of premises are assumed for the application of the heterogeneous nucleation model. First, the substrate is assumed to be rigid, and second, the nucleating entities are assumed to be the individual ions. Third, the model for the nucleus is thermodynamical (with constant interface energies and solubility products) while the growth is dealt with with standard steady state models. Finally, in order to be able to use these models, sufficient data should be available. To comment first on the latter aspect, solubility products are not easily measured but are available for $CaCO_3$ (Table 1), although different authors do present somewhat different results. Further, normally constant values for β, ξ, and σ are assumed; however, the relative area, represented by ξ, may change during the process and both the shape, represented as β, and the interface Gibbs energy σ may change with ξ. Moreover, they may be influenced by the formation of complex species in the liquid phase which show a different adsorption behavior as compared with the initial compounds. Shape information has to be put in via the value for β if quantitative final data are requested.

There are further complications with this model. Intrinsically, the model is difficult to apply for neutral species, since the supersaturation is usually defined in terms of the solubility product and activities of ions Ca^{2+} and CO_3^{2-}. Moreover, in the conventional approach for heterogeneous nucleation, the substrate is taken to be flat and the nucleus is a spherical cap. The model has been liberated from the flat−substrate condition recently by Liu et al. by generalizing the substrate geometry model to spherical.[28]

The modification to a faceted nucleus has also been recently established.[29] Incorporation of the latter aspect, in particular, makes sense, since in many cases a faceted nucleus is observed. It appears, though, that the influence of the faceting is negligible as long as the ratio $(\gamma_{SF} - \gamma_{SN})/\gamma_{NF} = \cos\theta \leq 0.25$ or $\theta < 75°$. Here, γ_{XY} denotes the surface energy of the X−Y interface (S = substrate, N = nucleus, F = fluid) and θ the contact angle (Figure 3a). Applying nucleation theory and the associated growth rate expressions, estimates can be made for the number of growth entities in

the critical nucleus, the interface energy σ, and the type of nucleation mechanism (diffusion limited, uninuclear or polynuclear, growth at edges or via dislocations) via the slope and intercept of the induction time equation. Typically low numbers of growth entities are calculated for the critical nucleus, e.g. four for vaterite on cholesterol,[37] five for aragonite on the xiphoid of the cuttlefish,[38] and two for vaterite on calcite in the presence of leucine.[39] Also, generally rather low interface energies result, typically below about 50 mJ/m^2. For example, for the systems mentioned before, $\sigma = 11$, 24, and 23 mJ/m^2, respectively. Independent other measurements and various models normally result in values of 100−500 mJ/m^2. The mechanism involved is inferred from the growth rate exponent, e.g. $n = 1$ for surface diffusion controlled spiral growth,[39] $n = 2$ for surface diffusion controlled growth,[37] and $n = 4$ for a polynuclear mechanism.[38] The usual objections for the inference of the mechanism for the growth rate exponent are 2-fold, namely that the consistency of the experimental data with a model is only indicative and that observed exponents not matching the models, as regularly happens, are difficult to explain. Nielsen[27] provides some analysis for what he refers to as compound growth mechanisms.

It must be said that, in spite of all the possible weaknesses, the nucleation model is capable of explaining many aspects. As an example, we briefly discuss the results of an intriguing set of experiments done by Liu and Lim.[28] Applying classical nucleation theory, they analyzed the growth of calcite using the influence of different degrees of supersaturation on the induction times (Figure 3b). The data for homogeneous nucleation were determined from experiments under microgravity. The authors argued that the growth plane should discretely switch from the plane with the lowest σ-value (deepest cusp in the Wulff plot) to the one with next lowest σ-value. Using the microgravity data, they were able to estimate the absolute values for the function $f(\theta)$. Indeed, the analysis showed a discrete jump from one value of $f(\theta)$ (one plane) to another value for $f(\theta)$ (another plane). Also, the interface energy σ could be estimated, yielding 170 mJ/m^2. This value is claimed by the authors to compare favorably with independent data.

2.2. Controlling Growth

2.2.1. Additive Controlled Growth

It has long been demonstrated that both organic and inorganic additives can have a distinct effect on crystal nucleation and growth.[40−43] These additives can adsorb to the primary particles, thereby influencing the growth rate of the various faces so that a critical nucleus cannot be obtained. On the other hand, the inclusion of the additives inside the mineral particles may enhance their solubility, increasing the minimum size for the formation of a stable particle. These effects may cause aggregation of small entities to occur, yielding either randomly oriented polycrystalline aggregates or, in favorable case, well-oriented, larger aggregates. Aggregation of crystals can also be due to the adsorption of additives changing the surfaces characteristics of crystals[15] or due to bridging of those additives between two or more crystallites.[42]

Alternatively, adsorption of additives may take place in the stage where mineral particles have already passed the nucleation stage. In this situation, the molecules may influence the development of the crystal by the inhibition of acceleration of growth at distinct crystal faces. This will hamper the formation of the equilibrium morphology, which often reflects the structure of the crystallographic unit cell. For example, Teng et al. studied the influence of aspartic acid on the growth rate of (10·4) calcite.[44] Using AFM experiments, they showed a direct influence of aspartic acid on the thermodynamics of the growth by measuring the step speed as a function of step length and the dependence of the critical step length on supersaturation. From these data, they calculated the edge Gibbs energy and the energy barrier to 1D nucleation. They show that the addition of aspartic acid leads to a lowering of the step edge energy. The authors propose that this may be due to the formation of an ordered adsorption layer on the facets which changes the equilibrium activity of solutions contacting those facets.

In connection with brushite ($CaHPO_4 \cdot 2H_2O$), citric acid was used to modify the growth rate of various crystal planes.[45] In this case, it was proposed that, in contrast to what is usually assumed, the step density rather than the step velocity is determining the development of the crystal. Another factor is the chirality of the additive, which may give rise to a macroscopic expression of the asymmetry in the appearance of the crystals, as was shown for the effect of D- or L-aspartic acid on the growth morphology of calcite.[46]

Furthermore, it was demonstrated by the application of a model that the interaction between a specific molecule and desired crystal faces can be anticipated. Using molecular simulations, Coveney et al. selected a specific diazo crown ether, a molecule that can take sufficient conformations, to inhibit not only one specific surface but all surfaces of $BaSO_4$.[47] This resulted in an almost round shape of the crystals, indicating that effective inhibition indeed took place.

In the beginning of this section, we discussed how the use of additives can lead to particle mediated growth of crystals. Related to this, increasing evidence has emerged indicating that ions are often not individually dissolved in the liquid but already form nanoassemblies in the liquid, the structure of which is codetermining, if not determining, the crystallographic structure of the precipitating nucleus. Evidence for such a mechanism has been found for many types of minerals, including calcium carbonate. For example, for the formation of silica in the presence of tetrapropylammonium (TPA), it has been shown that the growth of SiO_2-TPA-MFI (MFI = framework structure code for the zeolite ZSM-5) occurs in two steps: a linear exothermic growth, followed by an endothermic, increasingly less-then-linear growth.[48] The first step is enthalpy driven while the second step is entropy driven. It has been made probable that growth occurs via orderly aggregation of reassembled 2−3 nm size primary TPA-MFI particles in a fully kinetically controlled process, except near termination, where thermodynamic control takes over.

Recently, also the formation of crystals through the assembly and transformation of amorphous precursor particles was demonstrated for $CaCO_3$ (Figure 2, path d).[49] In addition, Cölfen has emphasized the importance of nonclassical, particle mediated growth through oriented attachment (Figure 2, path d) and mesocrystal formation (Figure 2, path c).[15]

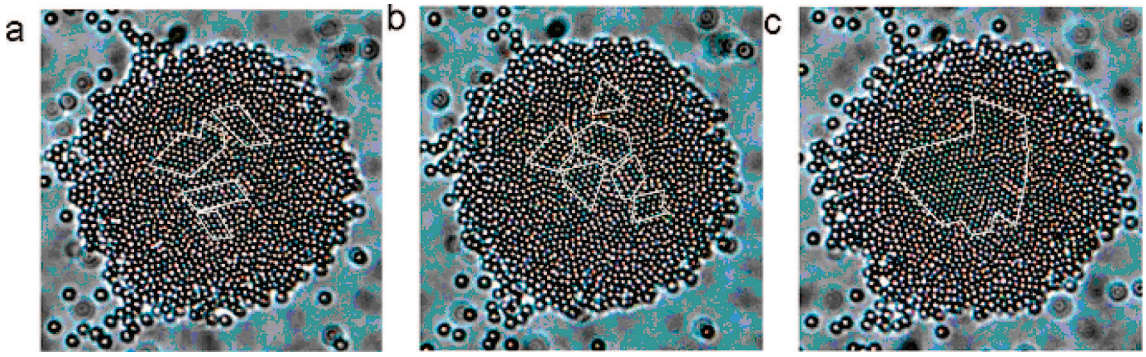

Figure 4. Evolution of crystalline structures inside the amorphous phase assembly of polystyrene spheres. (a) Small subcrystalline nuclei are initially created in the droplets that disappear and (b) reappear until they fuse to form (c) a stable mature crystalline nucleus. (Reprinted with permission from ref 55. Copyright 2007 American Chemical Society.)

2.2.2. Templating: Heterogeneous Nuleation

The nucleation of calcium carbonate on substrates generally has been discussed in terms of three mechanisms: epitaxy, charge/polarization matching, and mutual templating.

In epitaxy, the crystallographic structure of the nucleus must fit within certain limits the crystallographic structure of the substrate. Relevant for biomineralization is that both peptides and crystals have a structural surface-repetitive, complementary basis for pattern recognition. Epitaxy generally assumes a rather rigid substrate (the concept is borrowed from inorganic materials science), and an estimate for the maximum allowable lattice mismatch for epitaxy to occur can be made.[50] However, there are many examples in which one expects epitaxy and it does not occur and vice versa. Therefore, researchers looked at other mechanisms that relax the stringent constraints of the epitaxial model.

For calcium carbonate, many authors find indications that the functional groups of the template have a spacing in only one direction, or even just an orientation, that matches that of the carbonate ions (see section 3.3), as opposed to a strict epitaxial match. Molecular simulation studies have also investigated the influence of templates, such as Langmuir films[51] or self-assembled monolayers.[52] These studies show that, for example, the presence of Langmuir films can strongly influence the surface structure of some crystal faces. Similarly, these calculations indicated that the presence of other ions, such as bicarbonate ions, can form a mediating layer between the crystal face and a self-assembled monolayer, thereby lowering the interface energy.[52] These studies, thus, clearly show the limitation of using only epitaxy-based arguments to understand the interaction between the template and the inorganic phase.

In charge/polarization matching, the distribution of charges as observed on planes of the nucleus is matched by the opposite charges in the substrate plane. Not only Coulomb charges but also Van der Waals and other interaction effects such as polarization are taken into account. Obviously, this model puts less stringent constraints on the interface structure. Examples can be found in which charge/polarization matching is possible, indeed leading to the expected type of nucleus. However, there are also examples where charge/polarization matching cannot be used as an explanation but nucleation nevertheless occurs. These considerations lead workers in the field to the model of mutual templating.

In mutual templating, the structure of the nucleus and the structure of the substrate mutually influence each other in such a way that an energetically and structurally optimum interface is realized. Molecular dynamics studies[51,52] indicate this effect. Also, experimental studies[53] indicate that a flexible substrate can influence the growth rate. For example, a study using Langmuir films of varying compression was used to nucleate crystals of several amino acids such as tyrosine, alanine, and asparagine, and an enhanced growth rate was observed for not fully compressed films. The authors consider that a high growth rate is present when a low interface energy results between the film and the nucleus. Dividing the interface energy E_i in a nucleus misfit contribution E_d, a film strain contribution E_s, and an overgrowth contribution E_o, they argue that, for epitaxy, $E_d + E_s \cong 0$, so that a minimum interface energy is obtained for minimum E_o. For matching electrostatic interactions, $E_d + E_s \ll E_o$, so that also in that case a minimum in E_i results from a minimum in E_o. For mutual influencing using a film with nonclose packing, the misfit can be accommodated by a low strain in the film, since such a film is more flexible than a crystal. Hence, with E_d being zero and E_s being small, a minimum in E_i is again determined by a minimum for E_o. Of course, as a drawback, in this process more then one configuration is normally possible, and this can lead to less specific results.

Moreover, it has been suggested that aggregation on a template might occur preferentially via an amorphous phase, only later to order to a crystalline nucleus.[54] This process was simulated beautifully by using polystyrene spheres of $\sim$1 μm and narrow polydispersity ($\sim$5%) in an electric field at the low volume fraction of 0.03%[55] (Figure 4).

The first process step that took place was the aggregation at the surface, leading to an amorphous cluster. Thereafter, a few crystalline nuclei arise, but they normally shrink and disappear as a consequence of thermal fluctuations. Eventually, a stable crystalline nucleus, typically 3 or 4 out of 20, is realized by coalescence of a few smaller crystalline nuclei. Resulting grain boundaries are eliminated by rearrangement during further growth, indicating the (near) absence of an energy barrier. This is probably due to the fact that the density of the dense clusters decreases gradually from the center to the border, rendering the difference between "solid" and "liquid" in a dense cluster rather small. Indeed, the boundaries between crystalline and liquid are hard to delineate. The authors reported a kinetic analysis to support their structural findings. They also discuss why the differences between a 2D and 3D situation are not expected to be large. In the 2D case, of course, a strong "epitaxial" effect is active due to the rather stiff glass surface, and it is well-known from both computer and analogue simulation studies on hard spheres that extensive measures have to be taken to

avoid hexagonal packing at a flat surface. However, for templating crystallization studies, the main results, crystal nucleation via merging and ordering of a few small crystalline nuclei in a sufficiently large amorphous cluster, as such are quite insightful without generalizing to 3D.

3. Oriented Nucleation

As discussed in the previous section, a crystal is formed by the association of ions to form prenucleation clusters which further assemble to form the nucleus. It is well established that above a critical size the nucleus can further develop to form a crystal. This process, however, contains several stages in which crystallinity develops, as was also discussed in the last section. During this process, organic molecules or surfaces can influence the development of the crystalline state by the stabilization of a certain polymorph or even a specific crystal face. The stabilization of a specific crystal face on a surface is referred to as oriented nucleation. Further growth of the mineral phase then leads to crystals that all have this specific crystal plane oriented parallel to the template surface.

Hence, organic surfaces can not only lower the surface free energy of developing nuclei and thereby promote heterogeneous nucleation over crystallization in bulk solution, but they can also direct the crystallization of calcium carbonate by the stabilization of specific crystal planes. This latter process is commonly referred to as templating and plays a major role in biomineralization, as it is the key to the formation of oriented crystals. For example, in their investigations of mollusk shells, Weiner and Traub found evidence for an epitaxial relation between the spacing in the antiparallel β-sheet arrangement in chitin and the *ab*-plane of the aragonite it is in contact with.[56] From the experiments discussed below, we will learn that, in contrast to the original proposals in the literature, an exact match between the structure of the template and the developing inorganic phase is not a general prerequisite for an organic surface to control the formation of the mineral.

Here we emphasize the importance of biomimetic studies in understanding the processes involved in template-directed calcium carbonate formation. For this we will concentrate on the question to what extent the interactions between the organic and inorganic phases actually involve the transfer of structural information from the template to the nucleating phase. From the experiments discussed below, we will learn that, in contrast to the original proposals in the literature, an exact match between the structure of the template and the developing inorganic phase is not required for an organic surface to control the formation of the mineral. However, when a situation arises where the surface of the template and that of the nucleating crystal face have a close structural match, a high level of control over the crystallization can be achieved in which even the growth in the lateral direction and the morphology of the crystal are controlled. Furthermore, it will be shown that, where possible, the templating surface will adapt itself to the requirements of the developing inorganic phase. Moreover, the possibility of the template to rearrange is shown to strongly influence its ability to promote the nucleation of oriented calcite. Unfortunately, the question to what extend an organized surface must be present to produce oriented calcite remains unanswered for the moment.

3.1. 2D Templating Surfaces

In 1985, homochiral Langmuir monolayers of amphiphilic amino acid molecules were prepared and demonstrated to selectively nucleate crystals of glycine from the subphase solution.[57] The observation of enantiomorphous pyramidal glycine crystals confirmed the transfer of structure from film to nucleated crystal. In the same year, the nucleation of calcite on polymer surfaces functionalized with proteins extracted from mollusk shells was reported.[58] The first report related to calcium carbonate biomineralization in which the nucleation was studied on fully synthetic surfaces was published by Addadi and Weiner.[59] This paper described the assembly of a synthetic model system for the nucleation site of nacre in mollusk shells. The authors used poly(aspartic acid) (polyAsp) adsorbed on sulfonated polystyrene as the nucleation platform and demonstrated specific nucleation of the (00•1) face of calcite. Importantly, Addadi and Weiner showed that it was essential for the activity of the templating system that the polyAsp was organized in a β-sheet conformation. This strengthened the notion that biomineralization was controlled by macromolecular templates displaying ordered arrays of functional, in particular acidic groups. Moreover, these observations suggested that this form of preorganization of the functional groups is a prerequisite for their ability to control the organization of the first layer of calcium ions in the inorganic phase.

It was against this background of knowledge that Mann, Heywood, Rajam, and Birchall announced the controlled crystallization of $CaCO_3$ under Langmuir monolayers of stearic acid (octadecanoic acid, $CH_3(CH_2)_{16}COOH$).[10] In these monolayers, a similar form of preorganization is achieved in which the organization of the functional groups is governed by the packing of the surfactant head groups. This paper should be considered as extremely important, as it placed the use of monolayer studies, a technique well established in the field of physical chemistry, now in the context of biomineralization. The authors proposed that the initial stage of mineral nucleation is the establishment of the Stern layer of bound cations. They also discussed the possible involvement of epitaxial lattice matching between template and crystal, which had been raised previously in biomineralization literature. The authors concluded that their own results, however, actually did not involve epitaxial lattice matching and suggested that stereochemical as well as electrostatic matching could override the structural mismatch. Importantly, the work noted that partially compressed films were optimal in inducing crystal formation, which was related to the possibility that the stearate molecules would adopt a Ca-induced local ordering resulting in a configuration tailored for nucleation of these crystals. This paper clearly was the onset for a large number of papers using monolayers to study the nucleation of calcium carbonate[60−63] and other minerals.

In the 1990s also the use of self-assembled monolayers was explored for the oriented nucleation of calcium carbonate.[64] Although the biggest volume of work in this area was done on self-assembled monolayers of thiols on gold (and silver), the first experiments were actually performed using self-assembled monolayers of chlorosilanes on the surfaces of silicon wafers.[65] The combined results obtained with the different types of monolayers have revealed many details about the heterogeneous nucleation of calcium carbonate at a templating surface. An interesting extension of this work is the use of colloidal gold particles. These were stabilized with thiols of which the end groups were able to direct the

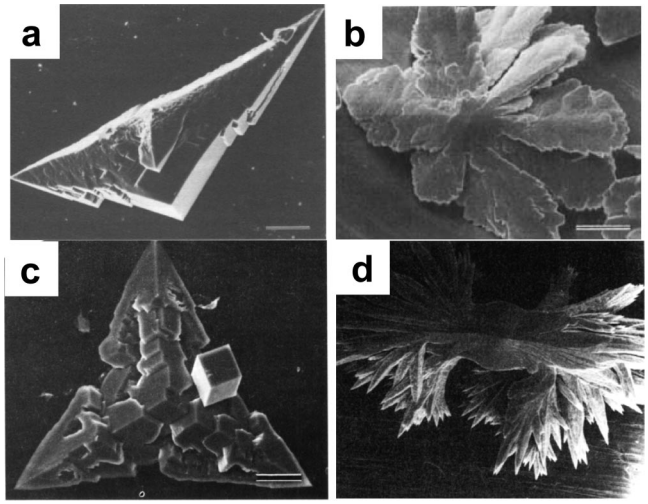

Figure 5. SEM images of $CaCO_3$ crystals formed under Langmuir monolayers of (a, b) stearic acid and (c, d) eicosyl sulfate: (a) (11•0) oriented calcite; (b) (00•1) vaterite; (c) (00•1) calcite; (d) (001) aragonite is formed in the presence of Mg^{2+} ions. (Parts a, c, and d are reprinted with permission from ref 70. Copyright 1990 Verlag GmbH & Co. KGaA, Weinheim. Part b is reprinted by permission from Macmillan Publishers Ltd: ref 10, copyright 1988.)

nucleation and growth of calcium carbonate, thereby introducing surface control in solution-based mineralization.[66−69]

In their early work, Mann et al. reported that when calcium carbonate is grown ($[Ca^{2+}] = 9$ mM) under monolayers of stearic acid, calcite is formed in its ($1\bar{1}.0$) orientation, i.e., with the *c*-axis of the crystals oriented parallel to the monolayer surface (Figure 5a).[70] Combined with the observation that under different experimental conditions also (00•1) vaterite could be obtained (Figure 5b),[10] the authors excluded the possibility of epitaxial matching of the carboxylate groups in the monolayer and the carbonate ions in the nucleating crystal plane. Instead, they proposed the involvement of stereochemical and geometric matching between the functional groups in the organic template with ions in the inorganic phase. This idea of stereochemical complementarity was strengthened by the nucleation of (00•1) calcite (Figure 5c) under two "tripodal" surfactants: *n*-eicosyl sulfate ($CH_3(CH_2)_{19}OSO_3Na$) and *n*-eicosyl phosphonate (CH_3-$(CH_2)_{19}PO(OH)_2$).[71] Both surfactants were thought to present three oxygen atoms able to interact with the (00•1) face of calcite, in which the carbonate ions are placed parallel to the crystal surface.

This group also showed that monolayers could be used to stabilize specific crystal faces in the other two anhydrous crystalline forms of calcium carbonate: vaterite and aragonite. A mixture of (00•1) and (11•0) vaterite was obtained by allowing the nucleation of calcium carbonate under monolayers of octadecyl amine.[70] For the nucleation of aragonite (Figure 5d), in the presence of Mg^{2+} ions, even more specific results were obtained: *n*-eicosyl sulfate and phosphonate both lead to the formation of (00•1) oriented crystals whereas the corresponding acid (arachidic acid, $CH_3(CH_2)_{18}COOH$) induces (11•0) oriented crystals.[71]

In a search for the mechanisms controlling the oriented nucleation of calcium carbonate, many studies have been reported in which organic assemblies with preorganized functional groups were employed. In the following sections, we will discuss in more detail the literature on this topic, focusing on the heterogeneous nucleation of calcite as studied at different "designer" interfaces.

3.2. Template−Crystal Interactions

Mann and co-workers demonstrated that under Langmuir monolayers of fatty acids, calcite predominantly nucleates from its ($1\bar{1}.0$) face.[71] The authors proposed that in this interaction the carboxylate groups of the template formed an auxiliary layer replacing the carbonate groups in the ($1\bar{1}.0$) face of calcite, similar to the proposed stabilization of the (00•1) face of calcite by the "tripodal" interactions with monolayers of eicosyl sulfate and eicosyl phosphonate (see section 3.1). Rather than using compressed Langmuir monolayers, Heywood, Mascall, and co-workers used monolayers consisting of self-assembled molecular ribbons of substituted melamine **1** and alkyl-modified cyanuric acids **2**. By modification of the melamine units, different functional groups (COOH, -OH, and -OPO_3H) were suspended from these monolayers (Figure 6).[72] In this way, self-organizing monolayers were formed with functional groups located at predefined positions that were used to induce the oriented nucleation of calcite.

The results obtained for the phosphate and the hydroxyl groups supported the previous results of Mann et al.; that is, crystals nucleated from the (00•1) faces and unmodified {10•4} calcite, respectively, were obtained. However, for the carboxylate moiety, the nucleation of (01•2) calcite was observed, instead of the ($1\bar{1}.0$) calcite that was observed for fatty acids. In this (01•2) crystal face, the carbonate ions have a tilted orientation with respect to the nucleation plane. This self-organized monolayer has a spacing of 4.5 Å between the molecular ribbon and within a ribbon a repeat distance of 9.5 Å for the functional groups. This means that the carboxylic acid groups have more space as compared to the head groups in a fatty acid monolayer and one could speculate that they could adopt a more tilted conformation to match with the orientation of the carbonates in the polar (01•2) face.

This suggestion is supported by the results obtained from self-assembled monolayers (SAMs) of thiols on gold. A number of ω-functionalized alkanethiols [HS-$CH_2(CH_2)_n$-X] were used to prepare SAMs on gold and silver surfaces[11,73] immobilized on silicon supports. Alkanethiols with -COO^-, -OH, -SO_3^-, and -PO_3^{2-} end groups (-X) induced the oriented nucleation of a series of specific crystal faces of calcite (Figure 7). On a silver support, a different set of orientations was observed, attributed to the different organization of the thiols depending on the underlying metal atoms. Self-assembly on gold or silver substrates, respectively, leads to the difference in the orientation of the alkyl chains of approximately 20°. In all cases, the orientations of the carbonates in the stabilized crystal planes matched the orientations of the carboxylates of the SAM very well (Figure 8).[74,75] This relationship was perfectly exemplified for monolayers of $HS(CH_2)_{15}COOH$ that change selectivity upon going from a gold support to a silver support.[76] The orientation of the *c*-axis changes linearly with the orientation of the alkyl chains with respect to the surface normal. Similarly, the carboxylates in the monolayer and the carbonates in the crystal keep their orientational relationship. This precise relation was further confirmed by comparison of different crystal orientations obtained from ω-carboxylate alkanethiols with different chain lengths on the same gold surface. Calculations indicated that variation of the chain length creates an odd−even effect inducing two different orientations of the carboxylic acid groups with respect to the substrate surface. These orientations can be matched

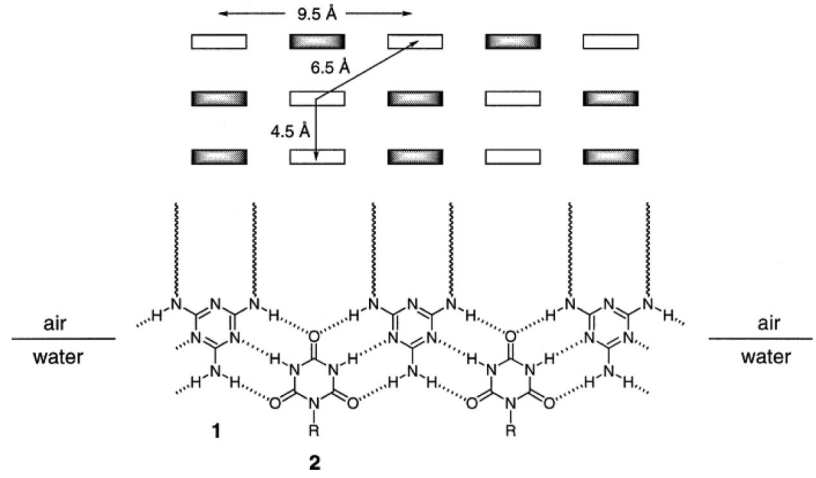

Figure 6. Representations of the melamine (1)−cyanuric acid (2) monolayer normal (top) and parallel (bottom) to the air−water interface. R = $CH_2CH_2CO_2H$, $CH_2CH_2CH_2OPO_3H_2$, $CH_2CH_2CH_2NH_2$. (Reproduced with permission from ref 72. Copyright 2000 Wiley-VCH Verlag GmbH & Co. KGaA, Weinheim.)

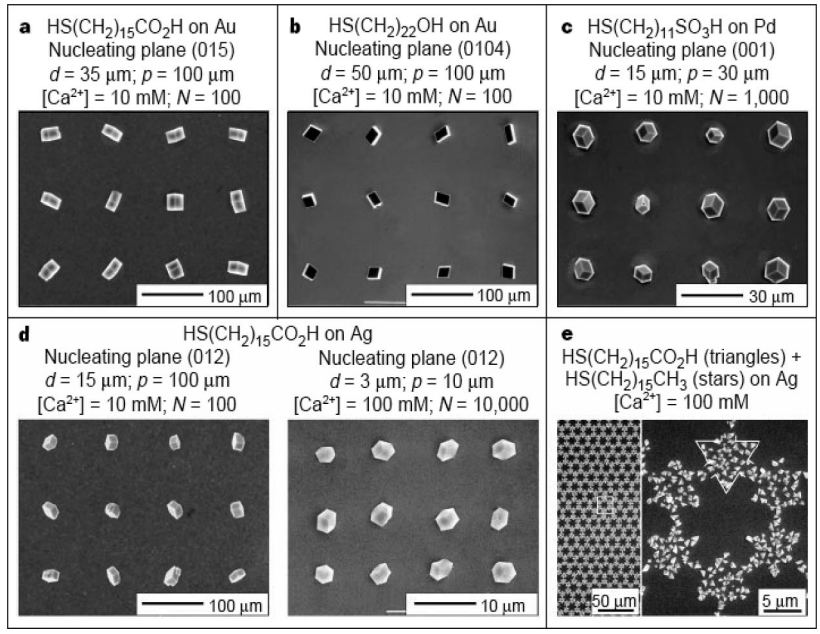

Figure 7. Ordered two-dimensional arrays of single calcite crystals grown on SAMs with different functional groups. (a−d) Single crystals. (e) An example of the fabrication of a more complex crystalline pattern: a continuous, polycrystalline structure. The low-magnification SEM (left) illustrates the high fidelity of the procedure; the high-magnification fragment (right) shows the formation of uniform crystals of submicrometer sizes. (Reprinted by permission from Macmillan Publishers Ltd: ref 11, copyright 1998.)

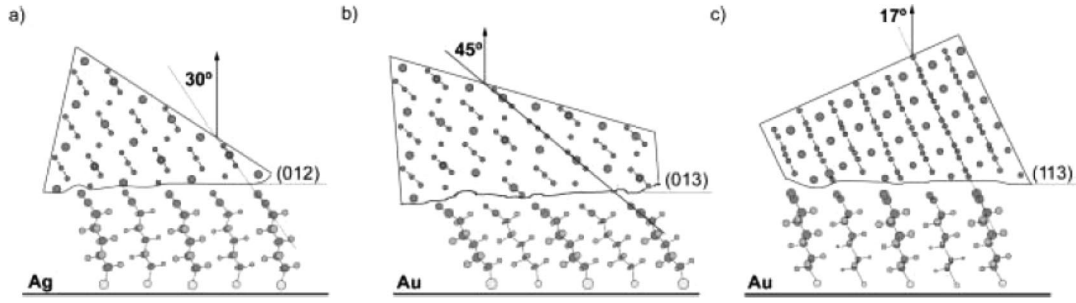

Figure 8. Schematic representations depicting the alignment of carboxylic groups on SAMs with the carbonate groups in calcite for (a) odd chain length SAMs on Ag, nucleation plane (NP) = (012), (b) odd chain length SAMs on Au, NP = (013), and (c) even chain length SAMs on Au, NP = (113). (Reproduced with permission from ref 76. Copyright 2003 Wiley-VCH Verlag GmbH & Co. KGaA, Weinheim.)

perfectly with the orientation of the carbonate groups in both observed crystal planes (Figure 8).

In contrast to the carboxy-terminated thiols, the monolayers with PO_3^{2-} terminal groups nucleated a group of crystal faces, rather than a single one. This was related to the rotational freedom of the phosphonate group with respect to the substrate surface. On gold, these included the (1 0•10), (1 1•12), and (0 1•14) planes, which share the common

feature that they all are oriented such that they make an angle of ~24° with the *c*-axis of calcite. The monolayer on silver stabilized a similar collection of planes, in this case with an average angle of ~40° with respect to the crystallographic *c*-axis. These angles coincide with the angles that the C−P bond makes with the surface normal of the monolayer. This suggests that the phosphonate groups coordinate in a tripodal fashion, forming a layer that replaces the carboxylates in the calcite lattice. In principle, the binding mode of the phosphate groups of the SAMs is the same as described for Langmuir films (although not as precise), but due to the tilted orientation of the molecules, the crystals have the above-mentioned orientations rather than the (00.1) orientation.

3.3. Epitaxy or Not?

In their initial paper, Mann et al.[10] clearly declined the need of epitaxial matching between the stearic acid [octadecanoic acid, $CH_3(CH_2)_{16}COOH$] monolayer and the nucleating crystals. Nevertheless, in a later report, they state: "Thus the first layer of the crystal will be determined primarily by the two dimensional spacings of the carboxylate binding sites. A comparison of these distances with those between coplanar Ca atoms in the $\{1\bar{1}.0\}$ face of calcite reveals a very close epitaxial match in two dimensions."[77] This statement was challenged by synchrotron X-ray studies which showed that monolayers of stearic and arachidic acid (eicosanoic acid, $CH_3(CH_2)_{18}COOH$) self-assembled to a well-ordered structure on a subphase of $CaCl_2$ even without compression.[78,79]

These monolayers were found to bind a layer of cations, but the density of this layer as determined by reflectivity measurements corresponded to only 1 Ca ion per four to five carboxylate groups in the case of arachidic acid and to one calcium ion per four to eight carboxylates for stearic acid monolayers (Figure 9). As these numbers cannot be brought in line with the crystal planes that nucleated under the organic films, the observations strongly argue against an epitaxial relation between the template and the nucleating crystal face for these monolayers.

The aforementioned revival of the theory of epitaxy was followed up by Aksay, Groves, and co-workers, who showed that monolayers of an amphiphilic porphyrin **3** bearing carboxylic acid groups nucleate the (00•1) plane of calcite (Figure 10).[80] This (00•1) plane forms an indentation in the corner of the rhombohedral crystals flanked by three {01•2} faces. The authors suggested the possibility of an epitaxial relation between the carboxylic acid groups and the (00•1) face of calcite, but they also indicate that the formation of the {01•2} faces that define the concave indentation may be related to the (bidentate) interaction with the carboxylic acid groups of the porphyrin.

Heywood and Mann already in 1991 described the formation of (00•1) calcite under a monolayer of eicosyl phosphonate.[71] In a later paper, Heywood and Mascal find the stabilization of the same (00•1) face of calcite also under self-organized monolayers of molecular ribbons with pendant phosphate moieties (Figure 6).[72] It is important to note that distinctly different spacings of the functional groups must be present in the two cases, again emphasizing that a precise matching between template and crystal plane is not the most important factor in regulating crystal nucleation.

Although the above clearly demonstrates that strict epitaxy is certainly not a requirement for the oriented nucleation of nonequilibruim faces of calcite, it is worth discussing in some detail to which extent there is a structural relation between

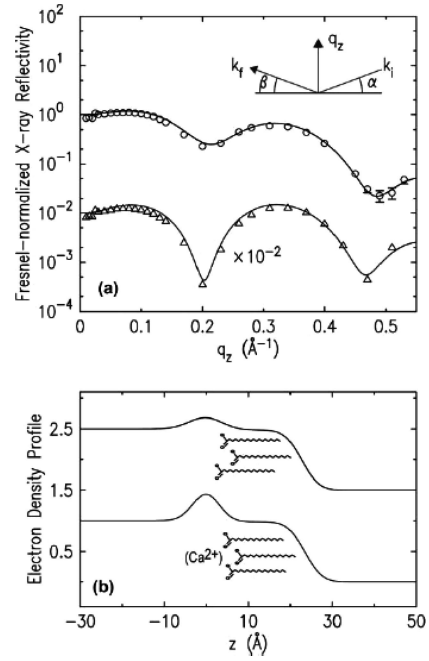

Figure 9. (a) Fresnel-normalized X-ray reflectivity data from stearic acid monolayers on water (upper trace) and calcium bicarbonate solution (lower trace) at surface pressures of 20−25 mN/m and (b) the related surface-normal electron density profiles on water (upper trace) and on calcium bicarbonate (upper trace) subphases. Schemes in part b show the positions of molecules at the surface. Increased density in the head group region shows that calcium collects at the interface of the bicarbonate subphase at an estimated ratio of four to eight stearic acid molecules per cation. (From ref 79 (http://dx.doi.org/10.1039/b309800a). Copyright 2003. Reproduced by permission of The Royal Society of Chemistry.)

the template and the nucleation crystal surface. In this respect, it is also interesting to mention the work of Kim et al., who demonstrated that nucleation of aragonite can be favored on inorganic surfaces with different degrees of mismatch with respect to the aragonitic lattice.[81] It was reported that under the conditions used the critical epitaxial strain for aragonite would be between 5.4 and 7.1%. Pokroy and Zolotoyabko found that epitaxial growth of aragonite on different oxide surfaces was even possible up to mismatches of 11%.[82] Moreover, they found that also in this setup stereochemical effects can overrule possible epitaxial relations, and they emphasize that for a full understanding of the mechanism these two effects should be treated separately.

Sommerdijk and co-workers presented evidence that orientational matching could suffice to stabilize the (10•0) face of calcite (Figure 11).[83] They used an amide-containing surfactant **4**, forming linear arrays of hydrogen bonds that defined their intermolecular spacing. Due to intramolecular hydrogen bonds, the phosphate head group is kept in a conformation such that only two of the oxoanions can bind to the mineral surface (Figure 11b), giving rise to a bidentate interaction explaining the stabilization of the (10•0) face of calcite. Molecular models indicated that the distance between the phosphate head groups as defined by the amide hydrogen bonds should be ~5 Å (Figure 11c). Although this distance approximately matches the 4.99 Å repeat distance of the carboxylate groups in the direction along the *a*-axis, no further matching of the 2D lattice could be found on the basis of the molecular parameters derived from Langmuir experiments.

The same group further investigated the relation between functional group organization and the nucleation plane using

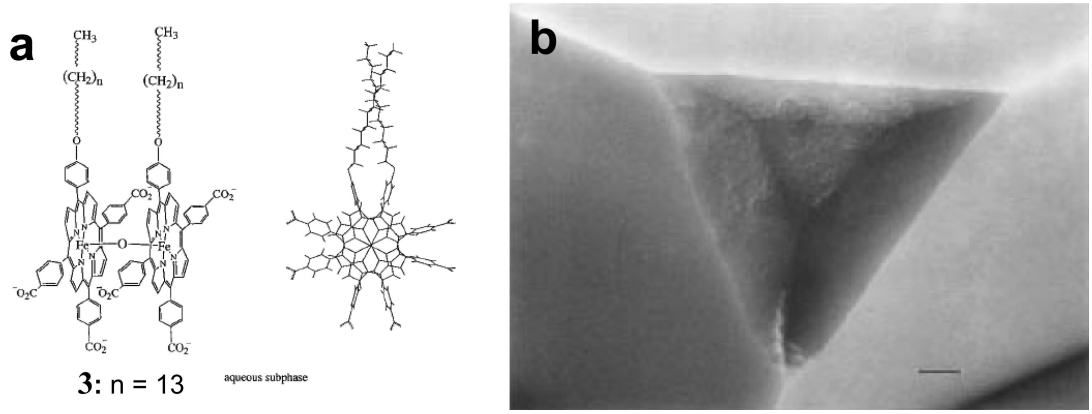

Figure 10. (a) Chemical structure of amphiphilic porphyrin **3** and (b) SEM image of a modified calcite crystal grown under monolayers of **3** displaying an indentation formed by three {01•2} planes and the (00•1) plane. (Reprinted with permission from ref 80. Copyright 1997 American Chemical Society.)

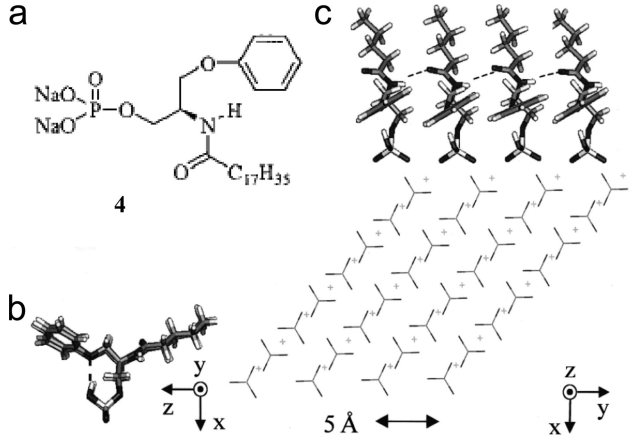

Figure 11. (a) Chemical structure of **4**. (b) Molecular model of **4** showing the H-bonding of the phosphate and the phenyl oxygen. (c) Proposed mode of interaction of H-bonding molecules of **4** with the (10•0) surface of calcite. (Reprinted with permission from ref 83. Copyright 2001 American Chemical Society.)

rigid surface adsorbed polymers (Figure 12).[84] Poly(isocyano peptides) **5** are a class of helical polymers with 4-fold symmetry, in which the peptide side chains form strong hydrogen bonds running in the direction of the backbone that stabilize the helical conformation even in aqueous media. This locks the carboxylate end groups of the dipeptide side chains in a predefined arrangement with a spacing of ~4.2 Å between two neighboring helical turns. These polymers adsorbed to glass slides induced nucleation of calcite from the (01•1) calcite face (Figure 12b), which has carbonate spacings of 4.05 and 4.99 Å. Computer generated models failed to indicate a match between the spacings of the carbonate ions in this crystal face and the spacings between the carboxylate end groups of the polymer. However, these models suggested that a match between the orientation of the carboxylate groups and the carbonate ions in the (01•1) face is well possible (Figure 12b).

More detailed information about orientational matching between the template and the developing inorganic phase was obtained by Berman et al. They used a diacetylenic carboxylic acid (**6a**) monolayer that was polymerized into a 2D crystal (**6b**) with domain sizes up to 3 mm (Figure 13).[85] After transfer to a solid support, calcite crystallized on this template in the (01•2) orientation, again suggesting a tilted orientation of the surfactant molecules with respect to the surface normal (see above). However, in this case, all crystals were oriented with the crystallographic *a*-axis along the polymer backbone and the projected *c*-axis perpendicular to the polymer backbone. Both the carbonate groups in the (01•2) face as well as the carboxylate groups in the template have a repeat distance of approximately 5 Å. The fact that the crystals have an asymmetric orientation with respect to the polymer substrate can be related to the approximately 30° angle the molecules make with the surface normal, which matches the angle of 28° the carbonates make with respect to the (01•2) crystal plane. The elongation of the crystals along the *a*-axis was attributed to a better match in this direction compared to the *c*-direction, which has a mismatch and is therefore inhibited. Indeed, when this mineralization reaction was performed in the presence of polyAsp, the interaction of the additive with the (11•0) faces delayed growth in the ⟨10•0⟩ direction, leading to elongation of the crystals along the *c*-axis.[86]

Travaille et al. made similar observations for the nucleation of calcite on highly ordered SAMs of ω-mercapto hexadecanoic acid on gold (Figure 14).[87] These authors found (01•2) calcite as the predominant phase with (01•5) as the minor product, in apparent contrast with earlier results described by Aizenberg et al.,[73] who found crystals with the latter orientation as the main product. These findings were attributed to the lower pH of the crystallization solution using the Kitano procedure instead of the ammonium diffusion method. This lower pH leads to a higher degree of protonation of the carboxylic acid groups, which subsequently induces a different orientation of these groups.[88] The gold domains employed by Travaille et al. had estimated sizes of 250×250 nm^2 and were oriented under 60°, following the symmetry of the mica that was used as a substrate. Strikingly, the ordered structure of the underlying mica and the gold layer had aligned their crystallographic axes together with those of the crystals over large distances. This also implies a precise relation between the calcite crystal structure and the underlying monolayer. Indeed, it was demonstrated that the orientation of the protonated carboxylic acid groups gives a near prefect match with the carbonate ions in the (01•2) plane along the ⟨10•0⟩ directions.[89] Han and Aizenberg used Mg^{2+} ions to influence the growth kinetics of oriented crystals in a similar system to change their shape.[90] By binding to the (0*k*•1) surfaces, increasing magnesium concentrations lead to a reduction in growth along the preferred ⟨10•0⟩ directions and to the elongation of the crystals along the *c*-axis. With this method, the growth kinetics of crystallization was varied on a variety of substrates, demonstrating an impressive control over both

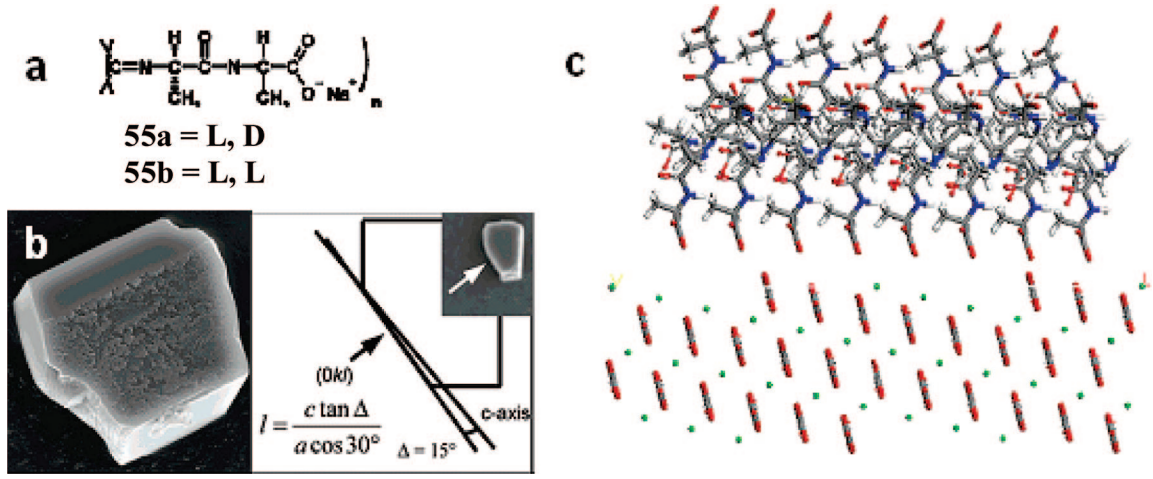

Figure 12. (a) Poly(isocyano alanyl alanine). (b) SEM image (left) and indexing of the (11·0) oriented calcite grown on surface adsorbed **5a** (right). (c) Computer generated model of **5a** and side view of the (0·11) surface of calcite showing the spacing of the carboxylate groups in the polymer and their proposed mode of interaction with the calcite surface (Reprinted with permission from ref 84. Copyright 2001 American Chemical Society.)

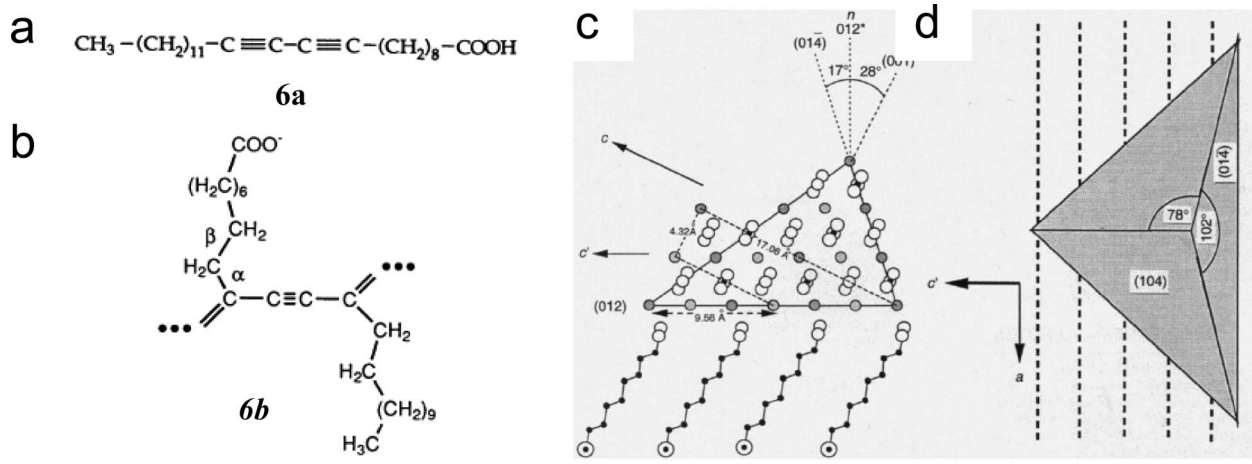

Figure 13. (a, b) Chemical structure of diacetylenic carboxylic acid (a) before (**6a**) and (b) after polymerization (**6b**). (c, d) Schematic representations showing the interaction of the polymerized Langmuir Sheafer film of **6b** with (01·2) oriented calcite. (c) Side view showing the alignment of the functional groups in the template with the carbonate ion in the mineral. (d) Alignment of the crystals with the polymer backbone (dotted lines). (Reprinted from *Science* (ref 85.)

shape and orientation. More recently, it was shown in more detail that each SAM, in addition to inducing the highly oriented crystal growth, induces a clear modification of the calcite shape.[91] These originate from the anisotropy of lattice mismatches that develop between the nucleating crystal face and the organic SAM in different directions. Pokroy and Aizenberg presented a model able to predict the shape of crystals grown SAMs, as a function of lattice mismatch, which correlated well with the experimental results.

The lateral orientation of the crystals discussed above shows that ordering of the monolayer is reflected in the crystallization results even though these gold domains (~250 × 250 nm^2) are still much smaller compared to the developing crystals, which become 10−20 μm in size. This means that even smaller domains of the SAM are able to induce this highly oriented crystal growth. Interestingly, Kwak and co-workers reported that these SAMs on gold do not show any long-range order in synchrotron X-ray scattering measurements (Figure 15).[92] The gold domains on which the SAMs were immobilized were determined to have a coherence length of only approximately 18 nm. Obviously, the coherence length of the SAM must be even smaller and was estimated to be 1−10 nm, since both before and after exposure to calcium ions the order of the monolayer was too low to be determined. This means that the interaction of the functional groups in the monolayer can act coherently only in the very first stages of nucleation. It should be noted, however, that these measurements were performed on dried samples, thereby eliminating the dynamics of the functionalized surface that may be present in contact with the mineralization solution. Indeed, in situ X-ray studies have shown that the binding of Ca^{2+} ions increases the order of the surface for carboxylic acid terminated SAMs.[93]

Volkmer et al. demonstrated that under monolayers of a tetrakis(carboxymethoxy)calix[4]arene (**7a**), (01·2) oriented nucleation of calcite single crystals occurs at low surface pressure (0.1−0.5 mN/m), where the monolayer displays a liquid-condensed phase (Figure 16).[94] This means that the monolayer under mineralization conditions is noncrystalline and highly dynamic during crystal maturation. Moreover, mineralization under monolayers of other amphiphilic macrocycles (e.g., tetracarboxyresorc[4]arene[95] (**8**) and calyx[8]arene[96] (**9**)) led to similar results: (01·2) oriented calcite is formed at similar low surface pressure (0.1−0.5 mN/m). These macrocycles do not have a prearranged organization of their functional groups, and the way these groups are exposed varies from molecule to molecule. This prompted the authors to bring forward the hypothesis

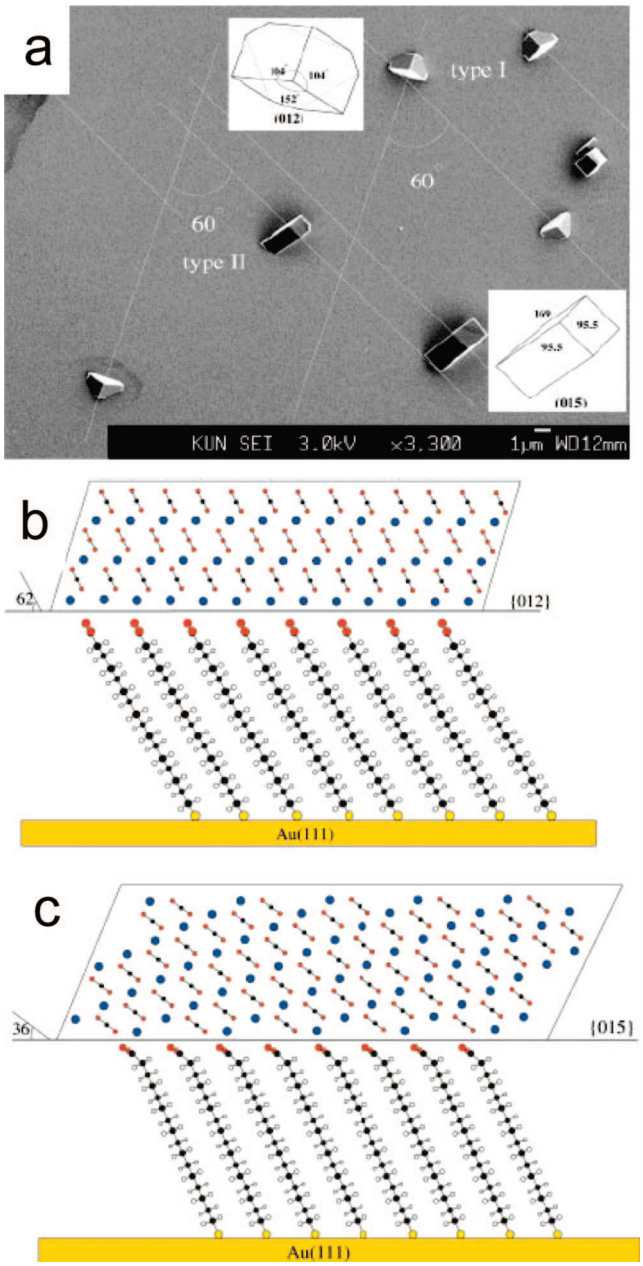

Figure 14. (a) SEM image of calcite crystals, grown on a SAM of 16-mercaptohexadeconoic acid (MHA). The lateral alignment of the calcite crystals with the hexagonal symmetry is shown with the white lines. The calcite crystals nucleate with two different faces: the {012} faces (type I) and the {015} faces (type II). The insets show the modeled calcite crystals that correspond to these two nucleation faces. (b, c) Schematic representations showing the interaction (side view) and the alignment of the functional groups in the template with the carbonate ion in the mineral for the (c) protonated SAM with (01•2) oriented calcite and (d) the deprotonated SAM with (01•5) oriented calcite. (Reproduced with permission from ref 87. Copyright 2002 Wiley-VCH Verlag GmbH & Co. KGaA, Weinheim.)

that not the precise organization of functional groups but charge density is the major factor in controlling calcium carbonate mineralization.[97] However, considering the results discussed above, the question remains whether or not it is possible for the pendant carboxylate groups of these macrocycles to orient themselves in such a way that they match the orientation of the carbonate groups in the (01•2) face of calcite.

3.4. Template Adaptability

In a 1996 review paper, Calvert and Rieke have pointed out the distinct difference between mineral growth at inorganic and at organic interfaces.[98] Where inorganic interfaces are rigid and stable and mineralization is largely determined by epitaxial lattice matching,[81,82] organic surfaces are inherently more flexible and may have specific binding capacities for the ions in solution.[98] As a consequence, the mineralization interface may change its structure due to the interaction of the two phases. Indeed, for several Langmuir monolayer templates, a change in surface structure is reported upon calcium complexation, as deduced from the shape of the surface pressure−surface area isotherms.[62,80,83]

Already in their first paper on calcium carbonate nucleation under Langmuir monolayers, Mann et al. observed that different degrees of compression influenced the nucleation density and hence the size of the crystals, but not the nucleation face of these crystals.[10] From these results they proposed that the organization of the monolayer adapts to achieve a "calcium induced local ordering of the stearate molecules into a configuration tailored for nucleation". It was suggested that the liquid phase monolayers were optimal for achieving a nucleation rate such that crystals with a narrow size distribution were obtained, i.e. that nucleation of most of the crystals occurred simultaneously and that the growing crystals competed with the nucleation of new ones. Related observations were made by Volkmer et al., who showed that, under monolayers of several calixarenes and resorcarenes (**7**−**10**), efficient modification of calcium carbonate growth only occurs at low surface pressure (0.1−0.5 mN/m) whereas, under compressed monolayers (5−20 mN/m), randomly oriented calcite is obtained[94−96] with reduced nucleation density.[99]

Dimasi and co-workers demonstrated that on a calcium containing subphase the stearate molecules self-assembled into highly ordered domains, which was independent of the compression state of the monolayer.[79] In line with these results, Meldrum et al.[100] showed for a series of fatty acids with varying chain lengths that the longer fatty acid monolayers had a higher tendency to form self-organized domains, also for uncompressed monolayers.[101] Brewster angle microscopy experiments indicated that calcium carbonate crystals nucleated predominantly under these domains, which suggests that they possess a preorganization that is favorable for the nucleation process. Interestingly, the nucleation density was found to be even higher at the domain boundaries. This observation most probably relates to the local higher mobility of the functional groups and their concomitant ability to adapt to the developing crystal.

Experiments of Aizenberg and co-workers on SAMs also suggested that the activity in nucleation of this type of templates depends on the possibility of the functional groups in the monolayer to reorganize their structure. Using patterns of metal-on-metal, they created domains of self-assembled monolayers of thiols with different degrees of order.[102,103] With ω-carboxyalkanethiols ($HS(CH_2)_{15}COOH$), these different surfaces showed different nucleation capability. Gold and silver have comparable lattice parameters; however, the functionalized alkanethiols on the gold films have a more tilted orientation (see Figure 14) and hence a tighter packing than on silver. In fact, the highest nucleation activity was observed at the boundary of the domains due to the local disorder in the monolayer (Figure 17), again similar to what was discussed for Langmuir monolayers.[100] In the case of

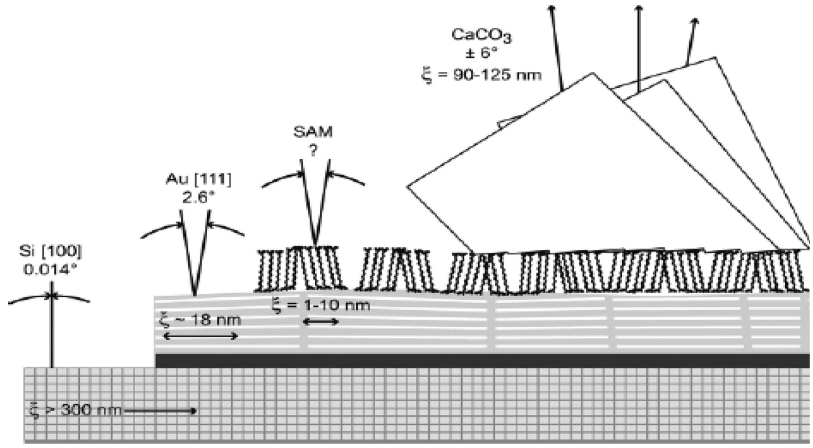

Figure 15. Schematic illustration of the buildup of a SAM on gold covered silicon, indicating the angular spreads and coherence lengths in each layer. (Reprinted with permission from ref 92. Copyright 2005 American Chemical Society.)

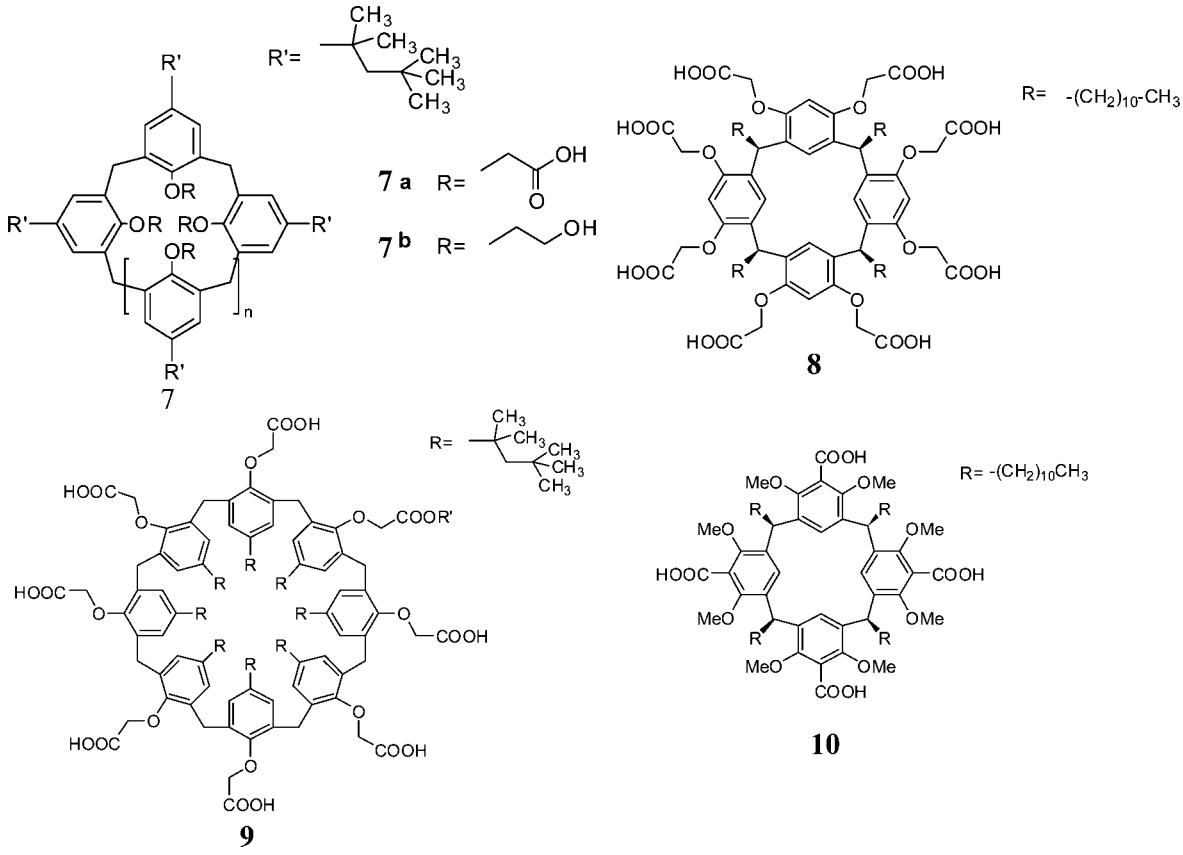

Figure 16. Molecular structures of macrocycles **7**−**10.**

silver and gold, the nucleation subsequently occurs on the edge of the silver islands, after which the silver islands are filled before nucleation on the gold occurs. Apparently, the ordering of the molecules within the monolayers is related to their nucleation activity, with the lower degree of packing of the thiols on silver being more efficient in promoting the nucleation of calcite than those on gold.

Lee, De Yoreo, and co-workers addressed the issue of monolayer reorganization using self-assembled monolayers of mercaptophenol on gold (Figure 18).[104] They used a precipitation method that involved the deposition of ACC that was temporarily stabilized in the presence of the monolayers but not in their absence. Using near edge X-ray absorption spectroscopy (NEXAFS) and photoemission spectroscopy, it was demonstrated that monolayers of 3- and 4-mercaptophenol were highly organized prior to exposure to the mineralization solution. Surprisingly, this order was completely lost upon deposition of the ACC on the SAM.

Nevertheless, crystal formation occurred with high selectivity for the {10·4} face of calcite. This points to a critical issue in the study of templated crystallization: does oriented crystallization need an ordered templating surface? Based on the above results, it appears that if this is indeed the case, this surface must be formed by a tiny, ordered domain in the mercaptophenol SAM, as was also proposed by Kwak and co-workers for ω-carboxy SAMs.[92,105] Alternatively, taking into account the aforementioned evidence of structural relationships between the organic and inorganic phases, the SAM reorders itself during the crystallization in a process in which the monolayer and the mineral template each other.

Such a rearrangement of surface functionalities to accommodate the nucleating crystals was beautifully demonstrated

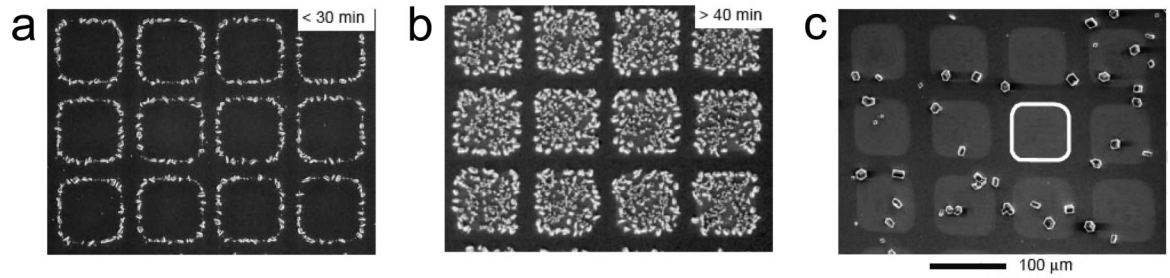

Figure 17. Scanning electron micrographs of calcite crystals grown on topographically patterned surfaces fabricated by depositing Ag (50 nm) on Au through a stencil mask followed by formation of SAMs. (a, b) Patterns of calcite crystals formed on SAMs of $HS(CH_2)_{15}CO_2H$ supported on the micropatterned metal surfaces. Crystals formed (a) after 30 min follow the outline of the patterns, and (b) after 40 min, preferential filling of the Ag regions is observed. (c) Nonpatterned growth of calcite induced by bare substrates supporting no SAM. (Reprinted by permission from Macmillan Publishers Ltd: ref 11, copyright 1998.)

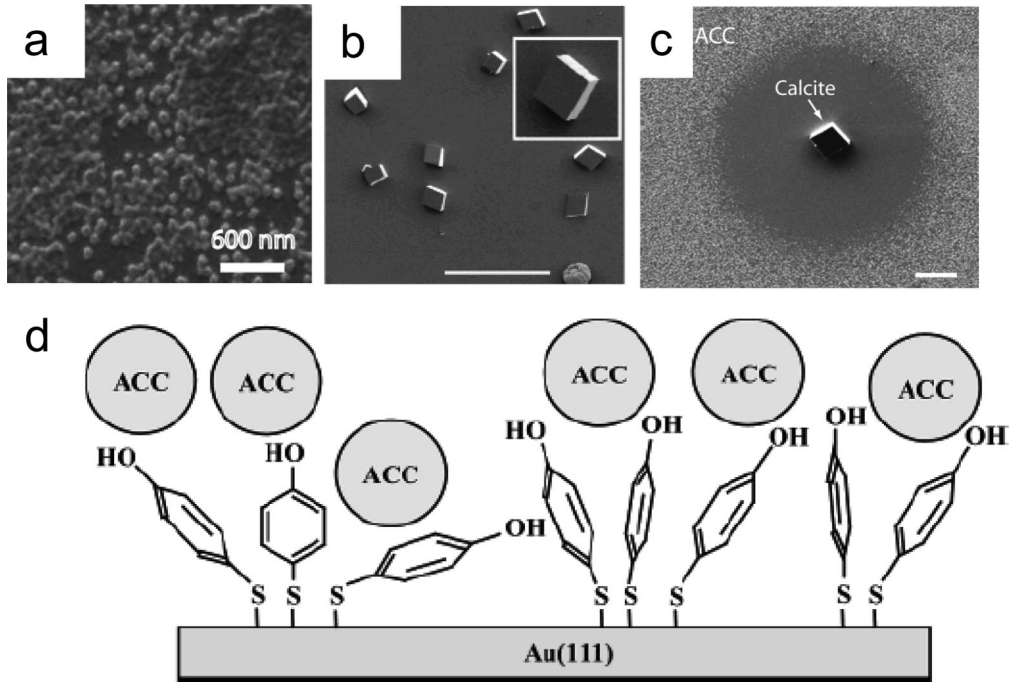

Figure 18. (a−c) SEM micrographs of (a) ACC precipitate prepared on a 4-MP SAM on Au(111); (b) crystalline $CaCO_3$ growth on a 4-MP SAM, scale bar 100 μm, inset = higher magnification image; and (c) a (10·4) calcite rhombohedron during the conversion from ACC to crystalline $CaCO_3$. The zone surrounding the calcite crystal is entirely depleted of ACC. The scale bar is 10 μm. (d) Schematic to illustrate an ACC/4-MP system in which the SAM is comprised of monomers with a random distribution of orientations. (Reprinted with permission from ref 104. Copyright 2007 American Chemcial Society.)

by Berman and co-workers.[85] They showed that the color of the poly(diacetylene) films (see also Figure 22) changed from blue to red upon exposure to the mineralization solution, indicating a restructuring of the template during the nucleation process. These observations were confirmed by FTIR measurements showing an increase in the intensity of the asymmetric methylene stretching band while the symmetric stretching band remained almost unchanged.[106] Theoretical calculations using classical electromagnetic theory indicated that this could be related to the reorganization of the alkyl chain structure. For stearic acid and octadecyl sulfate, a more precise description of the changes in orientation during mineralization was offered. Stearic acid was demonstrated to go from an almost parallel orientation to the surface normal on water or aqueous calcium chloride to a more tilted orientation during the outgassing of a supersaturated calcium carbonate solution and the concomitant formation of (01·0) calcite. For the octadecyl sulfate, an expansion of the monolayer was deduced from the observed order to disorder transition of the alkyl chains during the mineralization of (00·1) calcite.[107] These results indicate that although a strict epitaxial relation cannot exist, the different systems try to optimize the match between the functional groups in the template and the carbonate groups in the developing crystal.

This issue was investigated further by Sommerdijk and co-workers, who used self-organizing surfactants to demonstrate how the ability of these molecules to adapt to the demands of the nucleating mineral phase determines their activity in calcium carbonate nucleation (Figure 19).[108] From a homologous series of amino acid derived bis-urea surfactants **11a**−**d**, two examples derived from glycine (Gly) **11a** and valine (Val) **11c**, respectively, showed how the rigidity of the monolayer affected both the nucleation density and the templating capability of this system. Langmuir experiments showed that the Gly-derived surfactant **11a** forms highly rigid monolayers that only very weakly respond to the presence of calcium ions or to the formation of calcium carbonate underneath. In contrast, the Val-based surfactant **11c** increased its molecular area upon exposure to calcium ions but remained stable during mineral formation, indicating that the initial complex is also the one that is present during the mineralization.

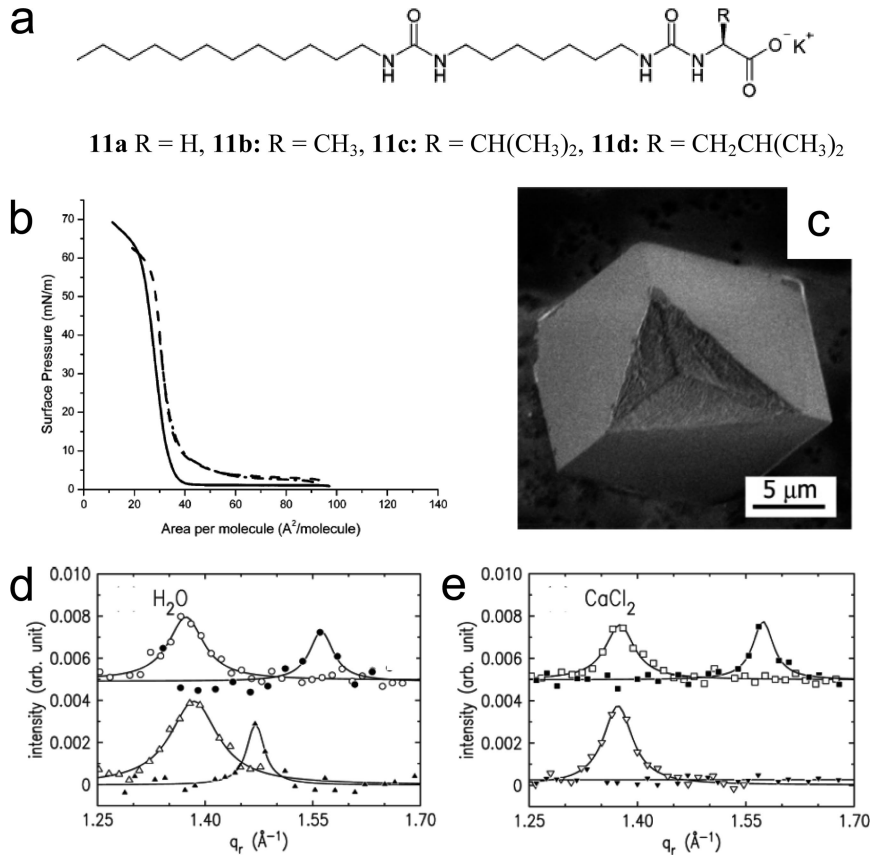

Figure 19. (a) Molecular structures of **11a**−**d**. (b) π−A isotherms of **11c**, on subphases containing water (solid line), 9 mM $CaCl_2$, and 9 mM $Ca(HCO_3)_2$ (two overlaying dashed lines). (c) SEM image of modified crystal with a concave indentation isolated from beneath a monolayer of **11c** after 4 h. Crystal viewed from the side that was exposed to the monolayer. (d, e) Background-subtracted grazing-incidence X-ray diffraction peaks for compounds **11a** (upper traces) and **11c** (lower traces) on (d) H_2O and (e) 9 mM $CaCl_2$ subphases. (Reprinted with permission from ref 108. Copyright 2007 American Chemical Society.)

These results are supported by X-ray diffraction studies which showed that, where the order of the Gly-based monolayer was undisturbed upon exposure to calcium ions, the 2D organization of the Val-based monolayer was lost and only the hydrogen bonding interactions remained.[109] The rigid Gly-based monolayer led to the formation of unmodified {10•4} calcite, whereas, in the case of the more pliable Val-based monolayer, the crystal predominantly showed modifications that were attributed to nucleation from the (10•0) calcite face (Figure 19c). Surprisingly, in this series of surfactants, the nucleation density increased with increasing monolayer rigidity, contrary to the observations on the systems described above.

For the alanine (Ala) **11b** derivative with an intermediate size side chain, the interaction with the different calcium containing subphases only led to small changes in the molecular area, and mineralization experiments yielded {01•2} calcite as the major product alongside other calcite modifications of the type {01•l} with $l = 1-2$, and a small fraction of (10•0) oriented calcite. These crystal planes are related by a rotation of the carbonate ions with respect to the crystal surface (Figure 20d−f). Moreover, in the earlier stages of the mineralization reaction, a different distribution of crystals was obtained: after 7 min, the {10•0} modified crystals were dominant, while, already after 15 min, equal amounts of {10•0}, {01•1}, and {01•2} modifications were observed, of which the last one became the major product after 4 h. The results most probably reflect the reorganization of the monolayer into a structure in which the molecules in time adopt a more tilted orientation with respect to the air−water interface. This suggests that also the adaptation rate is an important factor in the templating process determining the homogeneity of the mineralization product.

Similar results were obtained for a series of amphiphilic lipopeptides (Figure 20).[110] These were prepared to decrease the water solubility of the $(Leu\text{-}Glu)_n$ ($n = 2-4$) **12** sequence that only has some amphiphilicity above $n = 4$. This modification would allow studying the activity of this β-sheet forming sequence in the nucleation of $CaCO_3$. The acetylated octapeptide *N*-acetyl-$(Leu\text{-}Glu)_4$ (**13**) indeed was long enough to form stable and very rigid monolayers and was used as a reference. Monolayers of **13** did not alter their organization upon the addition of calcium carbonate ions nor during the first half-hour of the crystallization process. After 5 h, modified calcite grown under these monolayers predominantly developed with (01•2) orientation while a minor amount (<5%) of indented crystals were present that were identified as (10•0) nucleated calcite. With time, increasing amounts of the indented crystals were observed, until after 48 h, this was the major product. These observations suggest that the monolayer slowly rearranged in favor of a configuration that promoted the formation of this crystal type. In line with this idea, it was demonstrated that during the whole process, continuously new (10•0) crystals nucleated while the (01•2) oriented crystals only grew in size rather than in number. In contrast, the DOPE-$(Leu\text{-}Glu)_4$ conjugate **14c** (Figure 20) formed a much more flexible monolayer which significantly adapted its organization at the air−water interface upon complexation of calcium ions, and even more upon exposure to a supersaturated $Ca(HCO_3)_2$ mineralization

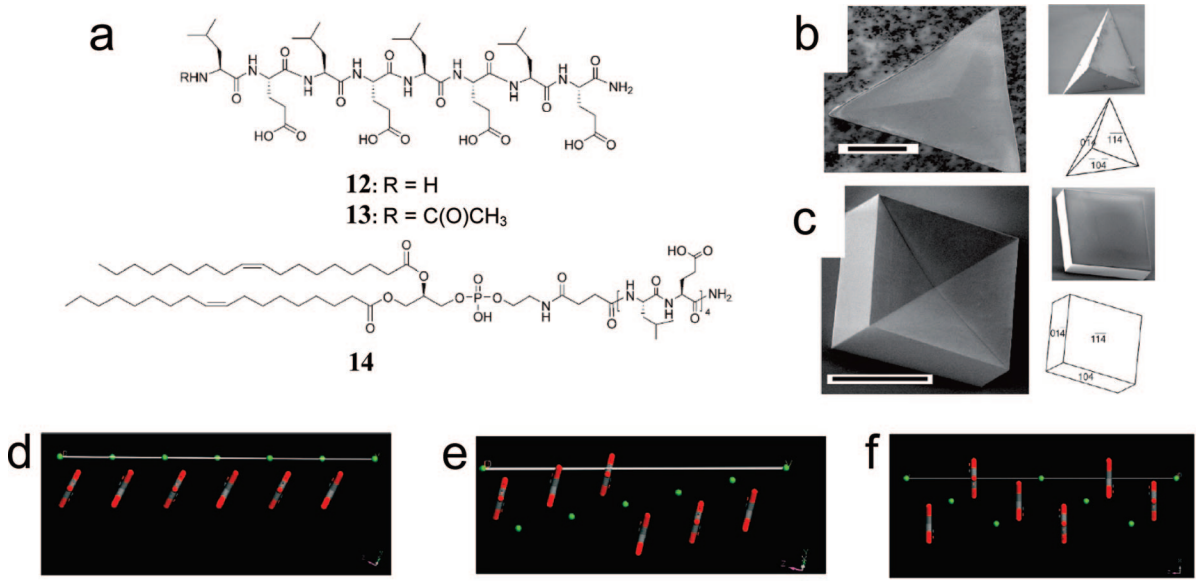

Figure 20. (a) Chemical structures of **12**−**14**. (b, c) SEM of (b) (01•2) oriented calcite and (c) indented (10•0) oriented calite crystals viewed from the side of the monolayer. Insets: calcite crystals observed from the side (top) and models of the crystals (bottom). (d−f) Models of the (d) (01•2), (e) (01•1), and (f) (10•0) faces of calcite. (Reproduced with permission from ref 110. Copyright 2006 Wiley-VCH Verlag GmbH & Co. KGaA, Weinheim.)

solution. Surprisingly, from this assay, the same two types of crystals were obtained, although now already after 5 h the indented crystals were dominant over the pyramidal crystals and this population only slightly increased with time. It was proposed that in this case the more flexible organization of the molecules allowed a quick adaptation of most of the monolayer to the (10•0) face of calcite, resulting in a more uniform reaction product, also in time.

Although the DOPE moiety distinctly altered the characteristics of the monolayer, grazing incidence X-ray measurements showed that both **13** and **14c** formed β-sheet structures. The activity of these compounds was related to their ability to form these ordered structures at the air−water interface. This was confirmed by a study of shorter peptide sequences **14a** ($n = 2$) and **14b** ($n = 3$) which do not self-assemble to spontaneously form β-sheets.[111] For **14b** ($n = 3$), β-sheet formation could be induced upon compression of the monolayer, in contrast to the amphiphilic tetrapeptide ($n = 2$) that did not form such well ordered structures. Importantly, the compression isotherm of the hexapeptide derivative indicated that this monolayer was even more flexible as compared to the DOPE-(Leu-Glu)$_4$ **14c** conjugate. Indeed, an even larger proportion of the indented crystals was obtained for the compressed monolayer of this compound, whereas the monolayer of the modified tetrapeptide did not show any activity in calcium carbonate nucleation.

4. Controlling the Phase Behavior of Calcium Carbonate

Many organisms demonstrate a very precise ability to select between the polymorphs of calcium carbonate that they use as a structural material. In mussel shells, we find a beautiful example, where calcite and aragonite are present in the neighboring prismatic and nacreous layers.[112] Several experiments have indicated that this polymorph selection is associated with the action of specific macromolecules. In one of these experiments, calcium carbonate has been precipitated in the presence of proteins isolated from calcitic or aragonitic layers. In vitro substrates were assembled from β-chitin, silk fibroin, and aspartic acid rich soluble macromolecules from a specific mineral layer.[113] It was demonstrated that the mineral originally associated with the proteins also formed in the in vitro system. However, the ability to form aragonite was only found in the presence of all three components of the system, indicating that only the presence of the soluble macromolecules does not suffice to specifically nucleate this polymorph and that the extracellular matrix also must play a role in this.

It is frequently found that the formation of the crystalline forms of calcium carbonate in nature is preceded by an amorphous precursor phase.[114−118] It is thought that this pathway allows the efficient transport of ions to the mineralization site and the formation of skeletal materials in complex shapes.[119,120] This indirect route to the different crystalline phases involves several distinct processes: transient stabilization of the amorphous phase, subsequent transformation into a stable crystalline phase, polymorph selection, and crystal orientation.[121] It has been suggested that polymorph selection may occur at the early states of the transformation, based on the observation that the transient amorphous phase already has the nascent order of the polymorph into which it will transform.[122,123]

The importance of the stabilization of the different polytypes lies in their different mechanical properties as well as in the differences in solubility characteristics they display. It is obvious that this has major consequences not only for the fabrication of calcium carbonate-based materials but also for the control of many processes where calcium carbonate precipitation is a main issue, e.g. in the form of scale formation.[124] Hence, this nicely underlines the need to look at biology and learn from it a strategy for controlling calcium carbonate polymorphism. In this section, we will discuss how additives and surfaces also in a synthetic environment allow the stabilization of the different forms of calcium carbonate that are less stable than the thermodynamic product, calcite. In order of increasing stability, these are the following: amorphous calcium carbonate, vaterite, and aragonite.

As calcite is the thermodynamically most stable form of calcium carbonate at ambient temperature and pressure, most

assays will have this polymorph as the final product.[125,126] Nevertheless, in many cases, its formation will proceed along a pathway in which one or more of the other forms is an intermediate.[127] There are several principle approaches to the formation and stabilization of one of the less stable forms of calcium carbonate. In general, these involve the modification of the activation energy barriers of nucleation, growth, and phase transformation. We will discuss this here along two main approaches: The first (section 4.1) is preventing the development of the more stable crystalline states, thus allowing the development of the less stable polymorphic forms. A second (section 4.2), principally different approach that has been mainly demonstrated for vaterite and aragonite, is the stabilization of specific crystal planes of these two polymorphs such that the transformation into calcite is prevented or at least delayed. This latter approach is the dominant route encountered for the specific nucleation of these less stable phases on surfaces and is best demonstrated in the absence of other additives.

Despite the fact that already for decades there has been an enormous activity in this area,[128] we will find that the factors which determine polymorph selection are still poorly understood.

4.1. Polymorph Control in Solution

In the subsections below, we will describe how the use of additives can inhibit the development of the energetically most stable product to obtain one of the other polymorphs.[129] For the formation of ACC, it implies that the nucleus must be stabilized before it has the chance to transform to the crystalline state. This can mean keeping its size below the critical size for the formation of the crystalline polymorphs or preventing its dehydration, as ACC must loose its included water for crystallization. Vaterite is also stabilized by the formation of nanocrystalline particles that are below the critical size for calcite formation. Similar to ACC, vaterite can also be stabilized by shielding it from the aqueous phase; in this case, however, the function of the additive is to prevent the dissolution−reprecipitation step necessary for its conversion to calcite. For aragonite, generally the above routes do not really apply, as its conversion into calcite under ambient conditions is so slow that aragonite can considered to be stable under these circumstances. However, we will see that a common approach for all thermodynamic less stable phases can be the inhibition of calcite growth by blocking specific steps and kinks on the surface of small crystallites. Nevertheless, for ACC and vaterite, this approach generally will only lead to a temporary predominance of this phase when not accompanied by an additional stabilization that prevents phase transformation into calcite in the long run.

4.1.1. Stabilizing ACC

Different methods have been reported for the generation of amorphous calcium carbonate; these include the bubbling of CO_2 through a solution of $CaCl_2$[130,131] or $Ca(OH)_2$,[132] the fast mixing of saturated solutions of calcium salts and carbonates,[133−136] the hydrolysis of dimethyl carbonate in a $CaCl_2$ solution,[137] the low temperature diffusion of calcium and carbonate ions,[138] the addition of ammonium carbonate to an ethanolic solution of $CaCl_2$,[139] and the diffusion of ammonium carbonate into a $CaCl_2$ solution in the presence of hydroxylated surfaces.[140−142] However, in none of these cases did the ACC show extended stability while still in contact with an aqueous phase unless additives, e.g. in the form of polycarboxylates,[140] polyphosphates,[132,143] or alcohols,[137,139] were present.

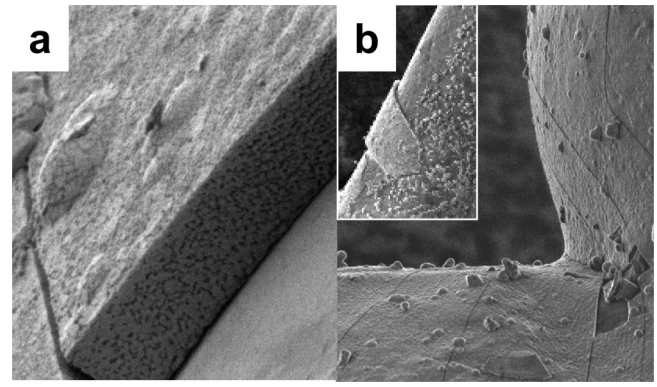

Figure 21. Scanning electron micrographs of the $CaCO_3$ films, 2 days after preparation, grown in the presence of 2.5×10^{-3} wt % DNA on (a) glass and (b) a poly(caprolactone)-based scaffold. Part (a) shows a 2 μm thick ACC film, and part (b) shows details highlighting the ability of the inorganic coating to follow the contours of the scaffold. The inset in part (b) shows lower magnification of a different area of the scaffold. (From ref 145 (http://dx.doi.org/10.1039/b710277a). Copyright 2007. Reproduced with permission of The Royal Society of Chemistry).

The amorphous phase can be effectively stabilized by the use of inorganic ions such as Mg^{2+} and phosphate but much more effectively by polymeric additives such as polyaspartate, polyglutamates, polyacrylate and DNA (Figure 21).[5,144,145] In particular, the polymeric additives have been explored to form thin films of calcium carbonate that slowly transform into one of the crystalline polymorphs depending on the type and quantity of the additive used.[146] In addition, the formation of the amorphous phase in the presence of magnesium has been used to effectively generate high magnesium calcite content (Mg^{2+} content > 35%). The precipitation of calcite with such high magnesium contents strongly contrasts the usual products of the precipitation of calcium carbonate in the presence of magnesium ions, which normally yields aragonite, as well as calcite with much lower (<15%) magnesium content.

Many kinds of low molecular weight organic ions that suppress crystal growth may be used to (temporarily) stabilize the amorphous phase. In particular, phosphates and phosphonates show a very strong inhibitor effect.[147] Sawada and co-workers investigated the effect of EDTMP [ethylenediaminetetrakis(methylenephosphonic acid)] (**15**) on the formation and transformation of calcium carbonate (Figure 22).[148] Various concentrations of EDTMP were added just after the mixing of calcium and carbonate ion solutions. Although the addition of EDTMP does not change the mechanism of the transformation, it strong1y retards the transformation of calcium carbonate polymorphs. The addition of 10^{-6} M EDTMP does not affect the conversion of ACC but slows down the transformation of vaterite to calcite such that it still is not complete after 3 days (Figure 22b). In the presence of 10^{-5} M EDTMP, the conversion of vaterite to calcite is stopped completely (Figure 22c). In the presence of more than 10^{-4} M EDTMP, the amorphous calcium carbonate (ACC) shows no more change and crystalline polymorphs are never formed (Figure 22d). The ACC solids thus obtained are quite stable and show no transformation to crystalline calcium carbonates after at least several days even if they are dried at 100 °C after filtration.

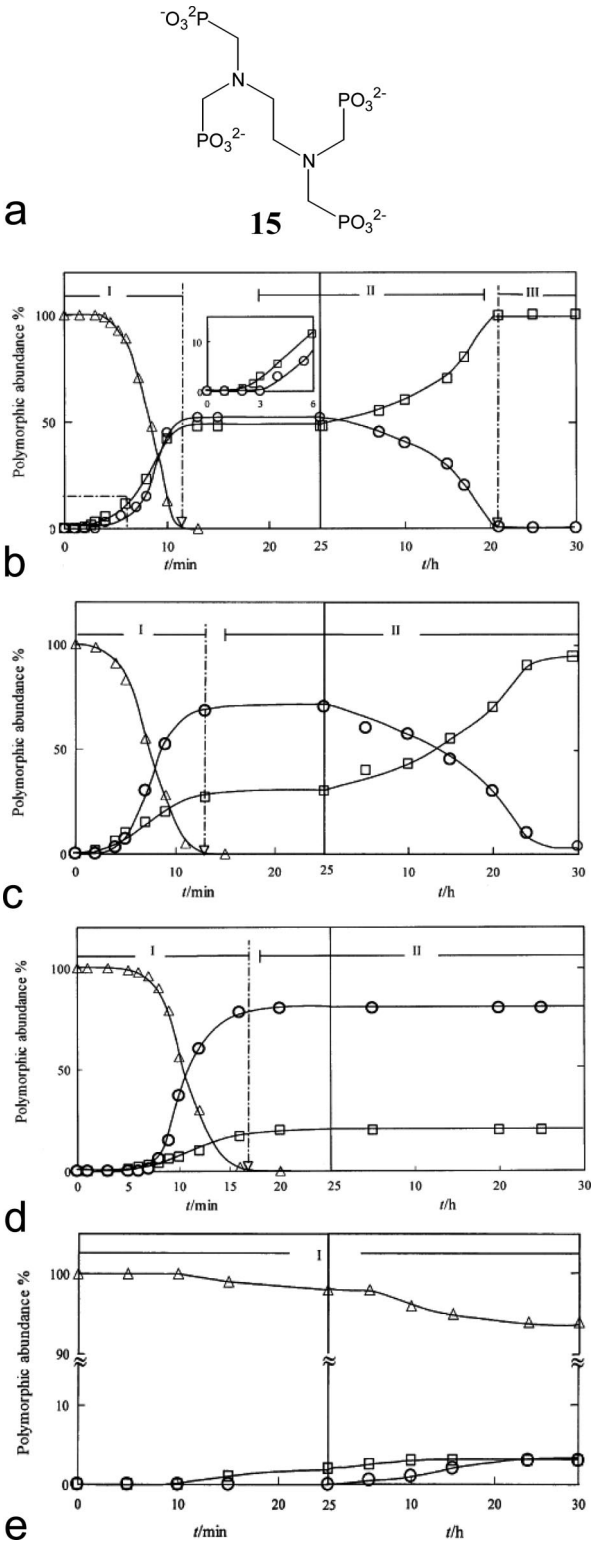

Figure 22. The change in polymorphic abundance of the precipitate in the bulk solution. (△) ACC, (○) vaterite, and (□) calcite under the influence of EDTMP [ethylenediaminetetrakis(methylenephosphonic acid)] (**15**). (a) The molecular structure of EDTMP **15**. (b) Effect of 10^{-6} M EDTMP on the change in polymorphic abundance of the precipitate. (c) Effect of 10^{-5} M EDTMP on the change in polymorphic abundance of the precipitate. (d) Effect of 10^{-4} M EDTMP on the change in polymorphic abundance of the precipitate. (Reprinted from ref 127, Copyright 2003, with permission from Elsevier B.V.)

Poly(propylene imine) dendrimers **16** modified with long aliphatic chains display amphiphilic behavior (Figure 23a). In aqueous dispersion, they adopt a "comet-like" conformation in which the hydrophilic core is in contact with water while the alkyl chains are oriented away from the aqueous phase, resulting in the formation of multilamellar, vesicular aggregates. The outer surface of these globular aggregates can be modified through the addition of **16** to dilute aqueous solutions containing octadecylamine; ODA (Figure 23b).[149,150] It was found that rigid polyhedral aggregates with a narrow size distribution resulted from the interaction of **16** with this amphiphilic molecule (ODA, Figure 23c).

In a supersaturated solution of $Ca(HCO_3)_2$, these aggregates became calcified, initially retaining their polyhedral shape (Figure 23d), before spherical ACC particles were obtained (Figure 23e).[149] In time, {10·4} rhombohedral calcite crystals developed by growing around the ACC particles (Figure 23f), suggesting that the ACC spheres play a role in the nucleation of the crystalline form. Aggregates prepared of **16** alone also induced the formation of ACC spheres. However, in this case, the amount of ACC was reduced and the transformation to calcite was more rapid than observed previously with the ODA-modified aggregates: after 24 h, 80% of the sample had been converted to calcite compared to 16% in the case of the **16**/ODA aggregates. The role of the template in stabilizing the amorphous phase is emphasized by the observation that, after 14 days, 20% of the calcium carbonate was still present in the form of spherical ACC. A main common feature of those two dendrimer-based aggregates was found to be their very high rigidity. The rigidity of the aggregates provides a charged, disordered, and persisting nucleating surface that probably at least temporarily stabilizes amorphous calcium carbonate against transformation into one of the crystalline polymorphs. The low charge density of the aggregates obtained from pure **16** and from **16**/ODA ($\sim +0.5$ per surface amino group) most probably also relates to the inhibition of the nucleation and growth of the crystalline polymorphs. Further growth of the particles is thought to involve incorporation of the dendrimer inside the particles, which both stabilizes the precipitated ACC and at the same time depletes the system from this stabilizing agent. This explains the later formation of calcite without dissolution of the amorphous phase, leading to the encased ACC particles.

Recently, Cölfen et al. reported the stabilization of amorphous calcium carbonate using inositol hexakis phosphate (**17**) (Figure 24).[151] The addition of this small polar molecule leads to the formation of hollow spheres of ACC which contained 5% of **17** as well as 15% of water. Interestingly, this is the same amount of water that is found in biogenic stable ACC, and indeed, the ACC spheres were found to be stable for more than 3 months. Increasing the concentration of the additive leads to smaller sized hollow spheres, which suggests that **17** acts as an inhibitor for the aggregation of the primary particles. Moreover, studies of the early stages show that initially small (<100 nm) but massive particles are formed that seem to transform into hollow spheres by a dissolution−reprecipitation mechanism. It was proposed that the primary particles consisted of hydrated ACC which lose their bound water, leaving a shell of anhydrous ACC. To our knowledge, the resulting hollow particles currently hold the record of being the most stable form of synthetic ACC produced to date.

4.1.2. Stabilizing Vaterite and Aragonite Using Additives

By the precipitation of calcium carbonate in the presence of (bio)polymers[7,14,15,152−157] as well as low molecular

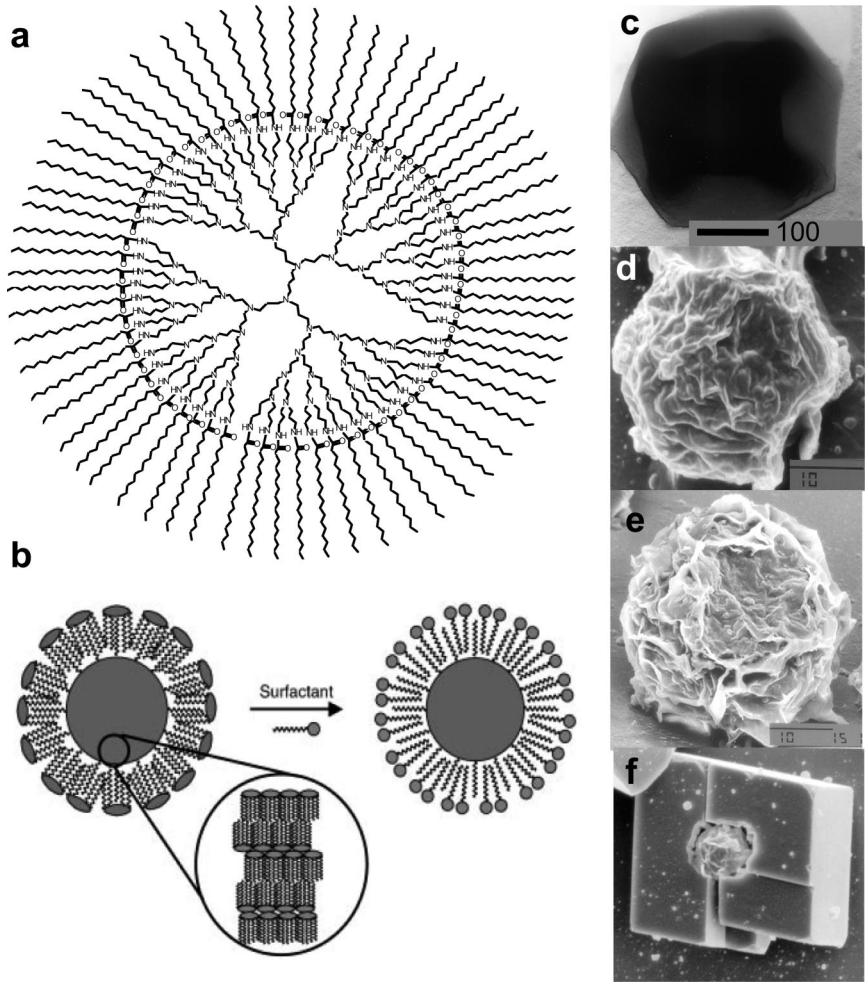

Figure 23. (a) Molecular structure of fifth-generation dendimer **16** modified with palmitate [-CO-$(CH_2)_{14}$-CH_3] end groups. (b) Schematic representation of the conformation of **16** and its aggregates in water and their complexation with a single chain surfactant. (c) TEM image of an aggregate of **16** and octadecyl amine (ODA). (d−f) SEM images of calcium carbonate grown in the presence of **16/ODA**: (d) amorphous particle after 1 day; (e) amorphous particle after 4 days; (f) amorphous particle overgrown with calcite after 14 days. (Reproduced with permission from ref 150. Copyright 2002 Wiley-VCH Verlag GmbH & Co. KGaA, Weinheim.)

weight additives,[126,147] many authors have managed to favor the nucleation of the less stable polymorphs vaterite and aragonite.[158] As the formation of aragonite in general requires the presence of magnesium ions or nonambient conditions, only a few accounts exist on the stabilization of this polymorph by the action of soluble additives only.[152,159,160] In contrast, studies reporting the formation of vaterite are abundant. For example, in view of their biological importance, many amino acids have been used as modification agents in mineralization experiments. Such studies have been reported for glycine,[161−165] L-alanine,[161−163,165] D-alanin,e[165] L-valine,[161,165] D-valine,[165] L-leucine,[161,166] L-serine,[161] L-threonine,[161] L-asparagine,[161] L-glutamine,[161] L-glutamic acid,[161,167,168] L-arginine,[161] L-cysteine,[169] L-tyrosine,[165,169] L-aspartic acid,[161,164,170,171] D-aspartic acid,[164] DL-aspartic acid,[169] L-lysine,[161,162,169] L-phenylalanine,[168] and L-histidine.[168]

However, to understand the results of these studies, it is very important to emphasize that the stabilization of vaterite is very dependent on the kinetics of the specific assay used. As a consequence, it is very difficult to compare the results presented in the different reports in which different precipitation methods have been used. A clear example of this is given in the following. While Manoli and Dalas have reported that the use of glutamic acid as an additive leads to the nucleation of vaterite as the only product, Kai et al. only find a small amount of vaterite (∼10%) alongside a majority of calcite crystals. The latter group also finds a similarly small vaterite inducing capacity for lysine, whereas Xie et al. report the formation of >95% vaterite for the same additive.

Also, the use of surfactants has been extensively explored in controlling the crystallization of calcium carbonate. The formation of vaterite has been reported for cationic surfactants (CTAB, hexadecyl trimethyl ammonium bromide),[172] for anionic surfactants [SDBS (sodium dodecylbenzenesulfonate)[173,174] and SDS (sodium dodecyl sulfate)],[172,175] as well as for nonionic surfactants [poly(oxyethylene) nonyl phenyl ether][172] and mixtures (calcium dodecyl sulfate/pentanol).[176] SDS has been the most investigated surfactant; however, also for this molecule the vaterite stabilizing activity has been demonstrated to be highly depending on the specific conditions used.[172,175,177−179] In addition, several other additives in solution have been demonstrated to lead to the formation of vaterite; these include alcohols,[180,181] polycarboxylates,[182−184] (poly)phosphates,[127,185] (poly)sulfonates,[184,186,187] acidic poly(amino acids),[188] carbon nanotubes (CNT-COOH),[183] and other functionalized carbon nanomaterials.[181] Also for these compounds a similar variety of mineralization methods has been used, and therefore, it is not possible to compare the results directly.

Nevertheless, several of these studies revealed some important clues as to the mechanism of these modifications:

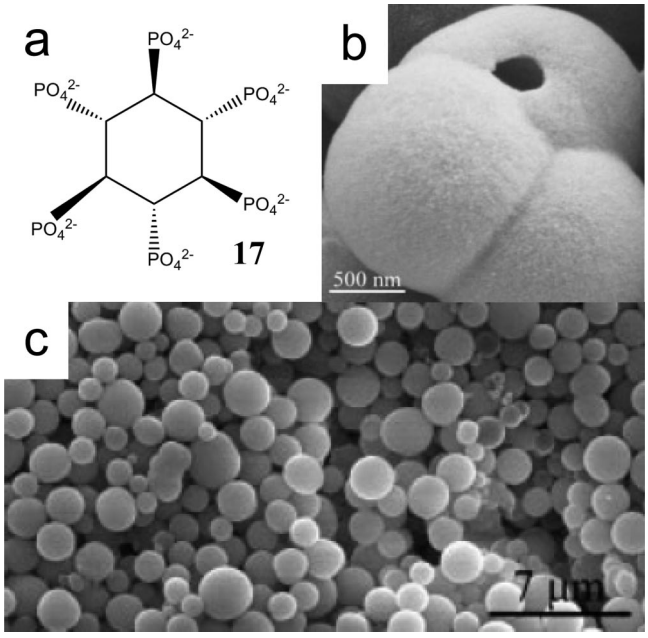

Figure 24. (a) Chemical structure of phytic acid (hexakis inositol phosphate) (**17**). (b, c) SEM images of ACC particles formed in the presence of **17**. Part (b) shows the hollow nature of the particles. (Reproduced with permission from ref 151. Copyright 2005 Wiley-VCH Verlag GmbH & Co. KGaA, Weinheim.)

Hou and Feng produced vaterite through the addition of glycine to the reaction mixture.[159] They proposed that this process is likely to be due to the inhibition of the calcite polymorph and showed by AFM that glycine blocked the growth of calcite by adhering to the (441) or (48$\bar{1}$) sites. This is in line with previous experiments by De Yoreo et al. in which the growth calcite was studied in the presence of aspartic acid. Also, in this work it was demonstrated that the binding of the amino acid to the step edges on {10·4} calcite depended strongly on its stereochemistry (see also section 5.1.4).[166] Related to this, some rather intriguing examples of polymorph switching were reported by the group of Tremel. They demonstrated that polymorph selectivity can be controlled by the stereochemistry of the amino acids used.[165] For example, L-alanine gave predominantly vaterite, and its D-enantiomer yields exclusively calcite. Similarly, L-valine leads to the formation of aragonite while the D-isomer gives only calcite. The origin of these remarkable observations is not yet fully understood.

A different mechanism was proposed by Tong et al., who pointed to the fact that vaterite particles formed in the presence of aspartic acid are composed from very small nanocrystallites (3−150 nm) that must be stabilized by the additive used. Based on quartz crystal microbalance measurements and TEM analysis, the authors proposed a mechanism in which the aspartic acid leads to the formation of a local high supersaturation and hence to a high nucleation density of these small vaterite particles.[170] It seems likely that the presence of the aspartic acid molecules prevents the fusion of these particles, which inhibits their conversion to calcite. In an extensive study using 12 different amino acids, Kai et al. were able to relate the amount of vaterite formed to the amount of the amino acid included in the vaterite particles. Also in this case, the dimensions and morphology of the particles suggest that the vaterite forming amino acids (Gly, Ser, Thr, Asn, and Asp) inhibit the growth of the microcrystals and thereby their recrystallization to calcite. From semiempirical molecular orbital calculations, they propose that the binding of the acid groups to the calcium ions is directly responsible for the observed effects and that the included amino acids may act as pinning centers preventing the transformation of the vaterite to the more stable calcitic polymorph.

The latter route is related to the work of Cölfen and co-workers, who have highlighted the formation of crystalline materials though a nonclassical pathway,[15] which in several cases was demonstrated to lead to vaterite structures (Figure 25).[189] This is exemplified by the formation of uniform hexagonal platelets of vaterite through the action of an *N*-methylammonium derivative of cellulose **18**. In the early stages of the reaction, nearly spherical nanoparticles were present that in time transformed into a polycrystalline product in which ACC and vaterite coexisted before complete conversion into the crystalline form was achieved. Through aggregation mediated crystallization of the nanoparticles, hexagonally shaped mesocrystals were formed.

4.1.3. Favoring Calcite over Aragonite

In addition, several authors have investigated the formation of calcium carbonate in the presence of additives under conditions that normally favor the formation of aragonite. Wada et al. investigated the effect of a variety of small acidic molecules in the presence of magnesium ions.[190] In this study, citric acid (**19**), maleic acid (**20**), tartaric acid (**21**), succinic acid (**22**), malonic acid (**23**), malic acid (**24**), acrylic acid (**25**), aspartic acid (**26**), glutamic acid (**27**), and furmaric acid (**28**) were used to obtain calcite formation under high Mg conditions (Mg/Ca = 1:1) that normally favor aragonite formation. The suggested mechanism involves the formation of small aragonitic nuclei that are slowed down in growth and hence convert into the more stable calcite. In a related study, Westin and Rasmuson investigated the effect of several low molecular weight polyacids on the nucleation and growth of calcite and aragonite (see Figures 26 and 27).[191,192] Crystal formation was studied by seeding a supersaturated solution with either calcite or aragonite crystals. Clear differences were found between the growth retarding capacities of the different compounds for calcite and aragonite. In agreement with the mechanism proposed by Wada et al., also in this case in general the inhibition of growth was stronger for aragonite than for calcite.

4.1.4. Polymorph Selection by Controlling System Kinetics

A systematic approach to polymorph control was adapted by Naka and co-workers, who showed elegantly that it is possible to control polymorphism by interfering with reaction kinetics during the mineralization process.[197] For this they used the double jet assay, which produces an extreme supersaturation locally by mixing Ca^{2+} and CO_3^{2-}, leading to instantaneous and homogeneous nucleation. By vigorous stirring, the nuclei are subsequently transferred into the dilute solution in which they are allowed to further develop. This technique perfectly allows one to study the effect of additives at already existing nuclei. The introduction of PAA was used to alter the kinetics of calcium carbonate formation at different stages in the reaction. As discussed above, the presence of PAA inhibits crystallization, in most cases leading to the formation of amorphous calcium carbonate that only later transforms into one of the crystalline polymorphs.[5] Indeed, when PAA was added at the beginning of the reaction, only small amounts of precipitate were ob-

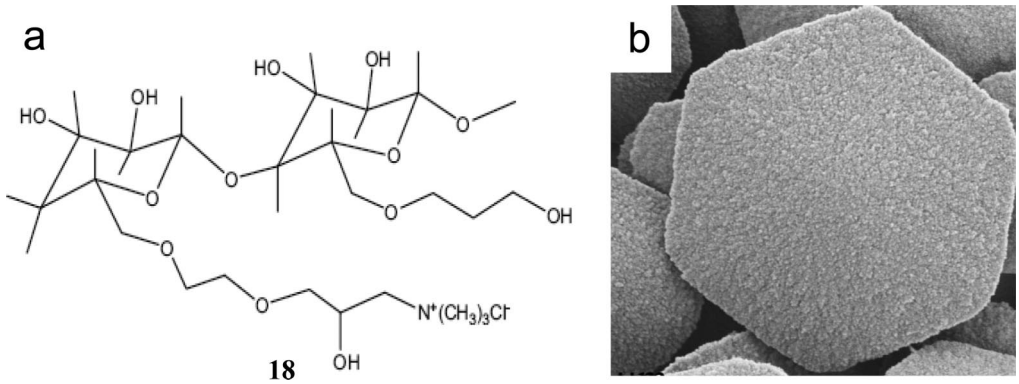

Figure 25. (a) Molecular structure of a monomer of an *N*-trimethylammonium derivative of hydroxyethyl cellulose **18** and (b) SEM image of the hexagonal vaterite particles formed in its presence. (Reproduced with permission from ref 189. Copyright 2006 Wiley-VCH Verlag GmbH & Co. KGaA, Weinheim.)

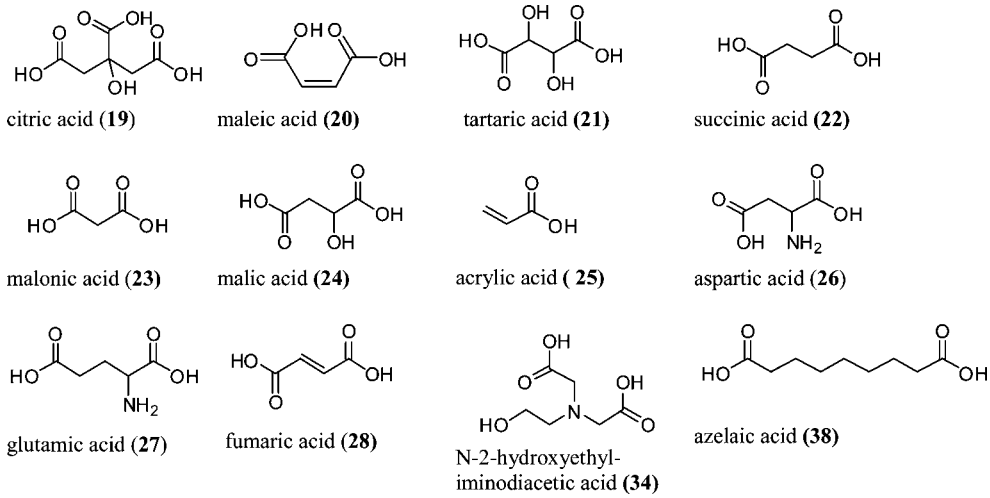

Figure 26. Chemical structures of additives.

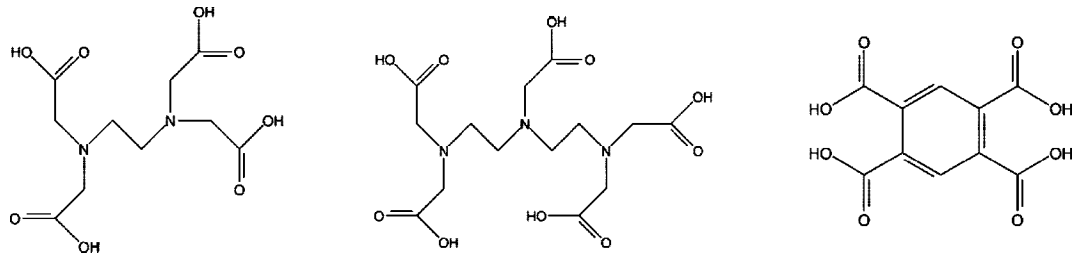

Figure 27. Molecular structure of DTPA (left), EDTA (middle), and PMA (right) used by Westin et al. (Reprinted from ref 191, Copyright 2005, with permission from Elsevier Inc.)

tained.[193] However, when the PAA was added after 20 min, small amounts of vaterite were observed.

In a second series of experiments, these authors used a so-called latent inhibitor approach (Figure 28).[194,195] In this approach, a reaction was performed at 30 °C in which sodium acrylate was added to the double jet system and polymerized after a certain amount of time to produce PAA that strongly interacts with the mineral formed.[196] The monomer did not interfere with crystal formation, as was demonstrated in control experiments. Also, when the acrylate polymerization was started after the reaction had proceeded for 20 min, standard rhombohedral calcite was isolated after 1 day. However, when the reaction was started after 3 min, vaterite was the predominant product (63%). When the polymerization was started after 1 min, aragonite became the main product. This implies that when present in the very early stages, the polymer either induces the formation of aragonite or stabilizes the aragonite crystals that have formed by homogeneous nucleation. Clearly, vaterite formed when the reaction was allowed to proceed for 3 min without the presence of the polymer. Also, for this phase it is not yet clear whether it forms by stabilization of homogenously nucleated crystallites or by polymer induced nucleation. Nevertheless, the above results show that the interference with the reaction kinetics can lead to the formation of the less stable polymorphs and that organic additives can prevent them from transforming into the more stable calcite.

With the same assay, this group also studied the ability of carboxy-terminated poly(amido amine) (PAmAm) dendrimers **29** to stabilize vaterite (Figure 29).[197] When different concentrations and different generations of dendrimers were added at the beginning of the experiment, vaterite was produced in all cases. Interestingly, when the authors used a delayed addition, i.e. when the dendrimers were added at a fixed time after the mineralization has started, distinct differences were observed. For the lower generation den-

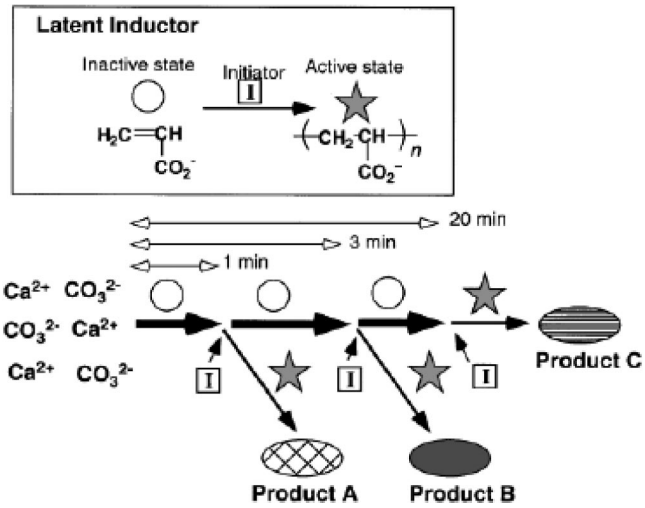

Figure 28. Schematic depiction for the control of crystal polymorph growth by a latent inductor product. A, B, and C correspond to aragonite, vaterite, and calcite, respectively. (From ref 194 (http://dx.doi.org/10.1039/b004649n). Copyright 2000. Reproduced by permission of The Royal Society of Chemistry.)

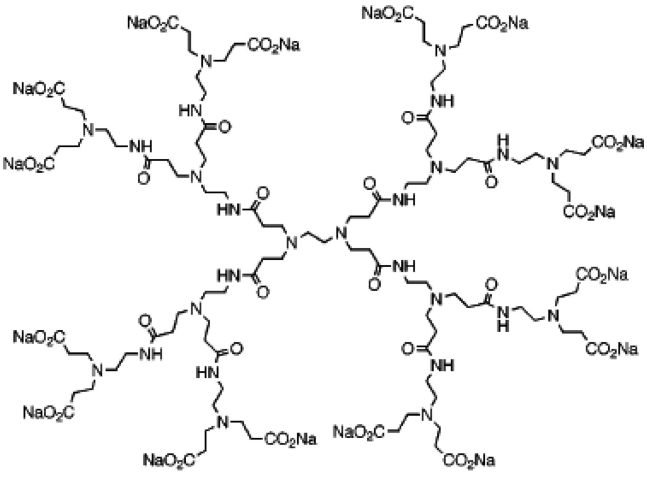

29

Figure 29. PAMAM dendrimer ($G = 1.5$) **29**. (From ref 200 (http://dx.doi.org/10.1039/a905618a). Copyright 1999. Reproduced by permission of The Royal Society of Chemistry.)

drimer ($G = 1.5$), added after 3 min, increasing amounts of calcite were observed whereas for the higher generation dendrimer ($G = 3.5$) all concentrations only produced vaterite. Moreover, the vaterite particle size increased with decreasing dendrimer concentration as well as with decreasing dendrimer generation. These results indicate that the binding of the dendrimer to the inorganic phase controls the stabilization of the vaterite polymorph but also the aggregation of the primary vaterite nanoparticles. It is important to note that this can be controlled not only by concentration but also by the dendrimer generation, as it was demonstrated that the higher generations were more effective than the lower ones at the same end group/calcium ratios. As the delay time increases, the amount of calcite increases, as does the size of the vaterite particles, which indicates that the interaction of the dendrimer with the primary nanoparticles prevents the formation of calcite. Most probably, the strong adhesion of the dendrimer molecules to the vaterite surface affects the subsequent dissolution−reprecipitation mechanism delaying the conversion to the thermodynamically more stable calcite. Indeed, the amount of dendrimer incorporated in the inorganic phase was found to be in agreement with the amount of dendrimers that adhered to these nanoparticles.[7]

Interestingly, control experiments show that, without the presence of the dendrimers, after 3 min, calcite is formed together with vaterite. Still, the addition of the higher concentrations of dendrimer even after 60 min leads exclusively to the formation of vaterite. This suggests that the addition of dendrimers reverses the formation of calcite up to a certain crystal size. Indeed, this reversal is no longer observed after a delay time of 120 min. A similar observation of vaterite formation was reported for the addition of PAA after 60 min to the same assay[198] but not for the generation of the PAA by in situ polymerization.

Surprisingly, when the same amounts of dendrimers were added to a carbonate diffusion assay, only a partial stabilization of vaterite was achieved.[199,200] In addition, although these particles contained more than 7% of the dendrimers, they transformed into calcite within 4 days, whereas the vaterite prepared by the double jet method was stable for more than 7 days. These results may be explained by lowering of the calcium concentration through the formation of dendrimer−calcium complexes in the diffusion-based method. This lowers the driving force for the formation of vaterite. In addition, the observed transformation of vaterite to calcite, which is a solution mediated process, suggests that in this case the dendrimers are less able to shield the vaterite from the aqueous phase.

4.2. Surfaces Promoting the Formation of the Less Stable Polymorphs

In section 3 we have seen that the nucleation of calcium carbonate on organic surfaces can stabilize the nonequilibrium faces of calcite by specific interactions of the functional groups with the ions in the crystal surface. Here, we will discuss how these interactions in several cases are effective in lowering the kinetic barriers such that the thermodynamically less stable polymorphs become accessible. It should be noted here that in this situation only one face of the crystal is shielded from the aqueous environment and that the other faces remain in contact with the mineralization solution. This means that transformation to the more stable polymorphs generally is only temporarily inhibited by the energy gained through the stabilization of the nucleating crystal face.

4.2.1. Nucleation of the Less Stable Polymorphs on Monolayers

Somewhat surprisingly, the first experiments, performed using Langmuir monolayers on a supersaturated $Ca(HCO_3)_2$ solution, yielded the metastable vaterite instead of the thermodynamically more stable calcite.[10] Although initially this observation was attributed to the use of lower supersaturation levels ($[Ca^{2+}] = 4.5$ mM) in the subphase, later experiments showed that in fact is was the outgassing rate of CO_2 that induced the formation of the kinetic polymorph.[79,100] It was clear that no epitaxial relation was possible between the observed (00•1) vaterite and the carboxylate groups in the monolayer. Instead, a model was proposed in which the carboxylate groups of the monolayer interacted with the Stern layer, forming an auxiliary layer of ions that through stereochemical complementarity lead to the stabilization of the (00•1) face. In later synchrotron X-ray experiments, Dimasi and co-workers showed that the nucleation of vaterite (00•1) indeed cannot be a strict

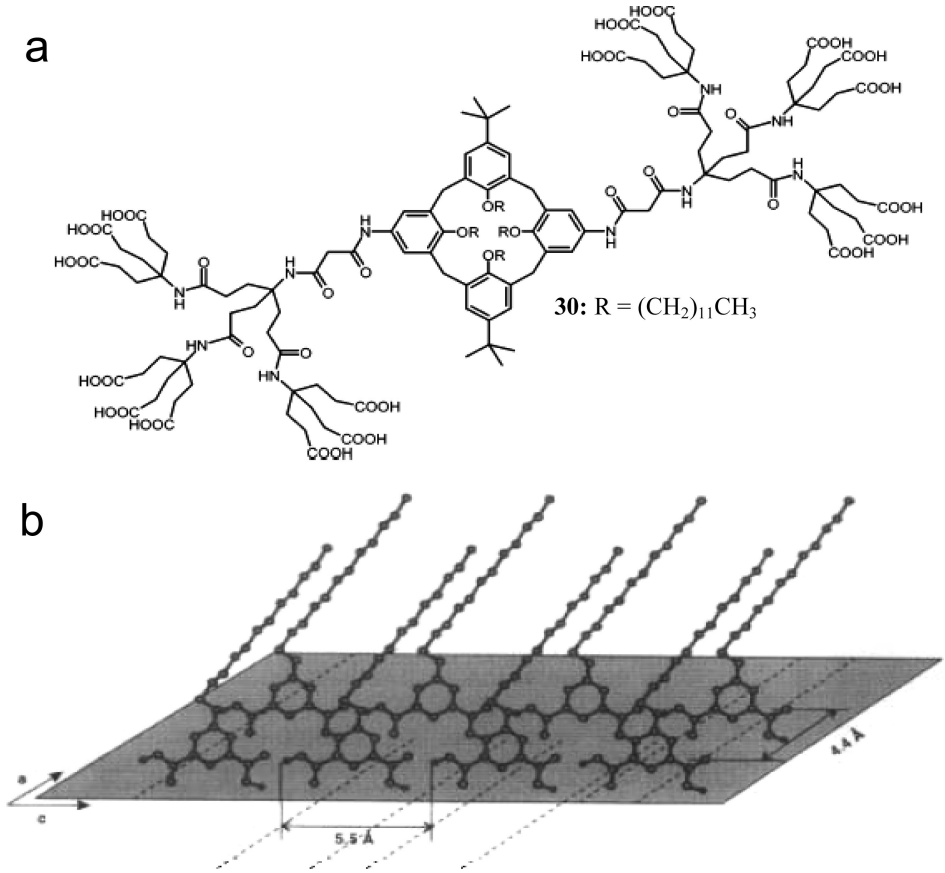

Figure 30. (a) Molecular structure of **30** (Reprinted with permission from ref 201. Copyright 2006 American Chemical Society.) (b) Schematic representation of the spatial relationship between a periodic monolayer of 5-hexadeyloxy isophthalic acid (**31**) and the ac-plane of aragonite. (Reproduced with permission from ref 211. Copyright 1997 Wiley-VCH Verlag GmbH & Co. KGaA, Weinheim.)

templating effect, as different periodicities were observed for the monolayer and the nucleating crystals.[79] In addition, it was shown that (as already mentioned above) only one calcium ion was bound under approximately four to eight stearic acid molecules but also that in the early stages of the reaction more than one orientation of vaterite was present.

Vaterite formation was also demonstrated by Volkmer et al. under a monolayer of an amphihilic calix[4]arene with dendritic head groups carrying 18 carboxylic acid moieties (**30**, Figure 30).[201] From comparison with other systems, it was proposed that the higher charge density of these monolayers is the dominant factor in triggering the formation of vaterite (see below). Nevertheless, it is interesting to note that the dendritic structure of the calixarene head group not only increases the charge density under the monolayer but also leads to the presentation of the carboxylate groups in a disordered manner.

That different degrees of organizations in a monolayer can lead to polymorph switching was demonstrated by the reorganization of the monolayer of leucine derivative **11d**.[108] Compared to its homologues (see section 3.4), this molecule has a larger side group and therefore is believed to rearrange more slowly into its final configuration in the monolayer. At earlier time points (i.e., 15 min), predominantly (00•1) aragonite formation is observed, whereas, in later stages of the reaction, domains with predominantly aragonite coexist with domains that produce predominantly calcite. The active compression of the monolayer resulted in a molecular organization that facilitates the nucleation of calcite, of which 70% consists of indented (10•0) oriented crystals, indicating that this calcite polymorph indeed nucleated under the more condensed domains. A similar phenomenon was also observed for monolayers of a glycine-based diacetylene surfactant [HOOC-CH_2-NH-CO-$(CH_2)_8$-$C_{(11.0)}$C-$C_{(11.0)}$C-(CH_2)-CH_3].[202] Using Brewster angle microscopy, it was found that these films induce the formation of vaterite in the condensed regions (π = 20−25 mN/m) and calcite in the coexisting liquid expanded and gas analogous regions (π = 0−5 mN/m).

Tremel et al.[203] and Lee et al.[204] reported vaterite formation in the presence of SAMs with a lower degree of organization. A similar effect was observed for the organization of HS-$(CH_2)_{15}$-COOH monolayers on gold. When these monolayers are formed on gold(111) surfaces, they template the formation of (01•5) calcite.[205] In contrast, when they are formed on gold films prepared by evaporation on Cr-coated glass (which generally have a higher surface roughness), they induce the formation of vaterite.[206]

This issue was investigated in more detail by the group of Tremel, who suggested that the disorder implicated by the roughness of the surface is an important issue in the induction of the nucleation of different polymorphs of $CaCO_3$.[207] They showed that, upon further increasing the roughness of the surface by using a poorly ordered monolayer of $HS(CH_2)_3SO_3H$, even the formation of aragonite was observed. Following from these results, monolayers of dithiols were prepared.[208] These sticky films allowed gold colloids to adhere, thereby creating very rough surfaces. Application of these roughened surfaces in a calcium carbonate crystallization assay indeed yielded aragonite as the predominant phase. Also, the increased roughness induced by the adsorption of hyperbranched polyethylene

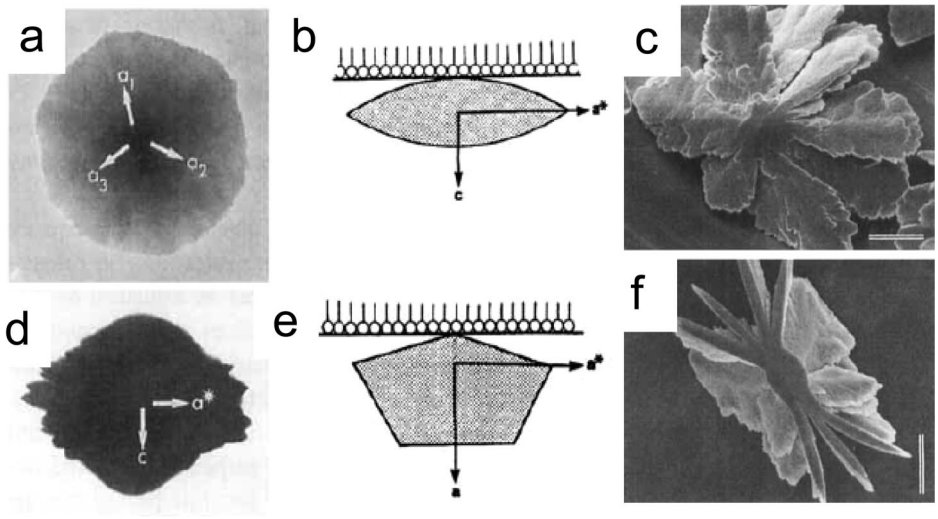

Figure 31. Crystallographic alignment of early crystals of vaterite grown under octadecyl amine (OA) monolayers. (a−c) [00•1] oriented vaterite disk viewed from (a−c) above the monolayer [(a) TEM, (c) SEM, bar = 10 μm]. (b) Schematic representation of the side view ([11•0] direction). (d−f) [11•0] oriented vaterite disk viewed from (d−f) above the monolayer: (d) TEM image; (f) SEM image, bar = 10 μm; (e) schematic representation of the side view ([11.0] direction). (Reproduced with permission from ref 70. Copyright 1990 Wiley-VCH Verlag GmbH & Co. KGaA, Weinheim.)

glycol to a methyl-terminated SAM drastically changed the results from the calcium carbonate mineralization assay.[209] Whereas the unmodified methyl-terminated SAM produced a mixture of polymorphs with calcite as the predominant product, the hyperbranched PEG-covered surface almost exclusively initiated the formation of aragonite. Based on reference experiments, it was concluded that both the presence of hydroxyl groups and a high surface roughness were required for the obtained results. Moreover, when calcium carbonate was grown on carboxylated SAMs in the presence of polyacrylate, nanowires were formed.[210] This phenomenon was related to the possibility of calcium−polymer complexes forming a surface attached bundle that would function as a templating structure for the assembly of the observed amorphous nanoparticles.

It is important to note, however, that also polymorph switching has been related to geometrical matching between the template and the nucleating crystal plane. Litvin et al. related the finding of [010] oriented aragonite under monolayers of 5-hexadecyloxy isophthalic acid (**31**) to the spacings of the head groups of the surfactant (Figure 30).[211] They presented a model in which the isophthalic acid derived molecules formed a rectangular array held together by hydrogen bonds that had dimensions similar to those of the (010) face of aragonite. The authors also compared the structure of the surfactant molecules to the β-sheet structures that stabilize specific crystal faces of aragonite. In a related experiment, it was demonstrated that different orientations of aragonite could be obtained under Langmuir monolayers in the presence of Mg^{2+} ions (Figure 5, section 3). Where eicosanoic acid (arachidic acid, $CH_3(CH_2)_{18}COOH$) stabilizes the (100) plane of aragonite, *n*-eicosyl sulfate and *n*-eicosyl phosphate stabilize the (001) plane. In all three cases, the template functional groups and the carbonate ions in the stabilized crystal planes show stereochemical complementarity, which is most likely related to the specificity of the observed effects.[71]

Tremel and co-workers demonstrated that this principle can be used to selectively switch beween calcite and aragonite also on hydrophobic SAMs.[212] For this the authors used alkanethiols which form a hexagonally packed structure, alongside an anthracene-modified alkanedithiol which packs in a centered rectangular lattice. At 45 °C the alkanethiols give rise to the nucleation of the (00•1) plane of calcite, whereas the anthracene-modified compound stabilizes (100) aragonite. The authors relate these observations to the similarity in the surface structure and symmetry of the template and mineral. The hexagonal structure of the alkanethiol has a near epitaxial match with the mineral surface, while the rectangular structure of the anthracene derivative fits the lattice distances of the (100) face of aragonite.

Mann et al. demonstrated the formation of a mixture of (11•0) and (00•1) vaterite under a monolayer of octadecyl amine (Figure 31).[60] This paper for the first time demonstrated that the formation of calcium carbonate did not depend on the direct binding of calcium ions. The authors suggested that the ammonium groups could preorganize the carbonate ions that subsequently may adapt to the specific requirements of the (11•0) and (00•1) faces. When these experiments were carried out with poly(α,β-aspartic acid) present in the aqueous subphase, still vaterite was formed; however, in this case, the crystals were irregular in shape and did not have a preferred orientation.[213] It is important to note that, in both the presence and absence of poly(α,β-aspartic acid) and in contrast to monolayers of carboxylic acids, the effectiveness of the cationic monolayers increased with their compression to a lower surface area, giving a more densely packed arrangement.

Vaterite was also observed under monolayers of self-assembled ribbons with pendant amino groups (Figure 6). The spacings of the active ammonium groups in these monolayers are distinctly larger compared to the spacings that are present in the monolayers of octadecyl amine. Although again the same two orientations of vaterite [(00•1) and (11•0)] were observed, it is important to note that the first crystal type, which has the lowest charge density in its nucleation plane, was clearly dominant (~95% of the population).

In a recent paper, Sommerdijk and co-workers also showed the formation of the same two vaterite orientations (see also Figure 31) under self-organizing monolayers of bis-urea

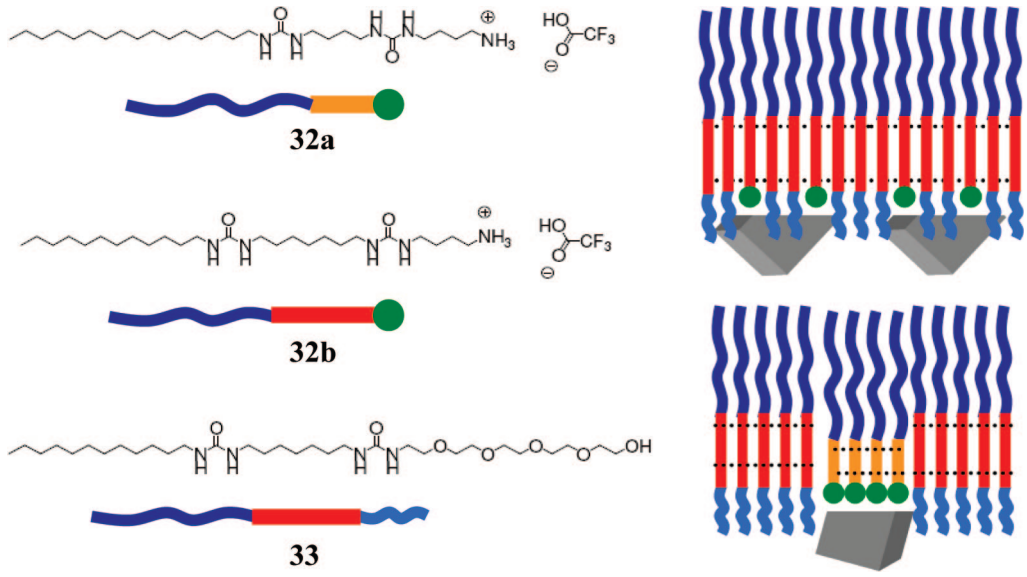

Figure 32. Left: chemical structures and schematic representations of bis-urea surfactants **32** and **33**. Right: schematic representation of the formation of crystals under two component monolayers with mixed (top) and phase separated monolayer stuctures. (Reprinted with permission from ref 214. Copyright 2007 American Chemical Society.)

surfactants containing ammonium head groups **32** (Figure 32).[214] Monolayers of two pure ammonium surfactants with different spacers (C_4 and C_7) between the bis-urea groups showed the same activity in a calcium carbonate crystallization assay: they promoted the formation of (11•0) vaterite alongside a similar amount of (10•0) calcite. When these two surfactants were mixed with an inactive penta(ethylene oxide) derived surfactant **33** with a C_7 spacer, the mixed monolayers behaved quite differently. The nonmatching pair (**32a/33**) showed the behavior expected for a phase-separated monolayer: the amount of modified crystals was proportional to the amount of active ammonium surfactant present in the monolayer. The matching pair (**32b/33**) surprisingly also showed phase separation. One phase consisted of the inactive penta(ethylene oxide) surfactant while the second phase consisted of a 1:4 mixture of this surfactant and the active ammonium compound. This composite phase gave rise to the formation of (00•1) vaterite in amounts proportional to the relative area of this phase, still in addition to (10•0) calcite, which now showed an indented morphology. As the density of the ammonium groups is higher in the pure phase as compared to the composite phase, it is surprising that the latter promotes the formation of the more highly charged (00•1) plane.

Volkmer et al. have demonstrated several accounts of polymorph switching (i.e., aragonite or vaterite formation) under macrocyclic monolayers.[215] The authors relate the observation of different polymorphs to differences in charge density in the monolayer and suggested that, above a critical charge density, the crystallization of calcium carbonate switches to these less stable polymorphs. It is interesting to note, however, that in several cases the compression of the monolayer to higher surface charge densities does not lead to polymorph switching but to inhibition of crystallization or, in the case of the calixarene with dendritic head groups, to a reduced selectivity, i.e. the formation of a mixture of calcite, vaterite, and aragonite.

In a recent paper, these authors review this work and propose a general scheme (Figure 33) in which polymorph selection and oriented nucleation are integrated, depending mainly on charge density in the templating monolayer. In this scheme, the authors leave room for new entries at charge density below zero electrons/nm^2, i.e. for cationic monolayers. It would be of interest to compare earlier results obtained with such cationic monolayers to the scheme presented by Volkmer and co-workers.

4.2.2. Polymorph Selection in Reverse Micellar Systems

In addition to Langmuir monolayers at the air−water interface and self-assembled monolayers at the solid−liquid interface, several research groups have explored the use of monolayers at liquid−liquid interfaces by using various reversed micellar or surfactant stabilized emulsion systems. Reverse micelles are formed at high surfactant/water ratios, where water droplets become enclosed by a monolayer of the surfactant of which the hydrophobic part is dissolved in the oil phase. In such a system, the calcium carbonate is grown inside the aqueous phase, where it can interact with the polar head groups of the surfactant. At room temperature, reversed micellar systems generally are dynamic and the water pools may grow by coalescence of different reversed micelles. Here we list several cases where the use of such systems leads to the formation of vaterite or aragonite.

The group of Mann was the first to demonstrate the formation of vaterite in reversed micelles (Figure 34).[216] They used an SDS/octane/aqueous $Ca(HCO_3)_2$ mircoemulsion system to produce what was termed vaterite microsponges (see also section 5.2.1 for a more detailed disussion on the shape of these structures). The formation of vaterite is attributed to the self-organization of the stabilizing surfactants at the oil−water interface giving rise to a high local charge density. This, due to the attractive interactions between the calcium ions and the sulfate head groups of the surfactants, locally induces a high supersaturation which favors the formation of vaterite. This idea was supported by the finding that, in a system without the octane, i.e. in the absence of an emulsion system, also vaterite was formed. It should be mentioned, however, that the dilution of the surfactant at the liquid−liquid interface through use of dodecanol as a cosurfactant did still lead to the formation of vaterite. It shows that the system is quite tolerant, also in

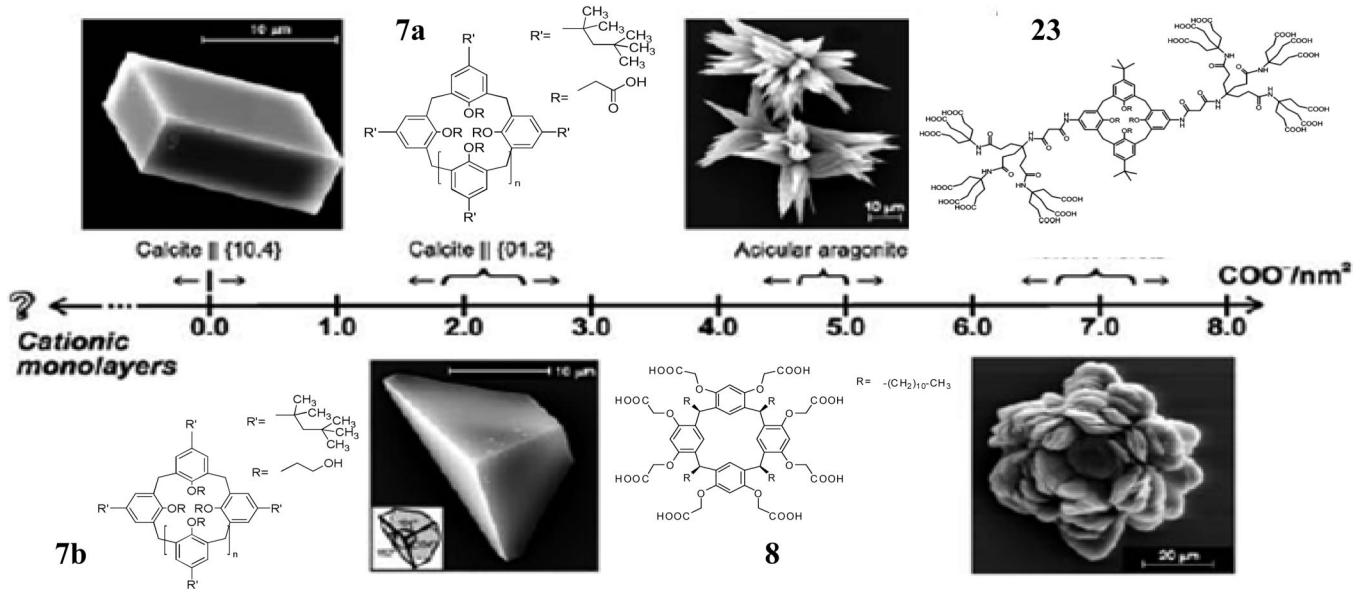

Figure 33. Overview of macrocyclic polyacids employed in studies on the growth of calcium carbonate beneath monolayers by Volkmer et al. The polyacids are arranged according to the increasing (negative) charge density (number of carboxylate residues per unit area) along with crystals forms of calcium carbonate formed under the monolayers. Charge density values were derived from Langmuir isotherms. (Reproduced from ref 215, Copyright 2007, with kind permission of Springer Science and Business Media.)

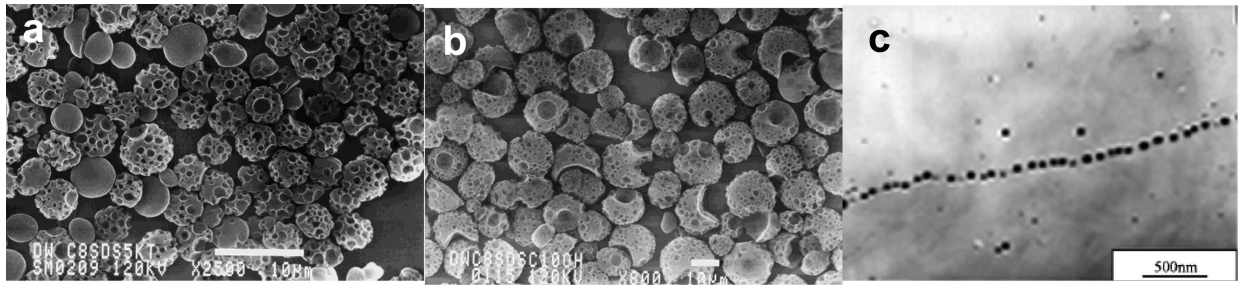

Figure 34. (a, b) SEM images showing spongelike vaterite spheroids prepared by evaporation from water-in-oil supersaturated microemulsions of (a) SDS/octane/$Ca(HCO_3)_2$(aq) and (b) SDS/octane/dodecanol/$Ca(HCO_3)_2$(aq): scale bars = 10 mm. (Reproduced with permission from ref 216. Copyright 1999 Wiley-VCH Verlag GmbH & Co. KGaA, Weinheim.) (c) TEM image of $CaCO_3$ nanocrystals prepared in a microemulsion of *p*-octyl polyethylene glycol phenylether (OP)/*n*-amyl alcohol/cyclohexane/water. (Reprinted from ref 228, Copyright 2007, with permission from Elsevier Limited.)

the amount of interfacial charge it requires for the stablilization of vaterite.

Kang et al. compared the formation of vaterite in SDS- and AOT-based reversed micellar systems and found that SDS is much more efficient in effecting the vaterite formation.[217] They find that for both systems above the surfactant/water ratio, i.e. the ratio above which stable reversed micelles are formed, vaterite is the main reaction product. These results suggest that the difference in efficiency for stabilizing the metastable polymorph is not related to an intrinsic capacity of these surfactants but may be related to their ability to stabilize a reversed micellar system.

A CTAB-based emulsion prepared by Liu and Yates was also shown to induce the formation of vaterite; however, in this case, the crystals were not stabilized and transformed into the more stable calcitic form within 4 days.[218] In addition, Tang and co-workers recently showed that the high interfacial charge density, and the concomitant increase in supersaturation, cannot be the only driving force for the formation of vaterite, as this polymorphic form can also be formed in a microemulsion based on the nonionic surfactant Tx100, although this surfactant is not as effective as SDS.[219] Similarly, Kandori et al. reported the formation of vaterite as well as aragonite in a nonionic emulsion system,[220] but also in this case, both these metastable phases transformed into calcite within 4 and 10 days, respectively.

The effectiveness of nonionic surfactants in the stabilization of vaterite was investigate in some more detail by Nakahara et al. (Figure 35)[221] in a pseudovesicular emulsion system.[222]

To this end, they prepared reversed micellar solutions of surfactant-stabilized droplets of aqueous K_2CO_3 in benzene. These emulsions were subsequently dispersed in another aqueous solution of $CaCl_2$, resulting in stable water-in-oil-in-water emulsions containing different surfactants. In this system, the calcium ions are shuttled through a layer of benzene surrounding the dispersed aqueous droplets. This causes the growth of the calcium carbonate phase within the boundaries of the inner surfactant layer under the exclusion of water and ionic byproducts. These researchers showed that vaterite was initially formed in all cases and that the effective yield of this polymorph in the product depended on the organization of the nonionic surfactant into a tight layer at the benzene−water interface and its ability to effectively interact with the crystals. This determines the extent to which the crystals are shielded from the aqueous phase and thereby the rate with which they transform into calcite.

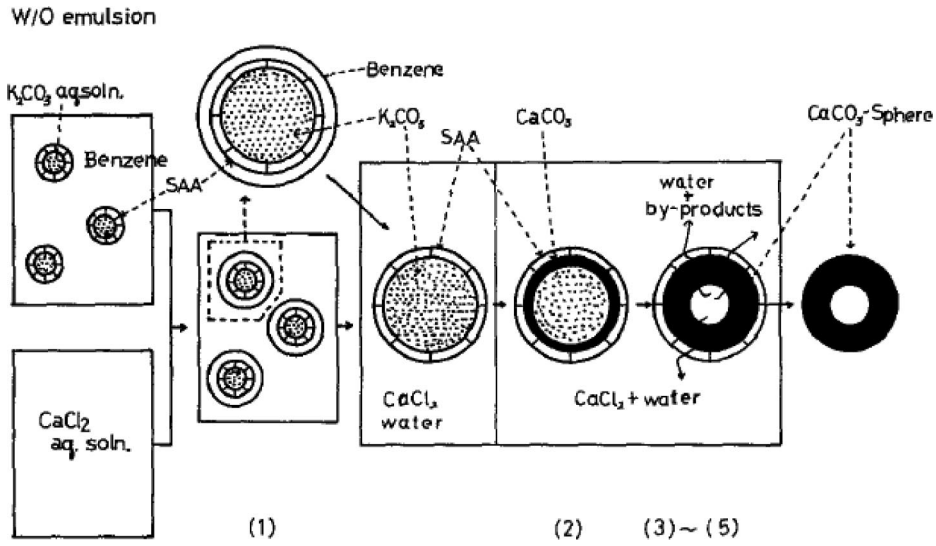

Figure 35. Schematic illustration of formation of the spherical $CaCO_3$ particles in the interfacial reaction method. Calcium carbonate particles of defined size are grown in a water-in-oil-in-water-emulsion. (Reprinted from ref 221, Copyright 1979, with permission from Elsevier Limited.)

This issue was also addressed by Mann et al. by mixing a dispersion of surfactant stabilized ACC particles with an AOT-based emulsion system.[223] As in some biological systems,[224] the ACC particles were used as a precursor phase that was allowed to crystallize upon interaction with the surfactants and the aqueous phase. By carefully changing the water/surfactant ratio, it is possible to tune the size of the aqueous compartments and thereby the amount of water present in each nanodroplet. At very low water/surfactant ratios ($w = 5$), the amount of water in the presence of the nanoparticle is so small that they do not crystallize. At somewhat higher ratios ($w = 10$), a conversion to vaterite is observed. The stability of this phase was attributed to the kinetic limitations given by the small volume of water and the presence of the stabilizing surface. Indeed, when the water/surfactant ratio was increased to $w = 20$, aragonite was formed.[225,226]

Moreover, the shape of the vaterite particles can be tuned, as the hydration is controlled by the ability of the surfactant to shield the particles from the interaction with water. It was demonstrated that the formation of vaterite structures significantly depended on the strength of the interaction between the surfactant and the vaterite particles by changing the Ca^{2+}/CO_3^{2-} ratio, which determines the net charge at the interface with the growing nanoparticles. At higher carbonate concentrations, this net charge is negative, reducing the interaction with the surfactant and leading to unrestricted growth of the vaterite. At higher calcium concentration, a stronger interaction with the surfactant leads to restricted growth and elongation only along the *c*-axis.

A more complex system was generated using a soluble additive to control the formation of the inorganic phase not only at the water−oil interface but also in the aqueous phase. Poly(phosphate) was used as an additive to control the formation of calcium carbonate in AOT-based microemulsions.[227] Increasing the concentration of poly(phosphate) reduced the amount aragonite that is formed without the presence of the additive, leading to mixtures of aragonite and increasing amounts of calcite. At concentrations of 2 g/L, aragonite was no longer found; instead a mixture of calcite and vaterite was obtained.

In a similar approach, Shen et al. showed that the nucleation and growth of calcium carbonate in a bicontinuous microemulsion consisting of *p*-octyl polyethylene glycol phenyl ether (OP)/*n*-amyl alcohol/cyclohexane/water lead to the formation of calcite nanocrystals (Figure 34).[228] However, the addition of DL-aspartate to the aqueous phase led to the formation of vaterite (up to 84% yield). Here the authors proposed a double role for the added DL-aspartate: the first is to interact with, and adsorb onto, the nonionic head groups of both the surfactant (OP) and the cosurfactant (*n*-amyl alcohol) to form a charged interfacial layer. Depending on the pH, this layer will attract either the positive or negative ions from solution, creating a supersaturation at the liquid−liquid interface which will promote the formation of vaterite. In addition, the adhesion of the amino acid molecules onto the developing nuclei was proposed to prevent their conversion into calcite, as was also demonstrated by Xie et al. (see section 4.1.2).[182]

5. Shaping the Inorganic Phase

Probably the most eye-catching aspects of biominerals are their beautiful and often complex shapes, as for example encountered in the exoskeletons of coccoliths.[229] In the current view, there are two main pathways along which organisms can control the shape of minerals. The first one involves the production of active (macro)molecules that interact specifically with certain crystallographic planes at the surface of the growing mineral phase, thereby favoring development of certain crystal faces above other ones. By switching on and off the growth along specific crystallographic directions, biominerals with predefined shapes can be formed. The second pathway involves growth of the mineral in a confined space with a predefined shape which acts as a mold for the developing crystal. One of the most important issues in this approach is the formation of molded single crystalline forms as opposed to the generation of polycrystalline aggregates with a specific shape. In the following section, we will focus on the experimental approaches that have helped to develop the present understanding of these approaches. As most of the experiments were designed to mimic only one of the approaches, they will be treated separately. Nevertheless, it may be expected that in many cases these two can act in a cooperative fashion.

5.1. Modification of Growth

In the past two decades, many experiments have been performed which, once put together, give a rather interesting overview of the factors involved in controlling the morphology and shape of a crystal. We will see that not just the type of the functional groups of the additive determines the interaction with the inorganic phase but that instead this process is dictated by the general collective of principles presently recognized as key factors in complex molecular interactions, such as cooperativity and (supramolecular) preorganization.

5.1.1. Cooperative Interactions

The first systematic studies into the effect of different additives on the formation of calcium carbonate were performed by the group of Mann. They investigated a complex series of inorganic and organic additives for their ability to modify the growth of calcite.[230] Of the inorganic additives, nitrate, sulfate, and phosphate were investigated. Phosphate was found to be extremely active in modifying the formation of calcium carbonate: even at very low concentrations ($[Ca^{2+}]$/[additive] = 10 000), a 40% reduction in number of crystals was observed. At higher concentration ($[Ca^{2+}]$/[additive] = between 1 and 10), the calcite crystals became characterized by a significant elongation along the *c*-axis. In contrast, similar concentrations of sulfate had only minor effects on the elongation along the *c*-axis, although a more rounded crystal shape was expressed. No such effects were observed upon addition of nitrate ions, not even at very high concentrations ($[Ca^{2+}]$/[additive] = 0.01). Hence, the above effects seem to be related to the affinity of the additive for Ca^{2+}.

By introducing an organic substituent on the phosphate [R−O−P(O)(−OH)$_2$; R = butyl, phenyl, and naphtyl], its effectivity in calcium carbonate modification dramatically decreased. For example, when using butyl phosphate, the ratio $[Ca^{2+}]$/[additive] needed to be increased to 10 for the observation of a clear effect. For phenyl phosphate and naphtyl phosphate, even higher concentrations were needed to observe a distinct modification. For the sterically less demanding methyl phosphonate, elongation of the crystals was observed still at a $[Ca^{2+}]$/[additive] ratio of 100. Diphosphonates on the other hand showed a much stronger ability to modify calcite growth. Methylene and ethylene diphosphonates already showed a strong effect at concentrations as low as $[Ca^{2+}]$/[additive] = 5000.

The importance of a cooperative action was already noticed in 1971 by Jackson and Bischoff. They described the recrystallization of aragonite to calcite in the presence of different amino acids (see also section 4.1.2).[231] They used arginine, serine, glycine, asparagine, aspartate, and glutamate and found that in the presence of these amino acids the rate of transformation to calcite increased quadratically with time, except for Asp and Glu. These two acidic amino acids result in stabilization such that the conversion shows a logarithmic reduction in rate. This observation was attributed to bidentate binding of the amino acids to the crystal surface and was related to the high content of acidic residues in matrix proteins.

Naka and co-workers,[194] and later on also others,[232] demonstrated that sodium acrylate, carrying only one carboxylic acid moiety, had no effect on the crystallization of calcite. However, polymerization of the monomer in early stages of the mineralization experiment leads to an inhibition of calcite and the concomitant expression of other polymorphs (see also section 4.1.2). The precipitation of calcium carbonate in the presence of *N*-2-hydroxyethyl-iminodiacetic acid (**34**) (Ca/additive < 20) even leads to rounded calcite crystals grown along the *c*-axis. This strong effect suggests a multidentate interaction of this molecule with the crystal faces oriented perpendicular to the plane of the carbonate ions (Figure 36).[233]

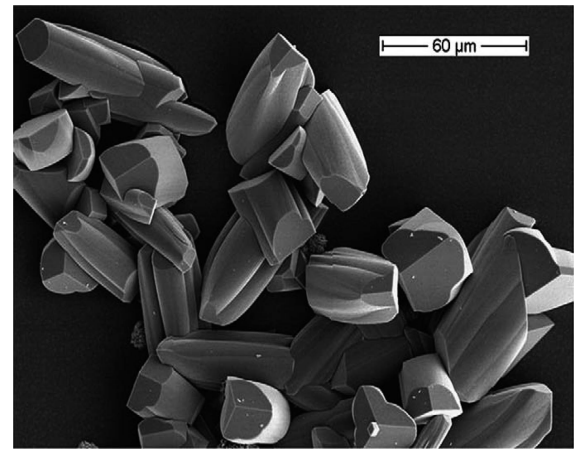

Figure 36. Elongated calcite crystals grown in the presence of **34**. (Reprinted from ref 233, Copyright 2006, with permission from Elsevier Limited.)

Also, other systems have been described in which the monomer was ineffective, while a multivalent derivative stabilized the nonequilibrium faces of calcite through specific additive−crystal plane interactions. For example, Estroff and co-workers synthesized an acid-modified pyridine trimer **35a** that induced the formation of needle-like calcite where the monomeric form had no effect. The isolated single crystalline needles had a sawtooth morphology expressing specifically the $(\bar{1}0 \cdot l)$ faces where $l = 0.5-1$ (Figure 37).[234]

Similarly, Imai et al. showed that calcite grown in the presence of silica at pH = 10.5 evolves with a needle-like self-similar structure with 3-fold symmetry (Figure 37).[235] This was attributed to the incorporation of silica in the crystal surface, as during the process of crystal formation the concentration of carbonate ions decreases and the influence of silicic acid ions becomes larger. Initially, the influence of the silicate anions is similar to what has been described for organic additives containing carboxylic acid groups (see above). In this mode, the silicic acid molecules are thought to attach with two of their silanol groups to the {11•0} faces of calcite, parallel to the *c*-axis. Only at higher surface concentrations do the incorporated silicate anions become polymerized and form linear polymers on the crystal surface that are strongly adsorbed and dictate the intricate complex shapes observed.

Recently, polystryrene sulfonate was used to control the morphology of calcite crystals by changing the kinetic pathway by which they developed (see also section 2).[236] In addition to the drastic changes in crystal morphology that were related to the nanoparticle assembly pathway, they also observed a stabilization of the (00•1) face. It is easily imagined how a large number of sulfonate groups can collectively bind to such a polar calcium exposing surface. Moreover, the tripodal coordination possibility of the sulfonate groups allows the stereochemical matching of the orientation of the carbonate groups in the (00•1) plane, which may be involved in stabilizing this crystal plane selectively.

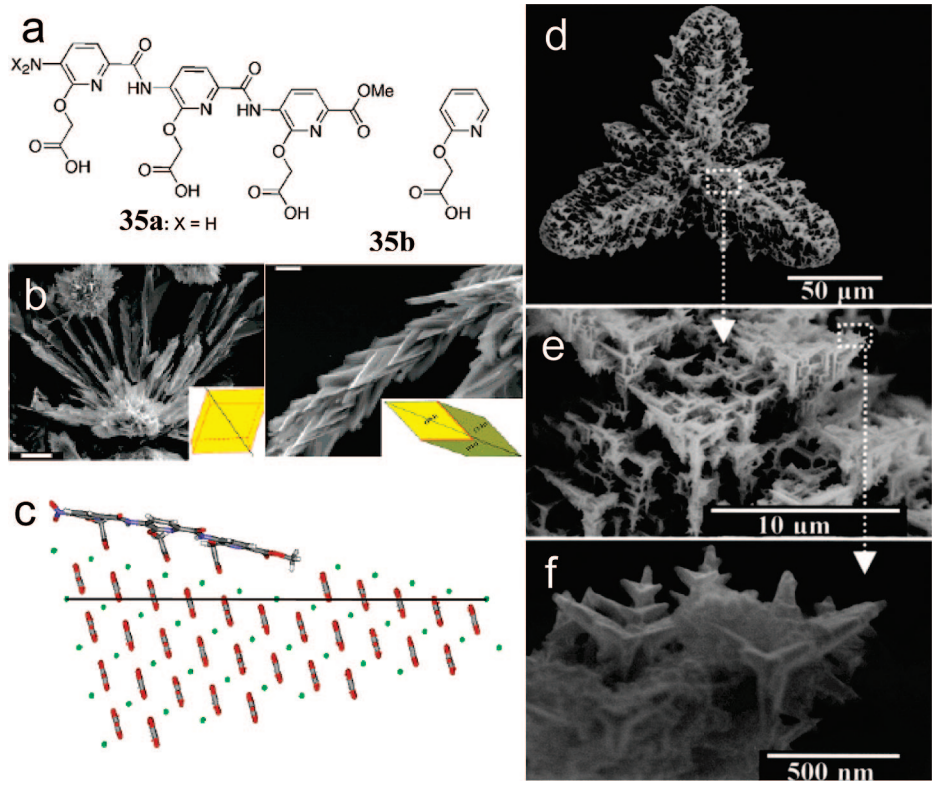

Figure 37. (a) Molecular structure of **35a** and the monomeric form **35b**. (b) SEM images of the crystals formed in the presence of **34a.** Scale bars: (left) 10 μm; (right) 5 μm. Insets: (left) calcite rhombohedron with the equilibrium morphology of six {10•4} faces; (right) calcite rhombohedron with six (11.0) faces. (c) Molecule of **34a** docked onto the ($\bar{1}$0•1) face of calcite (black line). Notice that the carbonates are projected almost perpendicularly out of the plane and the angle is matched by the carboxylates (Reprinted with permission from ref 234. Copyright 2004 American Chemical Society.) (d) Calcite grown in the presence of silica ions, exposing the (11•0) faces. (e, f) Enlargements of part (d). (From ref 235 (http://dx.doi.org/10.1039/b211240j). Copyright 2006. Reproduced by permission of The Royal Society of Chemistry.)

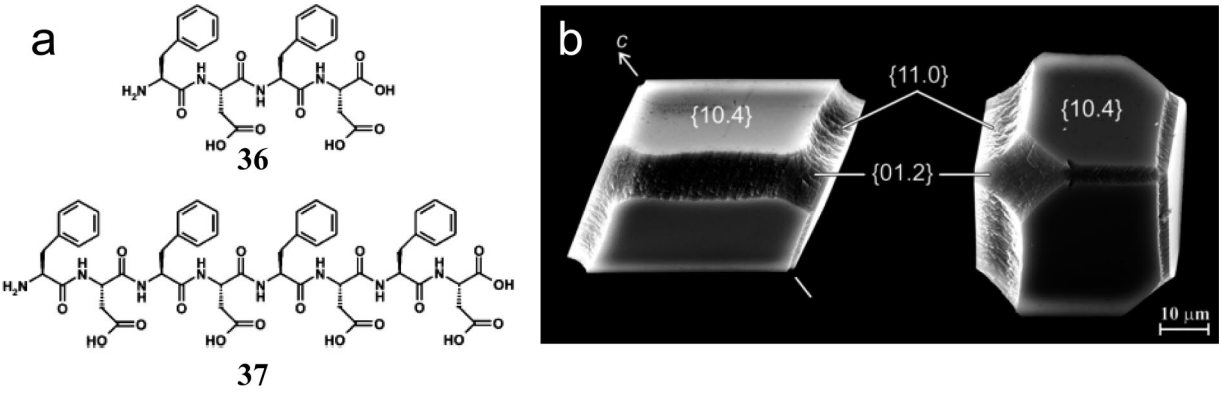

Figure 38. (a) Chemical structure of the tetrapeptide **36** and octapeptide **37**. (b) SEM images of calcite crystals grown in the presence of **37** (ratio of **37**/Ca = 1:180). Crystals isolated after 5 h. (From ref 237 (http://dx.doi.org/10.1039/b405613b). Copyright 2004. Reproduced by permission of The Royal Society of Chemistry.)

In a systematic study, Volkmer et al. showed that (Phe-Asp)$_2$ **36** and (Phe-Asp)$_4$ **37** affect the growth of calcite by inhibiting the (11•0) and the (01•2) faces (Figure 38).[237]

In line with the discussion above, the extension of the peptide chain from four to eight residues did not change the selectivity but only the effectivity of the interaction. This suggests that also in this case a cooperative effect was observed: where (Phe-Asp)$_2$ showed the abovementioned crystal modification at [Asp] = 2 mM, (Phe-Asp)$_4$ showed a similar effect already at [Asp] = 0.4 mM. Moreover, even at a concentration of 3 mM, monomeric aspartic acid did not show this effect but still led to the formation of {10•4} calcite.

5.1.2. Preorganization of Functional Groups

As discussed, the importance of cooperativity was already noted in the 1993 paper of Didimus et al.[230] In addition, these authors also found that preorganization of the functional groups could add to the effect. A homologous series ranging from malonate (**23**) with only a single methylene unit between the two carboxylates to azelaic acid (**38**) containing seven methylene units showed that the cooperative effect was strongest for malonate. Although far less effective than the corresponding diphosphate (clear effects were only observed for [Ca^{2+}]/[additive] ratios > 8), malonate (**23**) caused a very selective expression of the {$\bar{1}$1•0} crystal faces parallel to the crystallographic *c*-axis. Extending the spacer

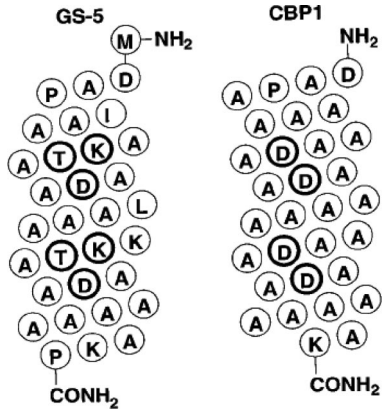

Figure 39. Helix net diagrams of the antifreeze polypeptide GS-5 and of the derived calcite binding peptide, CBP1, showing respectively the putative ice-binding (KTD) and calcite-binding (DD) motifs on one side of each helix. (Reprinted with permission from ref 238. Copyright 1997 American Chemical Society.)

between the carboxylates led to a rapid decrease in effectivity; for succinate (**22**) (containing two methylene units), the formation of truncated rhombs together with rounded crystals was observed; for the higher homologues, only minimal morphological effects were observed. As the binding constants for calcium did not differ much between the compounds, it was suggested that the observed decrease in effectivity was related to the entropy loss associated with the simultaneous binding of two carbonyl groups at the crystal surface for the longer chains.

Interestingly, maleate **20**, having a double bond that preorganizes the carboxylates, showed a stonger effect than the conformationally less restricted succinate (**22**). As expected, the *trans*-isomer fumarate **39** did not show any effect under the conditions used. The authors showed that the activity of macromolecules can be far greater than that of the low molecular weight additives. Although not well defined, for osteocalcin, the modification of calcite growth was even observed at a $[Ca^{2+}]$/[additive] ratio of 20 000. However, not all poly acids tested showed this strong multivalent effect. Macromolecules such as polyglutaronic acid showed little or no effect. This indicated that, apart from the presence of functional groups, also their local concentration is a major point in the controlled interaction with mineral surfaces. Moreover, these results pointed to the importance of molecular conformations and the role of preorganization of functional groups with respect to the points of interaction at the inorganic binding sites.

In line with these thoughts, DeOliveira and Laursen designed an α-helical peptide that contained calcium binding residues at predefined positions.[238]

They synthesized a poly(alanine)-based peptide equipped with two Asp couples at positions 10 and 13 and at positions 21 and 24 (Figure 39). When this polypeptide is in a helical conformation, these positions give an approximate match with four calcium ions in the $\{1\bar{1}.0\}$ prismatic faces of calcite. They showed that at 4 °C, when this calcite binding peptide (CBP1) is in an α-helical conformation, the further growth of calcite seed crystals indeed results in the formation of prismatic crystals with rhombohedral end faces. The quality of the design was demonstrated by the high efficiency of the interactions; the observed effects were already demonstrated at template concentrations equivalent to a [Ca]/$[COO^-]$ ratio of approximately 100. Unfortunately, the authors were not able to distinguish between binding of

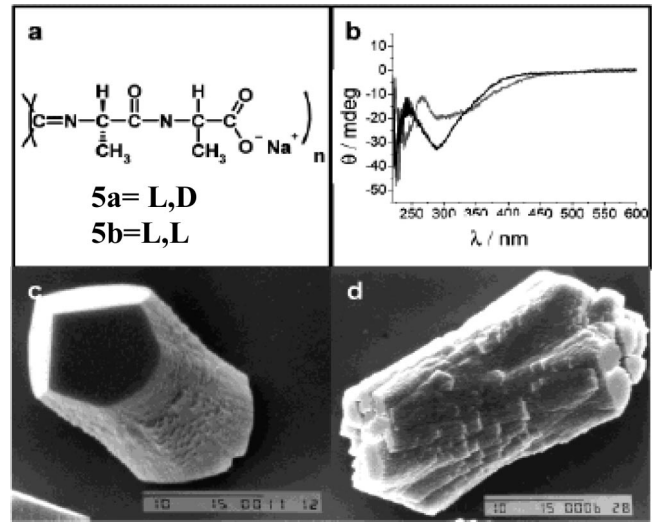

Figure 40. (a) Chemical structures of polymers **5**. (b) CD spectra of aqueous solutions of **5a/**Ca^{2+} (black) and **5b/**Ca^{2+} (gray); Ca^{2+}/repeat unit = 1:1. Scanning electron micrographs of calcite grown in the presence of (c) **5a** and (d) **5b**. (Reprinted with permission from ref 84. Copyright 2002 American Chemical Society.)

CBP1 to the $\{1\bar{1}.0\}$ or the $\{11.0\}$ prismatic faces of calcite due to the irregularity of the exposed crystal faces. However, the specificity of the interactions was demonstrated by performing an experiment at room temperature where a large proportion of CBP1 adopts a random coil conformation. Under these conditions, the peptide just showed an unspecific interaction with the growing crystal such that it blocks the development of nonequilibrium faces and causes the development of studded shapes by epitaxial growth of the $\{10\cdot4\}$ faces.

Expanding on these thoughts, Sommerdijk et al. designed two stereoisomeric peptide-based poly(isocyanides) as potential growth modifiers for calcite.[84] It has been demonstrated that the helical conformation of poly(isocyanides) in solution can be stabilized and rigidified by the presence of secondary interactions, e.g. hydrogen bonds, between the side chains.[239] For alanyl-alanine-derived poly(isocyanide)s **5**, the helical structure persists even in aqueous media presenting a regular distribution of carboxylic acid terminated side chains (Figure 40; see also Figure 12). Moreover, whereas in the absence of Ca^{2+} the intensity of the circular dichroism (CD) signal gradually decreased over a period of 24 h, in the presence of the calcium ions, the helical structure remained stable.[240] The presence of the poly(isocyanopeptide)s in crystallization assays in both cases leads to the formation of calcite crystals with a dogbone-like shape, elongated along the *c*-axis and expressing the rhombohedral $\{10\cdot4\}$ end faces. Both polymers showed a very high activity, which was observed already at a [Ca]/$[COO^-]$ ratio of 2000. This effect can be attributed to the high number of repetitions of functional groups in both polymers [for **5a**, degree of polymerization = 1520 (polydispersity index (PDI) = 1.9); for **5b**, degree of polymerization = 760 (PDI = 1.4)] and again underlines the importance of cooperativity in these recognition processes.

Importantly, the specificity of the interaction between **5a** and the growing crystal was demonstrated by comparison of the above results with those obtained with L,L-isomer **5b**. Polymer **5b** has a less well-defined structure, as evidenced by its CD-spectrum, which consisted of two superimposed bands. Indeed, crystals grown in the presence

AP7-N (DDNGNYGNGMASVRTQGNTYDDLASLISYL)
AP24-N (ADDDEDASSGLCNQYNQNVTTRPNNKPKMF)
n16-N (AYHKKCGRYSYCWIPYDIERDRYDNGDKKC)

Figure 41. Amino acid sequences for the proteins AP7, AP24, and n16. (Reprinted with permission from ref 243. Copyright 2004 American Chemical Society.)

of **5b** were less well-defined than those grown in the presence of **5a**, both in shape and in size [For **5a**, dimensions: 28 (±2) × 15 (±1) μm. For **5b**, dimensions: 31 (±4) × 14 (±2) μm].

The above results confirm that the preorganization of the functional groups can play an important role in the specificity of binding to specific crystal faces. In this view, it is interesting to speculate whether also in other investigations self-organization of the additive on the cystal surface may play a role. For example, Volkmer et al. showed that the octapeptide $(Phe\text{-}Asp)_4$ had a distinctly stronger effect on the development of calcite than the corresponding tetrapeptide.[237] These alternating peptides were selected due to their ability to form well defined β-sheet structures.[241] Therefore, it is not unreasonable to assume that the efficiency of these peptides may be related to their ability to form such a β-sheet conformation. Similarly, for a related series of peptide lipids based on the glutamate−leucine $(Glu\text{-}Leu)_n$ motif, it was shown that the hexapeptide- and the octapeptide-derived molecules can form monolayers with β-sheet structure, whereas the tetrapeptide-derived molecule only adopts a random coil structure.[242]

5.1.3. Relevance to Biomineralization

In this subsection, we will give some examples that further strengthen the notion that preorganization of additives indeed is an important factor in controlling mineralization also in a biological environment. Evans and co-workers investigated the influence on calcite growth for three different 30 amino acid long N-terminal mineral binding domains from biomineralization proteins AP7, AP24, and n16 (Figure 41).[243,244] AFM showed that AP7 and AP24 had very similar effects, i.e. binding at the obtuse steps, but also inducing the formation of rounded, possibly amorphous deposits on the terraces of the growth hillocks. However, their activities were distinctly different, with AP24 being the more active of the two. Both the AP7 and AP24 sequences have a disordered structure and so-called interactive sequence clusters, i.e. organized arrays of residues that may assist e.g. in water displacement or in the organization of carbonate ions.[245] Nevertheless, these domains also have distinct structural differences. For example, the kinetically more active AP24 not only has a larger array of acidic residues (5) and the tendency to form a more planar backbone, it also shows a higher conformational response to the presence of calcium ions.

In contrast to AP7 and AP24, the n16 sequence leads to pinning at the corner sites of the junction of the obtuse and acute steps. As these three proteins are all originating from the nacreous part of mollusks, these results show the diversity of function which is necessary for complementary and simultaneous protein control, as needed during biomineralization processes.

Substitution of Asp to Asn and Glu to Gln take away the ability of AP7 and n16 to modify the growth of calcite crystals.[246] This substitution was accompanied by changes in the secondary structures of the sequences. CD spectroscopy indicated that, after substitution, AP7 adopted a α-helical conformation. For n16, of which the structure is in equilibrium between a random coil and a β-strand conformation, substitution was found to lead to larger random coil content. This indicates that the presence of the acidic residues is crucial not only for the calcium binding of the sequence but also for its folding. This underlines once more that the preorganization of the control agents often is crucial for their activity.

Vaiyaveettil et al. investigated peptide sequences derived from the calcium binding sequence in the goose eggshell matrix protein ansocalin for their activitiy in modifying the formation of calcium carbonate.[247] The basic $R_2E_2W_2D_2$-$R_2E_2W_2D_2$ form ansocalin was modified by replacing R (arginine) for K (lysine) ($K_2E_2W_2D_2$-$K_2E_2W_2D_2$), by incorporation of P (proline) between the repeat ($R_2E_2W_2D_2$-P-$R_2E_2W_2D_2$), and by performing both substitutions ($K_2E_2W_2D_2$-P-$K_2E_2W_2D_2$). All the peptides showed a concentration dependent aggregation behavior. Those containing the rigid proline linker formed larger aggregates than those without. CD spectroscopy in the presence of calcium ions showed that in the aggregated form both 16 amino acid residues were in an extended β-sheet conformation. It further was found that incorporation of the proline residue induces a β-turn in the structure of the 17 amino acid peptides. All these modifications were active in influencing calcium carbonate precipitation by yielding aggregates of small intergrown calcite crystals, similar to the parent protein ansocalin. In contrast, control sequences with a disordered secondary structure did not show any significant activity. Interestingly, R to K substitution at low peptide concentration leads to a distinctly different secondary structure of the peptides, accompanied by a lower calcite modifying activity. Only at higher concentrations (2 mg/mL), i.e. where $K_2E_2W_2D_2$-$K_2E_2W_2D_2$ is present in its aggregated form, are modified crystals the predominant product of the crystallization assays. This suggests that the β-sheet conformation of the peptide sequence is essential for its activity in biomineralization. A remarkable observation is also that under these conditions $K_2E_2W_2D_2$-$K_2E_2W_2D_2$ compared to $R_2E_2W_2D_2$-$R_2E_2W_2D_2$ produces morphologies that are closer to those induced by the full protein. The introduction of the β-turn in $K_2E_2W_2D_2$-P-$K_2E_2W_2D_2$ leads to an activity that is even closer to that of ansocalin; moreover, this activity is already present at low peptide concentrations and, thus, apparently independent of the aggregation behavior. Apparently, also here the preorganization of the peptide enhances its activity, despite the fact that a β-turn is introduced which is not present in the native peptide.

5.1.4. Unraveling the Mechanism of Additive−Crystal Interactions

Significantly, in most experiments described above, additives were used which carried carboxylates as the functional groups. Most of these stabilized crystal planes in which the carbonate ions have an orientation perpendicular to the surface of the crystal. Consequently, these modifications have been predominantly described as arising from bidentate interactions with the carboxylates of the additive. Also, the substituted phosphates, described by Didymus et al., show the stabilization of the closely related $\{4\bar{4}.0\}$ faces,[248] suggesting that they also work through a similar bidentate interaction.[230] This is somehow surprising, considering the

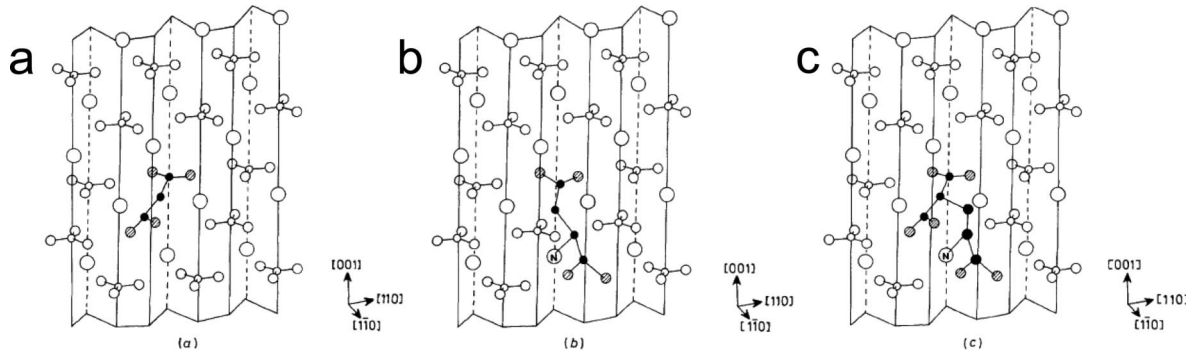

Figure 42. (a) Perspective drawing of the (1$\bar{1}$·0) face of calcite showing the possible malonate binding site. (b) Possible aspartate binding site showing α-aminocarboxylate interactions. (c) Possible γ-carboxyglutamate binding sites showing α-aminocarboxylate and γ-carboxylate (malonate) interactions. Large open circles = Ca, hatched small circles = carboxylate oxygens, small black circles = carbon atoms of additive molecules. (Reprinted with permission from ref 249 (http://dx.doi.org/10.1039/FT9908601873). Copyright 1990. Reproduced by permissin of The Royal Society of Chemistry.)

fact that the phosphate groups in principle are able to interact through a tripodal interaction replacing the carbonate in the (00·1) plane *perpendicular* to the *c*-axis, as was observed for example in eicosyl phosphonate monolayers.[71] Only in the case of phenyl phosphonate, is the {01·2} plane stabilized, which suggests that the steric hindrance of the phenyl group does not allow the same type of binding and forces the interaction to be tripod-like.

The homologous series of α,ω-dicarboxylic acids investigated by Didymus et al. was extended to include aspartate (**26**).[249] Interestingly, the introduction of an amino group completely changed the activity of the dicarboxylic acid moiety: even at a [Ca^{2+}]/[additive] ratio of 17, the addition of aspartate led to a clear expression of the prismatic {1$\bar{1}$.0} side faces in a manner that exceeds the effect of malonate (**23**). These results suggest a specific role for the amino group in recognizing a specific carbonate ion with defined positioning with respect to two calcium ions in the {1$\bar{1}$.0} planes (Figure 42). This specific recognition motif is indeed lost for the interaction with glutamate (**27**), so apparently the extension of the distance between the carboxylates overrules the extra stabilization given by the amino group. Conversely, when an extra carboxylic acid group is introduced at the γ-position of the glutamate, and thereby a malonate moiety is created, the interaction with the {1$\bar{1}$.0} planes again is enhanced, and a [Ca^{2+}]/[additive] ratio of 85 even was enough to stabilize these planes.

After Didimus and co-workers gave a detailed proposal for the interaction of diacids and amino acids with the {1$\bar{1}$.0} face, and following the early work on Langmuir monolayers,[10] many other researchers searched for epitaxal relations between the organization of the stabilized crystal plane and the functional groups of the interacting organic molecules. However, in the beginning of this century, it became more and more clear that in many cases it was impossible to define such a clear-cut relation. As discussed above, it was demonstrated for several systems that the match between the carbonate groups in the stabilized crystal plane and the carboxylates of the interacting molecules can at most be found in an orientational relation. A similar relation was suggested by Estroff and co-workers for the interaction of trimer **35**a and the stabilized {$\bar{1}0l$} faces (Figure 37).[234]

Volkmer demonstrated that the tetrapeptide $(Phe\text{-}Asp)_2$ **36** as well as the octapeptide $(Phe\text{-}Asp)_4$ **37** stabilized both the (11·0) and the (01·2) faces of calcite.[237] Here the stabilized faces share a common feature, i.e. an almost perpendicular orientation of the carbonate groups to the stabilized crystal plane. Although it is tempting to suggest that a relation exists between the orientation of the carboxylate groups of the aspartate residues and the carbonate ions of the two crystal planes, the reason why two different crystal planes are selectively stabilized is unclear. Moreover, Jones et al. demonstrated that calixarenes modified with four glutamate moieties (**40**) also selectively stabilize to the (11·0) and (012) faces (Figure 43).[250]

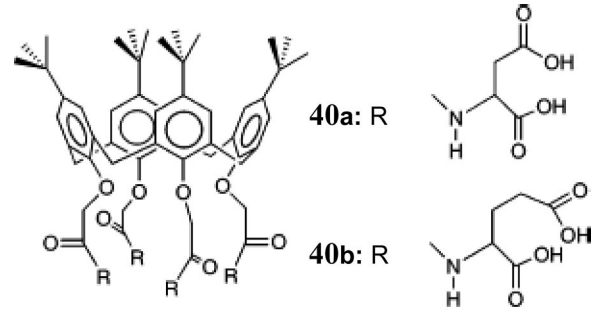

Figure 43. Molecular structure of amino acid-modified calix[4]arenes **40**. (Reprinted with permission from ref 250. Copyright 2005 American Chemical Society.)

In this molecule, the positioning of the carboxylic acid groups does not have any obvious relation with the two expressed crystal faces, suggesting that no specific interaction but maybe more general electrostatic forces are responsible for the stabilization of these faces. It should be noted, however, that, in analogy to the observations of Dydimus et al.,[10] that also in this case the substitution of the glutamates for aspartates (**40a**) lead to much stronger growth modification of the crystals.

De Yoreo et al. demonstrated how the morphological changes observed upon addition of aspartatic acid to a mineralization solution were related to its binding to the calcite surface.[164] Addition of aspartic acid leads the acute steps on a developing calcite surface to adopt a rounded shape. However, the symmetry around the glide plane is broken when only one of the enantiomers is used. This led to the formation of mirror image morphologies for the D- and L-forms of aspartatic acid (Figure 44a,b). It was concluded that, as the crystal was not nucleated in the presence of the additive, the growth modifications must arise from interactions with the growth step edges. This was supported by the observation that the step growth speed at moderate concentrations ([Asp]/[Ca] ratio ~ 2 to 200) was not concentration dependent, which would have been the case if the impurity would be included in the bulk.[251] When

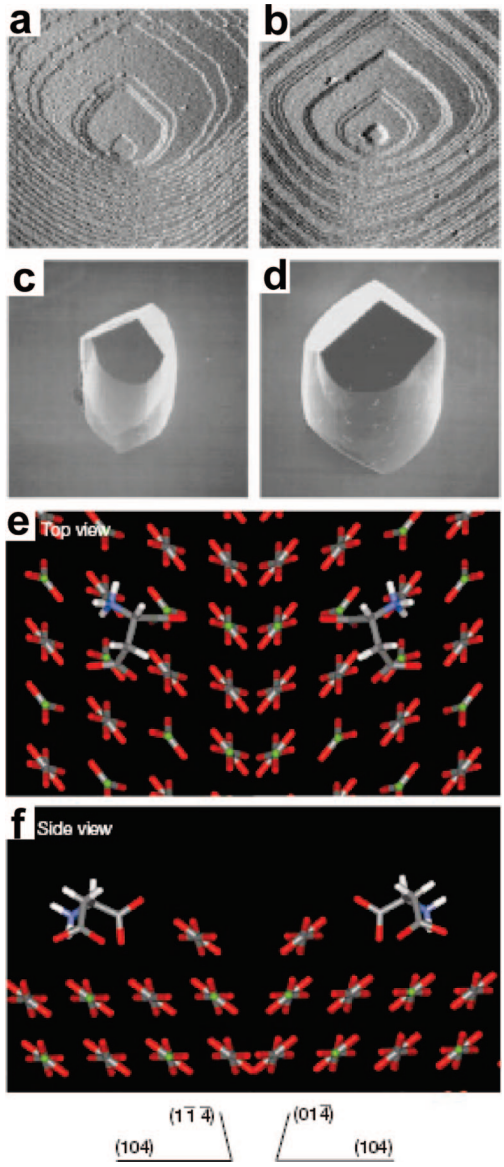

Figure 44. (a, b) AFM images showing growth hillocks following addition of supersaturated solutions containing (a) 0.01 M L-aspartic acid and (b) 0.01 M D-aspartic acid. (c, d) SEM micrographs of calcite crystals nucleated on COOH-terminated regions of patterned self-assembled monolayers of alkanethiols and grown in the presence of (c) 0.01 M L-Asp and (d) D-Asp. (e, f) Geometry of binding for aspartic acid adsorbed on the single (104) steps of calcite. (e) Top view and (f) side view of L-Asp (left) and D-Asp (right) binding to the steps of calcite with (1$\bar{1}\cdot\bar{4}$) risers and (0$\bar{1}\cdot\bar{4}$) risers, respectively. The crystal surfaces are rotated and aligned to show the mirror symmetry of binding. (Reprinted with permission from ref 164. Copyright 2001 Nature Publishing Group.)

crystals were grown in solution in the presence of one of the two enantiomers, a new set of {$hk\cdot0$} facets appeared, giving rise to crystals elongated along the *c*-axis of calcite. The cylinder-like crystals are capped by {10·4} faces, of which the appearance (Figure 44c,d) closely resembles the atomic steps seen with AFM (Figure 44a,b). It was described that also here the obtuse steps were unaffected by the additives and form straight ridges connecting the cap facets, whereas the curved acute steps form the rounded base of the cap. The binding of aspartatic acid to the {$hk\cdot0$} facets is in good agreement with the experession of the (11·0) faces of calcite as described by Mann et al. However, it should be noted that the results from De Yoreo et al. show that the binding does not occur at the exposed crystal face but rather at the growth steps on this face. Moreover, because of symmetry considerations, the chiral effect implies that the binding takes place at both the step riser and the terrace. Indeed, D-Asp was found to preferentially bind to the step between the (10·4) terrace and the (0$\bar{1}\cdot\bar{4}$) riser, where L-Asp has a preference for the step with the (1$\bar{1}\cdot\bar{4}$) riser (Figure 44e−g).

In a related study, Elhadj et al. reported a surprising additional effect of extending the length of oligo(aspartate) chains Asp_n ($n = 1-6$) on the development of calcium carbonate growth.[252] In this study, the development of growth hillocks was monitored with AFM. The formation of roughened growth steps was observed for all additives Asp_{1-6} at decreasing critical concentrations, with longer oligomers as expected. Remarkably, whereas Asp_1 and Asp_2 inhibited the growth of the acute steps, the longer chains (Asp_4-Asp_6) blocked the growth of the obtuse steps. By semiempirical modeling calculations, the authors were able to relate these effects to the binding mode of the different additives to the calcite surface (Figure 45). These calculations showed that the two short additives (Asp_1 and Asp_2) displaced more water on the obtuse steps then on the acute steps, whereas the reverse was the case for the longer chains (Asp_{3-6}). This experiment underlines a generally neglected issue for crystal−template and crystal−additive interactions; that is, that either dehydration of the interface must occur before complexation can take place or water molecules form a layer in between the interacting species.

By combining data from small molecules[252] as well as from protein fragments,[253] Elhadj et al. showed how organic molecules can be used to control calcite growth not only by reducing growth rate but also by catalyzing the growth under certain directions (Figure 46).[254] It was demonstrated that whereas at higher concentration additives inhibit the growth of calcite, at low concentration such peptides and protein fragments are able to accelerate crystal growth. At additive concentrations of 0.1 μM different dipeptides, oligopeptides, and small protein fragments increase the rate of obtuse step growth at the calcite {10·4} faces. The apparent relation between step acceleration rate and the peptide net charge was considered insufficient to accurately explain the differences in activity between smaller peptides. In view of the possible mechanism involved in the acceleration of step growth, the role of hydrophobicity was considered as a major factor. Indeed, the molecular hydrophobicity of the additives showed a linear relation with the step growth acceleration $\ln(v/v_0)$. This molecular hydrophobicity was related to the effect of the additive on the water activity at the mineralization site. As the growth of a crystal is strongly influenced by the interactions of water molecules with the crystal surface, the growth units, and the additives, the local activity of water is thought to play an important role in this process. It was proposed that the hydrophobicity of the additive may influence the rate of dehydration of the growth units and thereby influence the rate of the step growth. Importantly, these experiments demonstrate how organisms possibly can regulate mineral growth not only by inhibiting specific crystal faces but also by accelerating the growth of certain other faces.

5.1.5. Complex Shapes in Solution

For the collective of the above experiments, we can say that, to be effective in the modification of calcium carbonate growth, an addive best should have multiple functional

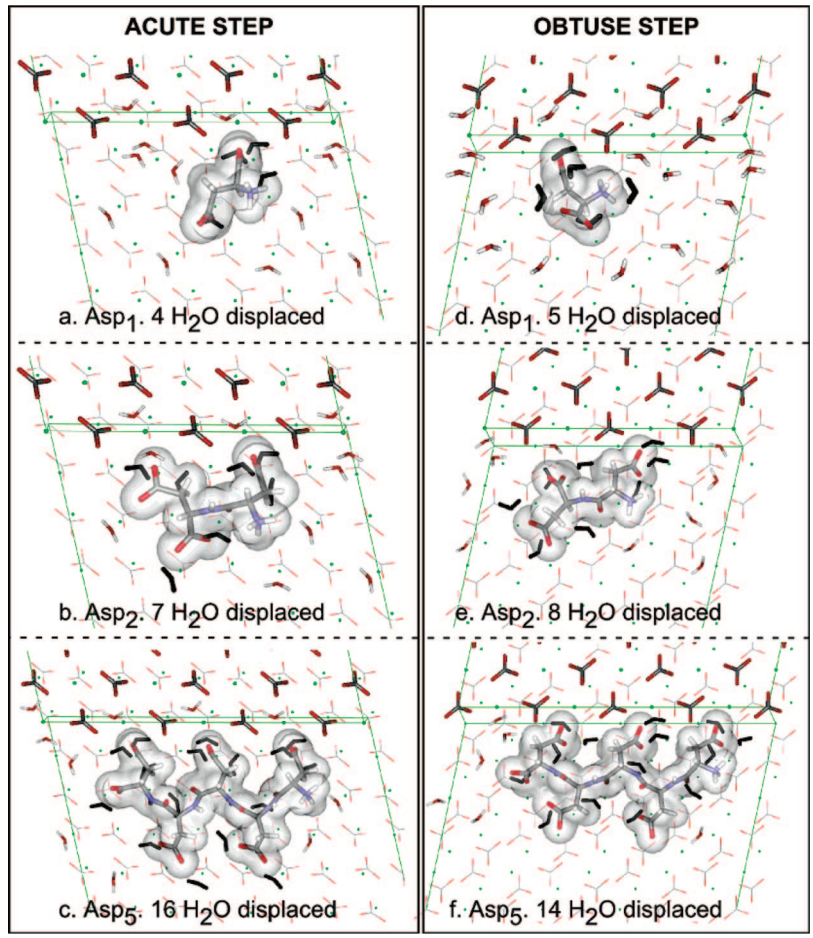

Figure 45. Computational model for a representative set of Aspn binding to the hydrated right acute (a−c) and obtuse (d−f) calcite steps for Asp1, Asp2, and Asp5. A green outline delineates the steps: (Ca) green, (C) gray, (N) blue, (O) red, (H) white. The contrast in water molecules displaced by the binding of Asp1 (a, d), Asp2 (b, e), and Asp5 (c, f) to the steps is shown, and the number of displaced H_2O molecules is depicted in black for emphasis. (Reprinted with permission from ref 252. Copyright 2006 American Chemical Society.)

groups that work coherently to influence the growth of specific crystal phases. This has been demonstrated for small molecules but seems to work most effectively for macromolecules or assemblies, in particular when their functional groups are preorganized, presenting an array of attachment points tailored to interact with the selected crystal plane. This interaction in most cases leads to an inhibition of growth for a certain crystal plane; however, it was also demonstrated that, at low addditve concentrations, this may lead to an accelerated growth of this face. Together these factors should allow us to design new additives that control the formation of minerals in a biomimetic manner. However, with this we would still lack one of the most exiting aspects found in biomineralization: the formation of ordered assemblies of these crystals. The possibilities for this will be discussed below, where we select some examples that demonstrate the complexity of the materials formed, concentrating mostly on low molecular weight additives, while being aware that there is a vast amount of reports on polymer controlled crystal growth leading to structures of similar beauty and complexity which are not within the scope of this review.[255,256]

Very unusual calcitic structures were reported by Yu, Cölfen, and co-workers using a block copolymer consisting of a poly(ethylene oxide) chain connected to a hexacylen moiety **41** (Figure 47).[257] This rigid hexacyclen block most effectively modifies the crystallization behavior of calcium carbonate when the amino groups in the ring are protonated. At a block copolymer concentration of 1 g/L, this leads to the formation of stacks of pancake-like morphologies. Time-dependent studies showed that these were formed through amorphous and polycrystalline precursor phases, apparently temporarily stabilized by the hexacylcen-based block copolymer. The diffraction pattern of the mature stack showed several peaks, of which the (01•2) and (02•4) reflections were among the stronger ones. Upon increasing the polymer concentration to 2 g/L, the morphology changed to spherical particles, while the (01•2) and (02•4) together with the (20•2) became dominant. From comparing the models of the stabilized crystal faces and the hexacyclen as well as their charge densities, the authors conclude that a complex interplay between particle stabilization, epitaxial matching, time for polymer rearrangement, and surface ion density determines how the polymer adsorbs to the exposed faces and thereby controls the morphology of the crystalline phase.

The use of 1,3-diamino-2-hydroxypropane-*N*,*N*,*N*,*N*-tetraacetate (**42**) leads to the formation of even more fascinating shapes in the form of nanotrumpets (Figure 48).[258] These are built up from long nanocrystals of calcite that develop in the course of 24 h, starting from plaques of calcite carrying ball-like calcite excrescences. Although architectures of similar complexity have been described previously using double hydrophilic block copolymers,[256] in particular for barium sulfate,[259] this was the first time such intricate structure was achieved with a small molecule. Unfortunately, the mechanism of formation of these trumpets is still unresolved.

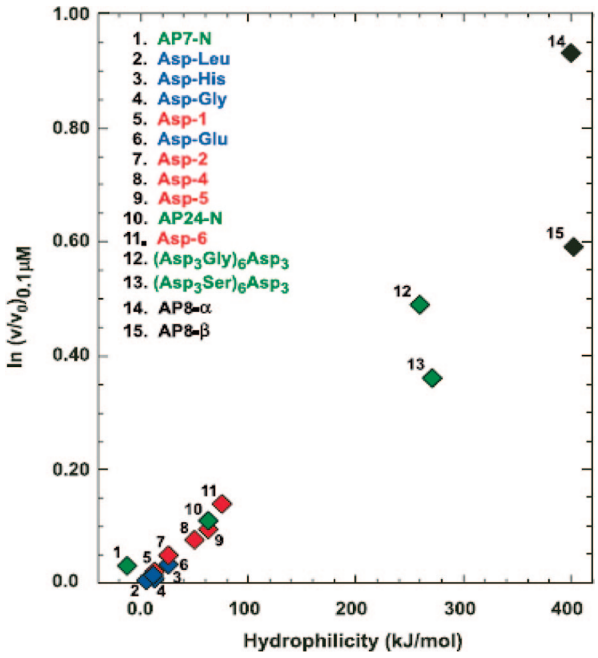

Figure 46. Graph showing the relationship between calcite growth and the hydrophilicity of the additive at a concentration of 0.1 μM. Logarithm of normalized step enhancement velocity (relative to the control) at a concentration of 0.1 μM (v/v_0), plotted against the calculated peptide hydrophilicity. Color codes indicate different classes of additives. (Reprinted with permission from ref 254. Copyright 2006 National Academy of Sciences of the United States of America.)

It was demonstrated that the effect of organic additives can work in concert with other additives such as magnesium ions (Figure 49).[40,260] Meldrum et al. precipitated calcium carbonate from saturated solutions of calcium bicarbonate in the presence citric acid (**19**) and malic acid (**24**). Both citric and malic acid interacted with calcite to produce crystals elongated along the *c*-axis. The degree of elongation increased with the organic additive/Ca ratio and was more pronounced for citric than malic acid. When, in addition, magnesium ions were also present, a range of generally rounded shapes, including lobes, dumbbells, oöids, and spherulitic structures (Figure 49), were found. These were identified as high magnesium calcite (Mg^{2+} content: single crystals ~10%, polycrystals up to 22%) rather than aragonite, which implies that the organic additives probably act by inhibiting crystal nucleation and growth (see also section 4.1.3). The action of the organic additives also in the presence of magnesium ions was highly specific, adsorbing on certain crystal faces during growth and producing crystals elongated along the $\langle 00\cdot 1\rangle$ direction.

5.2. Growth in Confined Space

The sites where biominerals are formed are generally sealed-off from the environment by barriers, often formed by vesicles. These barriers regulate the diffusion of ions but are also involved in shaping and positioning the generated mineral particles. It is evident that the design of synthetic systems for the growth of minerals in confined space offers possibilities to control the size as well as the assembly of the crystals and, thereby, in many cases, the properties of the resulting materials. Indeed, micellar systems,[261,262] protein capsules,[263] vesicles,[264,265] synthetic membranes,[266] and microemulsions[267] have been used as container systems for the restricted growth of a large variety of minerals.

Controlling the shape of biominerals by growing them in a confined space that acts as a mold requires two main challenges to be overcome. The first one is the preparation of the mold. This scaffold should, under the mineralization condition used, have or adopt the desired 3-dimensional shape. When using self-assembling systems, one of the main difficulties in achieving this is that very many organic (macro)molecules undergo conformational changes upon interacting with calcium ions and thereby change their self-assembling properties. As a consequence, the shape of the aggregates after addition of the calcium ions may be difficult to determine in advance. Moreover, the growing mineral will impose a force on the template by which it may deform. The second challenge is to prevent the formation of polycrystalline aggregates when single crystals are desired. As many different sites inside the mold can induce heterogeneous nucleation, a special measure must be taken to allow single crystals with the predefined shape to be formed.

In recent years, there has been increasing evidence that in many cases an amorphous precursor phase plays an important role in the formation of complex calcium carbonate structures, as it delays crystallization, thereby, in many cases, avoiding the formation of polycrystalline assemblies in favor of single crystalline forms.[144]

Here Loste and Meldrum demonstrated how crystals with a predefined 3D shape could be formed by using track-etch membranes as a mold.[138,268] In this approach, the calcium carbonate was deposited as an amorphous phase which was temporally stabilized using low temperatures. In a similar approach, Li and Qi recently produced a single crystalline calcite replica of a colloidal crystal.[269] The colloidal crystal composed of polystyrene beads with a poly(methyl methacrylate−acrylic acid) corona was infiltrated with the mineral by sucking it through a solution of ACC. After this, the $CaCO_3$ crystallized and the beads were removed by a dissolution/calcination step, yielding impressive mineral structures. In an alternative approach, Gower and co-workers produced intricate calcite structures using poly(asp) as a structure directing agent (Figure 50).[270] In the following subsections, we will treat the formation of complex calcium carbonate architectures according to the method used.

5.2.1. Self-assembled Systems

Droplets in microemulsions can act as a closed compartment in which mineralization can be performed and therefore mineralization can be confined to the shape of the droplet. However, an important issue in the synthesis of mineral phases using self-assembled templates concerns the shape persistency of these molds under the mineralization conditions. During the process in many cases, a delicate interplay between the organic and inorganic phases gives rise to several transitions before the structure of the resulting material evolves.[271] Also, in the case of reverse micelles, most of the systems are highly dynamic and coalescence can be an important factor contributing to the growth of the inorganic phase. It is obvious that control over the stability of the template is essential for its successful transcription on both the atomic and the mesoscopic levels.

The first report on the use of an emulsion system to control the formation of calcium carbonate was published by Nakahara et al. already in 1979.[221] As discussed previously,, these authors used nonionic surfactants to prepare water-in-oil-in-water (W/O/W) dispersions consisting of droplets of aqueous K_2CO_3 prepared inside a volume of benzene that

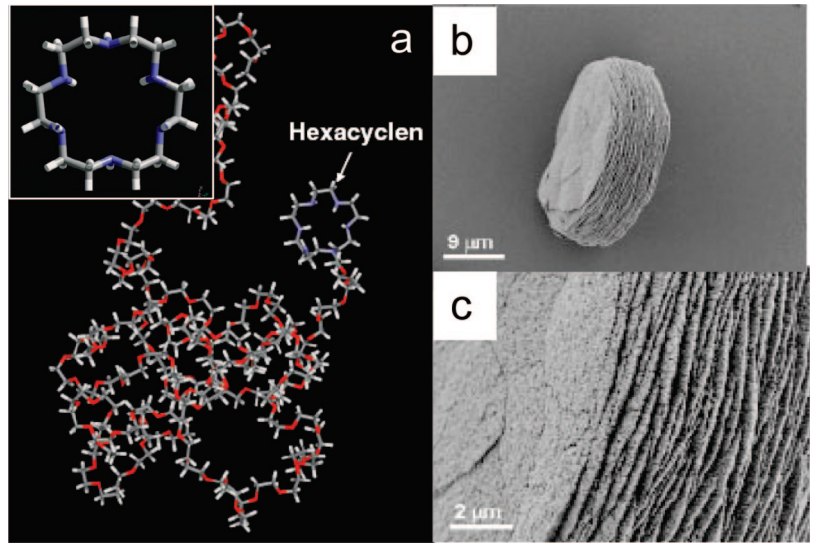

Figure 47. (a) Molecular model of the poly(ethylene oxide)−hexacylen block copolymer **41**. Inset: model of the hexacyclen structure. (b) SEM images of stacks of the pancake-like calcite crystals. The stacks had diameters of 26−29 μm and a thickness of ~8 μm. (c) Stacks at higher magnification. (Reproduced with permission from ref 257. Copyright 2005 Wiley-VCH Verlag GmbH & Co. KGaA, Weinheim.)

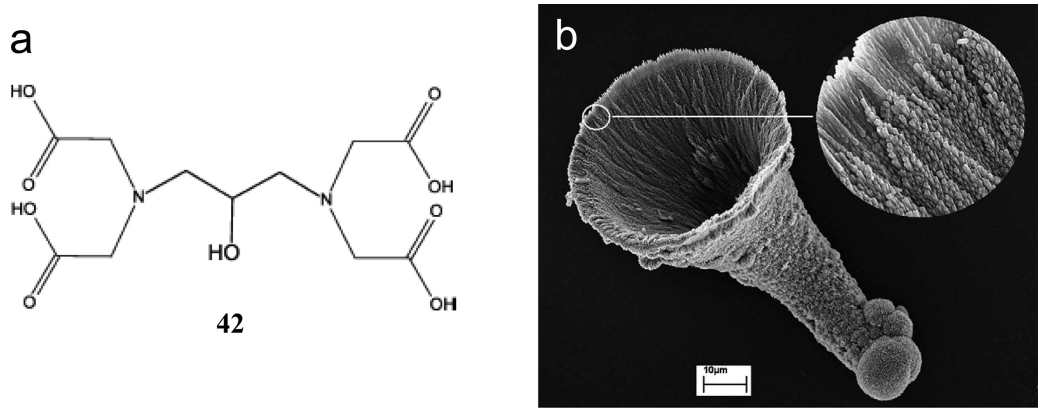

Figure 48. (a) Molecular structure of 1,3-diamino-2-hydroxypropane-*N*,*N*,*N*,*N*-tetraacetate (**42**). (b) A calcite microtrumpet formed in the presence of **42**. (From ref 258 (http://dx.doi.org/10.1039/b401754d). Copyright 2004. Reproduced by permission of The Royal Society of Chemistry.)

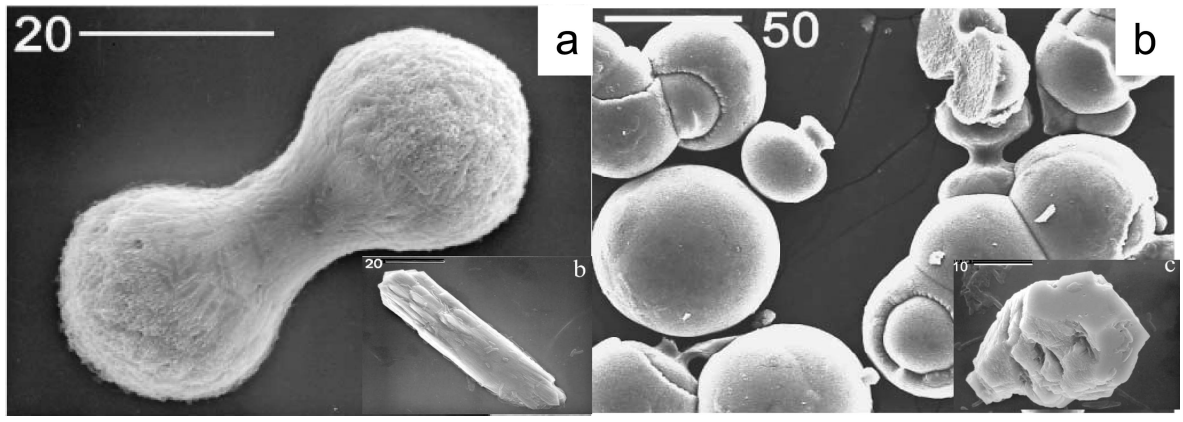

Figure 49. (a, b) High magnesium calcite particles formed in the presence of magnesium ions and organic additives. (a) Dumbbells formed in the presence of citric acid (**19**) and oöids formed in the presence of (b) malic acid (**24**). Insets: crystals formed in the presence of the organic additives but in the absence of magnesium ions. (Reprinted from ref 40, Copyright 2001, with permission from Elsevier Limited.)

in turn is stably dispersed in an aqueous calcium chloride solution. In this system, the calcium ions are transferred into the internal aqueous phase, where they form vaterite spheres that are confined to the dimensions of the internal aqueous phase. Although excellent control over polymorph selection was obtained, the polydispersity of the reverse micelles led to a broad range of particle sizes with diameters ranging from 1 to 15 μm.

In a related system, Hirai and co-workers found similar results with a related surfactant for a kerosene-based emul-

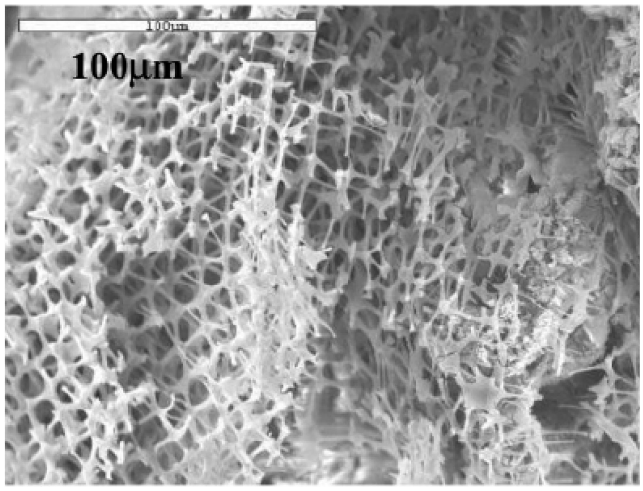

Figure 50. PHEMA replica of a sea urchin spine mineralized in the presence of a polymeric process-directing agent. A region of the calcite after calcination in which the structure appears similar to the central core region of the urchin spine. (Reprinted with permission from ref 270. Copyright 2006 American Chemical Society.)

sion in which they used bis(2-ethylhexyl)phosphoric acid (D2EHPA, **43**) to efficiently shuttle calcium into the inner aqueous compartment.[272] Also, this pseudovesicular double emulsion produced spherical particles of vaterite with diameters in the same range as those for the "vesicles". In this case, however, the authors demonstrated that the particles are hollow, which implies that the mineralization reaction indeed takes place at the oil−water interface. More in particular, as the nonionic surfactant used (Span-83) is not expected to efficiently interact with the ions in the inner aqueous compartment, the localized mineralization as well as the selectivity for vaterite can be attributed to the high local supersaturation caused by the efficient shuttling action of the D2EHPA.

It was demonstrated also that single W/O emulsions can be used as microreactors in which the formation of the inorganic phase is restricted by the dimensions of the aqueous phase. Mann et al. demonstrated that the dispersion of an outgassing supersaturated solution of $Ca(HCO_3)_2$ in octane, using SDS as the surfactant, leads to vaterite particles with a sponge-type appearance (see section 4.2.2 and Figure 34).[216] These arise from confined growth in the reversed micelles around the evolving gas bubbles. Studies of particles isolated during the early stages of the reaction showed that they were formed initially at the oil−water interface and around the bubbles that are trapped at this interface, and then grow inward to the core of the droplet. The subsequent entrapment of the CO_2 bubbles then leads to the formation of interconnected pores. Recently, Kang and co-workers demonstrated in a cyclohexane-based microemulsion stabilized by either SDS or AOT that the size of the vaterite particles indeed can be related to the water/surfactant ratio and hence to the size of the aqueous droplets.[273]

The uniformity in size of the vaterite spheroids described by Mann et al. was significantly improved by the use of dodecanol as a cosurfactant (Figure 34b). As dodecanol is known to interpenetrate the surfactant (SDS), thereby stabilizing the emulsion droplets, the observed decease in polydispersity suggests that the coalescence of emulsified droplets is a main issue in obtaining a homogeneous product.

Following a similar approach, Shen et al. investigated the growth of calcium carbonate inside the aqueous phase of the four-component bicontinuous emulsion system *p*-octyl polyethylene glycol phenylether (OP)/*n*-amyl alcohol/cyclohexane/water.[228] The confinement of the mineral to the aqueous phase was nicely demonstrated by the observation of strings of nanocrystals (see section 4.2.2 and Figure 34c).

In contrast, Liu and Yates described the growth of calcium carbonate in a CTAB/pentanol/water/cyohexane-based microemulsion in which the mineral overrules the boundaries given by the aqueous phase. The system initially stabilizes hexagonal vaterite crystals that within 4 days transform into a unique type of prismatic calcite rods (Figure 51).[218] It is obvious that in this case the organic phase is being reassembled by the growth of the inorganic phase rather than predefining the shape of the latter.

Walsh and Mann presented a unique type of cellular framework consisting of a single crystal of aragonite (Figure 52a).[274] The authors prepared a bicontinuous emulsion of supersaturated $Ca(HCO_3)_2$ solution mixtures of hexadecane and tetradecane using didodecyl dimethyl ammonium bromide (DDAB) as the stabilizing surfactant. The mineralization solution was diluted with aqueous magnesium chloride to yield a $[Ca^{2+}]/[Mg^{2+}]$ ratio of 1:5, aiming at the formation of aragonite. It appeared, however, that the outgassing of the CO_2 was severely restricted, possibly by the low solubility of the CO_2 in the oil phase. Only upon application of the emulsion onto a solid substrate and subsequent washing, was the formation of a phase-separated structure induced that subsequently acted as the template for the mineral formation. This method could also be applied to form these cellular frameworks around polystyrene spheres that were later removed by dissolution in organic solvent (Figure 52a, inset). It should be noted that, even though the mineral growth did not truly follow the templating structure laid out by the bicontinuous emulsion system, the formation of these single crystalline hollow shells of mesoporous aragonite is still one of the most complex and intruiging biomimetic structures achieved to this date.

As explained earlier (section 4.2.2), the same group explored the use of surfactant-stabilized ACC precursor particles to grow crystalline calcium carbonate inside the aqueous compartments of a reverse micellar system.[223,225] In this system, the shape of the particles is controlled to some extent through the strength of the surfactant−crystal interactions, which, in turn, depend on the net charge of the crystal surface. The conversion from ACC to vaterite to aragonite is controlled by regulating the amount of water that is available in the compartment to mediate the dissolution−reprecipitation process. In the case of a higher water/surfactant ratio ($W = 20$), this leads to the formation of a complex network of interconnected nanofibrils (Figure 52b) with an average width of 12 nm that assemble to form large well defined micrometer sized doughnut-like structures (Figure 52b, inset). This again exemplifies how complex hierarchical structures can evolve from the dynamic interplay between an adaptable template and the developing inorganic phase.

5.2.2. Patterning Crystals

As was mentioned before, metal-on-metal patterns can be used to create self-assembled monolayers with different packing densities of the same ω-functionalized alkanethiol. Aizenberg and co-workers demonstrated that these patterns consisted of three regions: the SAM on metal 1, the SAM on metal 2, and the interfacial region, which have different

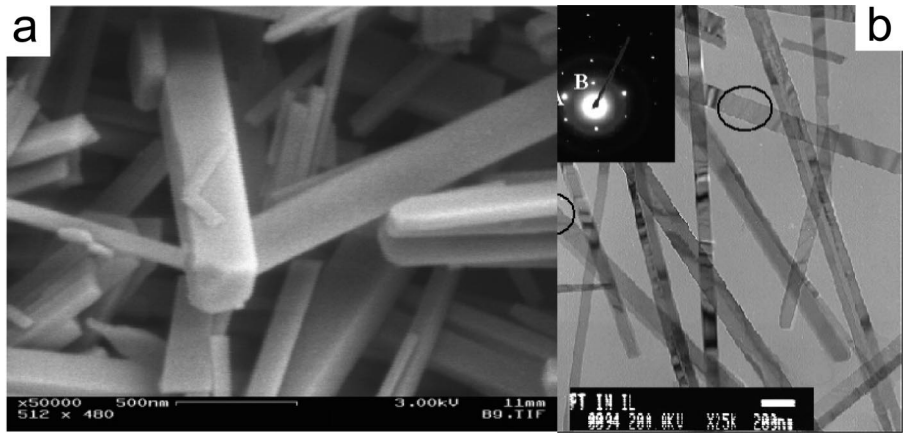

Figure 51. SEM (a) and TEM (b) images of rod-shaped prismatic calcite crystals synthesized in CTAB/pentanol/water/cyohexane microemulsions. Inset: SAED pattern of [11•0] calcite. (Reprinted with permission from ref 218. Copyright 2006 American Chemical Society.)

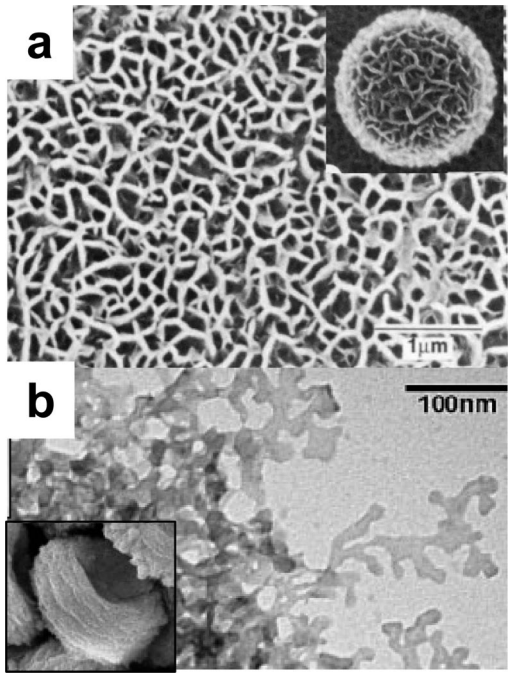

Figure 52. (a) SEM from a cellular framework of aragonite produced from a bicontinuous microemulsion. Inset: cellular frameworks formed around polystyrene spheres. Image recorded after removal of the polystyrene (Reprinted with permission from ref 274. (b) TEM image of a porous network synthesized from surfactant stabilized ACC nanoparticles inside a reverse micellar system. Inset: SEM image of the doughnut-like superstructure formed by the porous network. (Reproduced with permission from ref 225. Copyright 2003 Wiley-VCH Verlag GmbH & Co. KGaA, Weinheim.)

nucleation capacities for calcium carbonate (Figure 17).[11] Due to the local disorder, the interfacial region has the highest nucleation induction power, which can be used to create line patterns of calcium carbonate crystals. The contours of the interfacial region control the patterning of the crystals, which in principle can be varied by changing the characteristics of the metal-on-metal pattern.

After this first nucleation at the interfacial region, crystals will start to nucleate preferentially on one of the two patterns; in the case of Ag/Au structures, crystal growth will take place on the SAM on silver. This allows the creation of surface patterns of crystals with different forms and shapes, depending on the shape and order of depositon of the metal layers.[275]

In a second approach, the same group showed that patterns of calcite crystals can be obtained by using the difference in nucleation power between active (e.g., carboxy-terminated) and inactive (methyl-terminated) surfaces.[276] This method relies on the concentration gradient that is induced by the local depletion of calcium and carbonate ions caused by the crystal growing at an active nucleation point.[11] This concentration gradient will give rise to a mass transport to the growing crystal, thereby lowering the ion concentrations in the region outside the active nucleation area to an understaturation level. In this way, the nucleation of new crystals outside this area is prevented. By choosing the appropriate supersaturation levels and the sizes and distances of the active nucleation areas, even patterns of discrete individual crystals of uniform size could be obtained (see also discussion on page 46, Figure 18). Moreover, by selecting the appropriate combination of metal surface and functional alkanethiol, the crystallographic orientation of these crystals can be chosen as well. In addition, the growth of these crystals into complex patterns can also be achieved.

5.2.3. Patterned Films of Calcium Carbonate

As was mentioned previously, several anionic polymers such as poly(aspartate), poly(glutamate), and poly(acrcylic acid) (PAA) are able to temporarily stabilize ACC. This feature, which has been excellently reviewed,[5] has been used by several groups to obtain thin films of ACC that subsequently transform into one of the crystalline polymorphs.[277−292] Gower and co-workers discovered that this process may involve a so-called polymer-induced liquid-precursor (PILP) phase.[281] This concerns a sequence of events that is not yet entirely understood but which involves a liquid−liquid phase separation resulting in droplets of a calcium-rich liquid. This liquid phase forms depositions and converts to a solid, but amorphous, material that subsequently transforms into a thin polycrystalline layer with a mosaic structure.[282,293] Although generally calcite is formed, more recently, also tablets of aragonite were obtained in the presence of magnesium ions.[293]

A structured template was prepared by using a phase-separated monolayer film of a polymerizable surfactant, **44**, that inhibits mineralization and stearic acid, which promotes mineralization (Figure 53).[294] With this 2D pattern, the growth of the PILP-derived calcium carbonate film can be

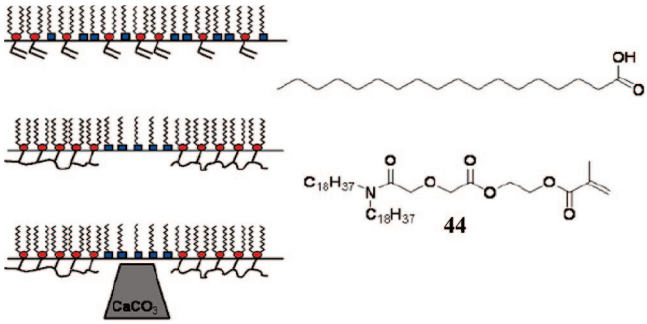

Figure 53. Schematic representation of the formation and polymerization of a phase-separated two component monolayer of **44** and stearic acid. As **44** inhibits mineralization, crystals only form under domains of stearic acid. (Reprinted with permission from ref 294. Copyright 2006 American Chemical Society.)

confined to predefined regions of which the size and shape can be regulated during the monolayer formation procedure.

The amorphous phase can also be used to produce pattered films of calcium carbonate with dimensions on the order of several hundreds of micrometers. In this work, the amphiphilic ABA block copolymer poly(hydroxylethyl methacrylate)-*b*-poly(methylphenylsilane)-*b*-poly(hydroxylethyl methacrylate) **45** was used to prepare a thin polymer film on a glass substrate (Figure 54).[295] By UV irradiation through a mask, exploiting the photolytic properties of polysilane block, this hydrophobic block was locally degraded but left in place. When exposed to a mineralization solution, discrete crystals (a mixture of calcite and vaterite) formed on both the irradiated and nonirradiated lanes. Whereas the crystals were firmly adhered to the intact polymer, from the irradiated areas, they could be easily and efficiently removed.

By using a PAA containing mineralization solution, a thin film of ACC with a thickness of $\sim$1 μm was deposited on both the irradiated and nonirradiated areas. Also in this case, the calcium carbonate layer strongly adhered to the intact polymer film but was easily removed from the irradiated areas by a simple washing with ethanol. This, however, was only possible as long as the calcium carbonate was still present in its amorphous form; after transformation to the crystalline polymorphs (a mixture of calcite and vaterite), the calcium carbonate persisted on the polymer film, whether irradiated or not.

A similar approach was employed by Vokmer, Klok, et al., who used photopatterned surfaces from which PMAA brushes were grown (Figure 55).[296] When exposed to a calcium carbonate mineralization assay, the resulting polymer pattern was accurately reproduced by the deposition of ACC that was transformed into calcite by heating. This method, however, not only allows the deposition of the patterned calcium carbonate film with a high fidelity in the lateral dimensions, it also allows a precise control over the thickness of the film though the length of the polymer brushes. A precise regulation of the polymer length can be easily achieved through the SI-ATRP method used by the authors.

Interestingly, in an earlier and very similar approach, the Qi group showed that the layer-by-layer deposition of alternating layers of a photodegradable nitro-diazo resin and polyacrylic acid can be used to create patterns of calcium carbonate (Figure 56).[297] These authors used a mask to create different patterns of the multilayer polymer structure with a PAA top layer. Calcium carbonate was formed in the presence of this template with additional PAA as additive in the solution.

The effect of the PAA was demonstrated to prevent the formation of individual single crystals and to lead to the formation of crystalline films. However, rather than smooth films generally observed in the presence of a crystallization inhibitor such as PAA, here the formation of rough films consisting of intergrown (10•4) oriented crystals was observed. This suggests that mineral deposition and crystallization occurred simultaneously. In this respect, it is interesting to compare these results to those obtained by Sommerdijk et al.[144] They showed that the crystallization of thin ACC films, formed with DNA as the inhibitor, was accelerated when these films were deposited on a LbL coating that also had DNA as the top layer. In a similar manner, the presence of PAA as a top layer may induce crystallization already to occur during the deposition process in the experiments of Qi et al.[297]

Exploiting the possibility to preferentially deposit calcium carbonate on surfaces with exposed polar functionalities, Gower and co-workers used patterned arrays of SAMs on gold (Figure 57).[298] The arrays contained a pattern of COOH terminated alkanethiols in a background of methyl terminated thiols. Mineralization in the presence of PAA leads to the formation of amorphous films that transform into large crystalline domains of calcite following the pattern of the carboxy terminated SAM. In two experiments, where only one of the two thiols was present against a background of bare gold, it was demonstrated that this effect was not due to specific interaction of the carboxylates with the $CaCO_3$. When a COOH-terminated thiol was used, this leads to the preferential, but not selective, deposition of the mineral on the SAM. In the case where the methyl-terminated SAM was used, this leads to the formation of a $CaCO_3$ pattern preferentially on the gold, with only a thin layer of mineral on the SAM. Also, in these examples, it is noticed that the mineral crystallizes rapidly on the carboxylated SAM while it remains amorphous on the noninductive gold surface or methyl-terminated SAM.

Inspired by the sophisticated arrays of calcium carbonate microlenses found in brittlestars, Aizenberg and co-workers demonstrated a synthetic system that allows the *predetermination* of not only the shape but also the crystallographic orientation of the inorganic thin film (Figure 58).[299] They used a carefully designed crystallization template consisting of a surface patterned with pillars around which a self-assembled monolayer was deposited. The monolayer was composed of a precise mixture of alkanethiols of different lengths and containing different end groups (-OH, OPO_3^{2-}, $-CH_3$). This monolayer inhibited the formation of calcite and induced the formation of amorphous calcium carbonate (ACC). Exposure of this surface to a mineralization solution resulted in the formation of a continuous, uniform film of ACC deposited around the pillars. The crystallization of this film was subsequently induced by a small region of COOH terminated alkanethiol also present in the SAM. Remarkably this led to the formation of single crystals of calcite with predefined shape of micrometer dimensions. X-ray diffraction measurements of the produced crystals showed the selective nucleation depending on the type of functional groups and the metal surface used.

It was demonstrated that the dimensions of the pattern were important for obtaining a patterned single crystal. In the absence of a pattern, the ACC transformed into a polycrystalline film. It was hypothesized that the holes in the inorganic film allowed the water confined in the ACC to be

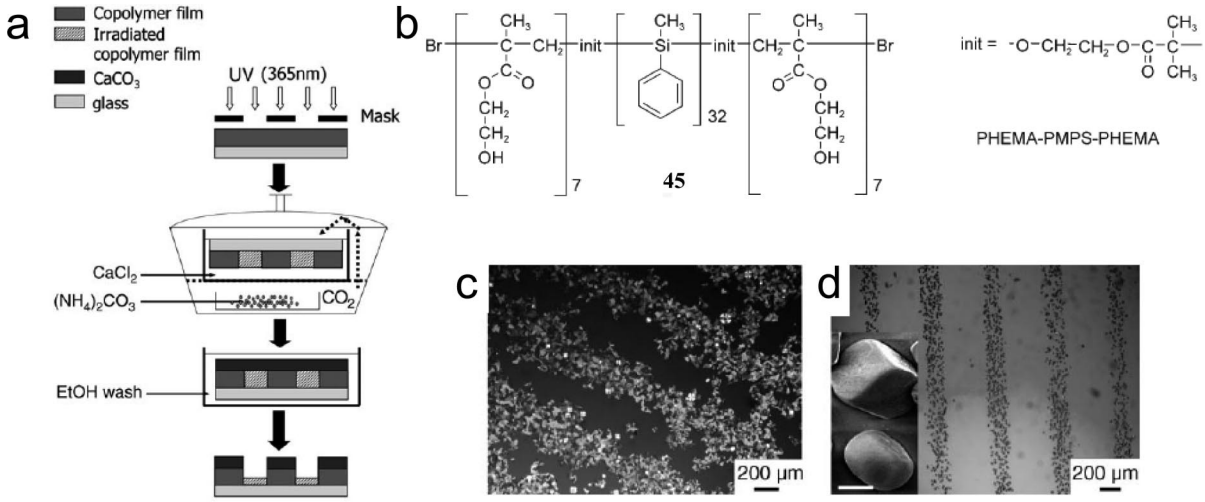

Figure 54. (a) Schematic representation of the experimental procedure for the generation of patterns of $CaCO_3$. (b) Structure of the PHEMA-PMPS-PHEMA copolymer **45**. Optical micrographs under cross-polarized light of (c) a patterned crystalline $CaCO_3$ film prepared in the presence of PAA and (d) a pattern of discrete calcite and vaterite crystals, obtained in the absence of PAA. Inset in part (d): SEM image showing a calcite (top) and a vaterite (bottom) crystal (scale bar: 10 mm). (Reproduced with permission from ref 295. Copyright 2006 Wiley-VCH Verlag GmbH & Co. KGaA, Weinheim.)

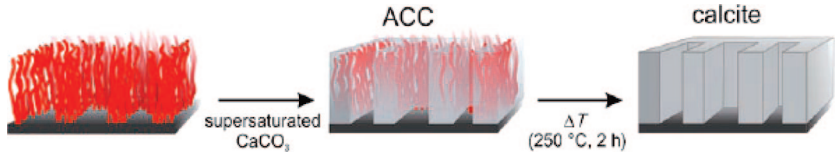

Figure 55. Schematic representation of the fabrication of microstructured calcite films. Left: Synthesis of PMAA brushes from photolithographically patterned ATRP initiator functionalized substrates. Middle: Directed deposition of a thin, metastable layer of amorphous calcium carbonate (ACC). Right: the subsequent temperature induced transformation of the metastable ACC layer into a microstructured, polycrystalline calcite film. (Reproduced with permission from ref 296. Copyright Wiley-VCH Verlag GmbH & Co. KGaA, Weinheim.)

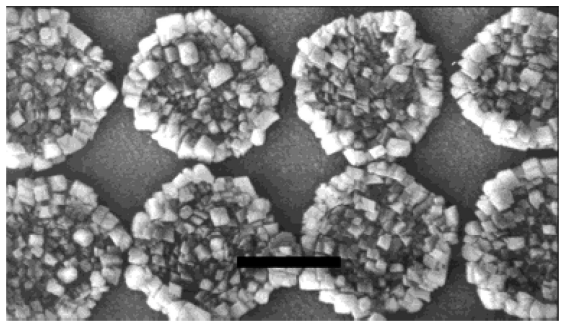

Figure 56. SEM image of an isolated island of $CaCO_3$ films grown on the micropatterned (nitro-diazo resin /PAA)$_6$ film produced using a photoresist mask. Scale bar: 5 μm. (Reprinted with permission from ref 297. Copyright 2004 American Chemical Society.)

expelled from the developing crystal. Using water soluble fluorescent dyes, the authors demonstrated that the water indeed ends up collected around the pillars and that the dimension of the pores in the film increases in going from the amorphous to the crystalline film. A progressing crystallization front that is preceded by a water layer, separating the front from the remaining ACC, argues for mass transport between the amorphous and crystalline phases rather than for a solid-state transformation. Such a mechanism was also demonstrated by experiments on mercaptophenol-based SAMs that clearly showed the dissolution of the ACC around developing calcite crystals (Figure 18).[104,300]

From these observations, the authors remark that "when single crystals are the biomaterial of choice and their formation occurs through an amorphous phase, the development of large, solid structures is unlikely because of mechanical stresses caused by the release of water and macromolecules".[299] This suggests that the organic material included in the crystals not only can act as as structural templates but also will provide sites for stress relaxation and impurity discharge, necessary for the formation of large, and consequently, microporous single crystals.[301,302] It should be noted that this mechanism is different compared to the process proposed for the PILP process,[281] in which the transition occurs in a pseudomorphic fashion, i.e. through the reorganization of the atoms within the boundaries of the amorphous phase, as in a solid state transformation, but aided by the presence of water molecules.

6. Preparing Hybrid Materials

In previous sections, we have described the interaction of designer molecules and surfaces with the different phases of calcium carbonate. In several cases, we may expect that the additives may become included in the inorganic phase. For example, the inclusion of surface bound molecules inside the crystalline forms of calcium carbonate may be expected during overgrowth experiments[278,303] but also during the formation of mesocrystals from polymer stabilized building blocks.[304−308] As in biominerals, the coprecipitation of organic matter is directly related to their unique materials properties; it therefore is interesting to analyze to what extent additives used to control the formation of calcium carbonate become part of the resulting mineral. However, in general, very little information is available on the inclusion of organic molecules in the inorganic phases. This is mainly due to the difficulty of analyzing these small quantities of organic

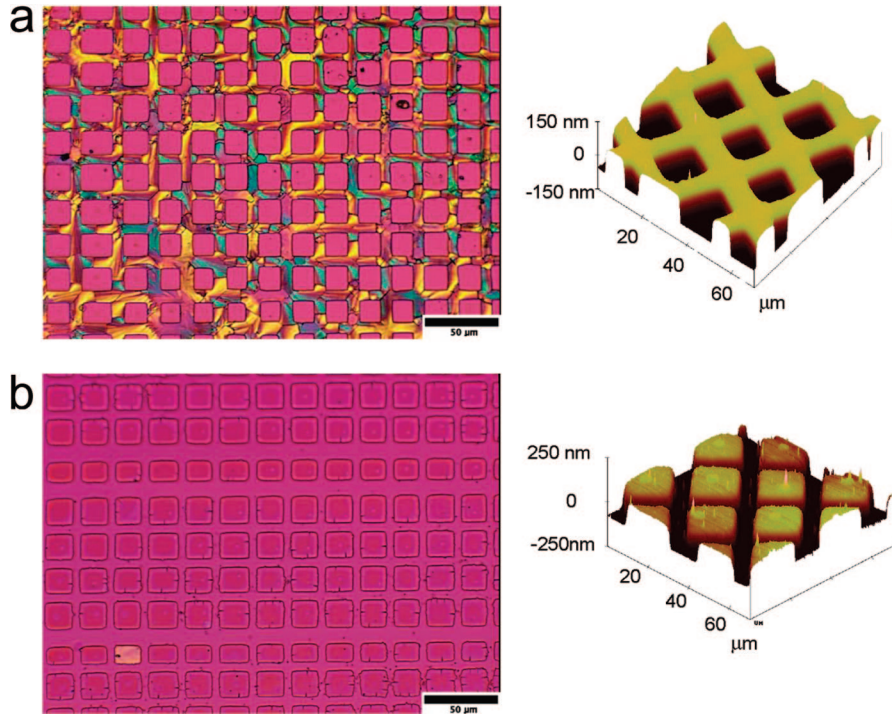

Figure 57. Optical micrographs (left) using crossed-polarizers and AFM 3-D height images (right) of calcium carbonate films formed through preferential deposition of mineral films on SAMs of different end-group functionality, 42 days after removal from the reaction solution. (a) Using surfaces patterned with COO^--terminated SAMs on the grid area and bare Au on the interior area (square regions) produced birefringent calcite films that match the exact pattern of the grid area of the SAM template. The surface topology from the AFM image (right) confirms that the mineral deposited selectively on the grid area (COO^--terminated SAMs). (b) Using surfaces patterned with CH_3-terminated SAMs on the grid area leads to the opposite patterning. The lack of birefringence indicates the films are still amorphous. The surface topology of the AFM image confirms the mineral deposited selectively on the interior square areas (on bare Au). (Reprinted with permission from ref 298. Copyright 2007 American Chemical Society.)

material. In a number of approaches, researchers have demonstrated the intimate mixing of the mineral and the intercrystalline organic phase, while, in a few cases, researchers obtained evidence for the inclusion of organic molecules in calcium carbonate crystals, as we will discuss below.

6.1. Organic Material in Biominerals

The structure of nacre is characterized by stacked tables of aragonite that are sandwiched between layers of organic material, consisting of an insoluble layer of chitosan and silk-like hydrophilic macromolecules with adhered acidic macromolecules (Figure 59).[112] One of the special features of nacre is its mechanical strength: it is ~3000 times more fracture resistant than pure aragonite, its main component. This outstanding mechanical characteristic has been attributed to its particular composite structure, in particular related to the intercrystalline proteins (Figure 59).[309] Inspired by the possibility to obtain new materials with improved properties, several research groups have investigated a variety of routes to obtain different calcium carbonate-based organic−inorganic hybrid materials.

Where in biominerals the presence of intercrystalline organic material has been clearly demonstrated, there is also compelling evidence that organic molecules are actually enclosed within the crystal structure. For example, a single crystal of inorganic calcite cleaves easily along the (10·4) planes.[310] The skeletal elements of sea urchins, which are also single crystals of calcite, however, not only fracture with more difficulty, they also produce conchoidal fracture surfaces, as generally are found in amorphous glasses. This behavior is most likely related to the acidic proteins present inside these elements.[311,312] It has been demonstrated that the proteins are only released upon dissolution of the crystal and must therefore be occluded inside the crystal as opposed to the intercrystalline material found, e.g., in between the nacreous plates of mollusk shells. Recently, intracrystalline material was indeed visualized by acetic acid etching of prismatic calcite crystals from mollusk shells.[313]

The perfect order in a crystal only exists over a relatively short distance, the so-called coherence length. After this characteristic length, the perfect translation of symmetry as defined by the unit cell is perturbed by imperfections or dislocations. It is obvious that the introduction of organic (macro)molecules inside the crystal lattice will cause additional disturbance and lead to a decrease of the coherence length.[311,312,314] In vitro experiments using acidic proteins extracted from the sea urchin spines have shown that the acidic proteins become located at the boundaries of crystal domains and that the average coherence lengths are significantly smaller than those of pure calcite crystals. Inside these crystals, the proteins are preferentially adsorbed on the set of {11·0} planes of the crystal, parallel to its crystallographic *c*-axis (Figure 59). As a consequence, these crystals also do not cleave along the {10·4} planes, but produce conchoidal fracture planes, as was observed for the sea urchin spines.

In addition, it has been found that, in biogenic calcite and aragonite, the inclusion of macromolecules in fact leads to a distortion of the crystal lattice, which can be released through the removal of the organic material by annealing.[315−317] High resolution powder diffraction studies subsequently supported the model that the inclusion of acidic macromolecules in

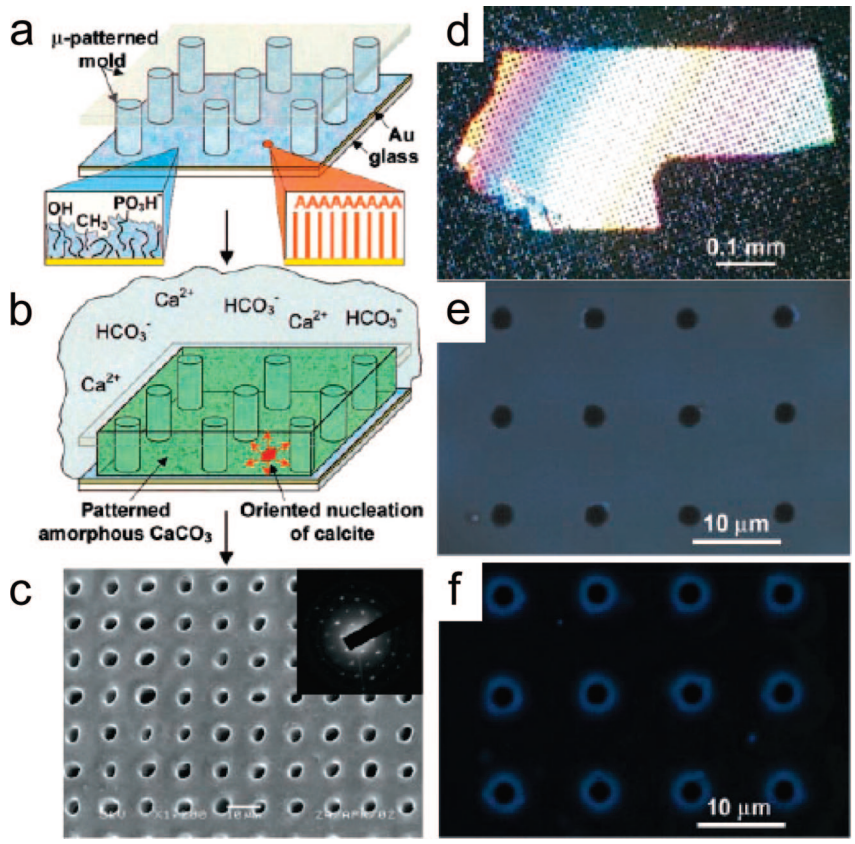

Figure 58. (a) Schematic representation of the micropatterns consisting of a square array of posts, with the feature sizes of $<10\ \mu$m and an aspect ratio of >1 coated with a transparent 5−10 nm-thick film of gold or silver. A nanoregion (red circle) of a SAM of $HS(CH_2)_n$-X (X = OH, CO_2H, SO_3H) that induces the nucleation of calcite in a controlled orientation. (b) Calcium carbonate deposition using the gas diffusion method leading to the formation and subsequent crystallization of the calcium carbonate film. (d) Polarized light micrograph of a micropatterned single calcite crystal in the [10•4] orientation formed within the ACC film. (e, f) Fluorescence micrographs of the ACC film and its corresponding calcite crystal grown in the presence of a fluorescent additive in the crystallizing solution. The even distribution of the dye in the ACC phase and its exclusion from the growing crystal and buildup at the post interfaces hint at the "microsump" function of the micropatterned framework. (From ref 299 (http://www.sciencemag.org). Reprinted with permission from AAAS.)

biogenic calcite occurs on the crystal planes that are parallel to the crystallographic *c*-axis.[318] This should occur by the specific interaction of the acidic (aspartic and glutamic) acid residues that can replace the carbonate ions in these planes. With such interactions, the lattice distortion would be maximal in the direction perpendicular to the plane of the carbonate ions, indeed in the direction of the *c*-axis.

6.2. Synthetic Hybrids with Intercrystalline Material

The preparation of the material most closely related to the natural nacre was reported by Cölfen and co-workers, who showed that a near identical nacreous assembly could be obtained by retrosynthesis.[319] This method involved the removal of the calcium carbonate and soluble proteins from the natural structure of *H. laevigata* and the subsequent reinfiltration of the remaining structure with PAA stabilized ACC using the gas diffusion method. The resulting materials were indistinguishable from natural nacre but for one important feature: the mineral phase consisted of calcite instead of aragonite. Nevertheless, its mechanical properties were certainly promising, as elastic moduli as high as 37.7 GPa were determined.[320]

Zhang and co-workers have mimicked the structure of nacre by using a layer-by-layer (LBL) approach in which organic polymer layers constructed by the LBL self-assembly method were alternated with layers of calcium carbonate prepared by the ammonium carbonate diffusion method (Figure 60).[321] By repetitively allowing PAA and diazo resins to adhere to the substrate, a polymeric layer was created of which PAA formed the first and the last layer. This film was then dipped into a solution containing calcium chloride and subsequently was exposed to ammonium carbonate. By the number of repeats, the thickness of the polymer film can be regulated while the time of exposure to ammonium carbonate determined the thickness of the calcium carbonate films that crystallized as a mixture of calcite, vaterite, and aragonite.

6.3. Inclusion of Organic Molecules inside $CaCO_3$ Crystals

As mentioned, recently, thin films of calcite and aragonite were grown under Langmuir monolayers of amphiphilic macrocycles with PAA as the additive and in the presence or absence of Mg^{2+} ions.[322] The diffraction patterns of both the calcitic and the aragonitic phases showed a distortion from the "pure" unit cells which is suggestive of the inclusion of polymer in the crystal structure.[323]

The occlusion of organic molecules in a calcium carbonate crystal was elegantly demonstrated by Estroff and co-workers, who performed mineralization experiments inside a self-assembled hydrogel of a bis-urea gelator molecule containing pendant acid groups **46** (Figure 61).[324] Initially calcite crystal with a normal rhombohedral morphology developed inside the gels. However, after a few hours, these

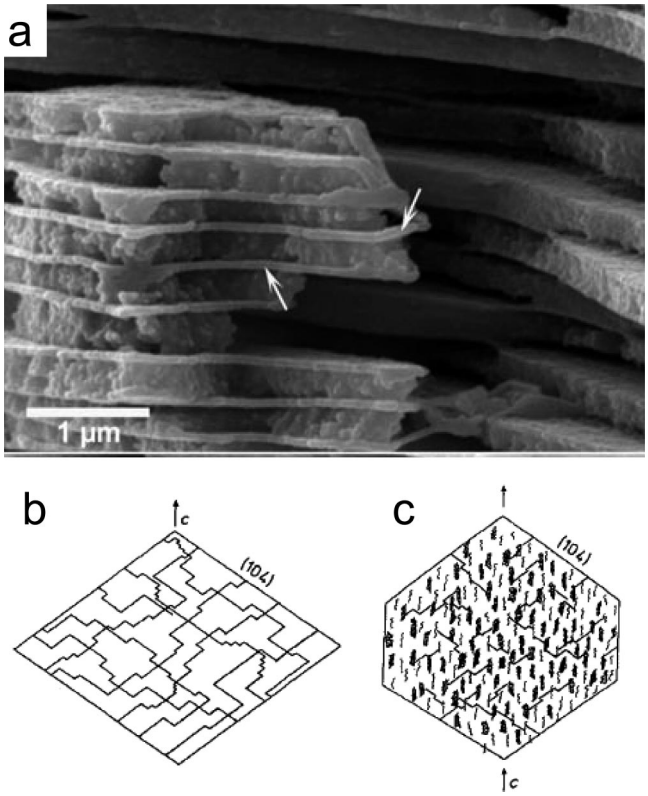

Figure 59. (a) Scanning electron microscope images of a fracture section of Nautilus nacre, the interlamellar sheets visible as layers between the etched mineral tablets (arrows). (Reproduced with permission from ref 112. Copyright 2006 Wiley-VCH Verlag GmbH & Co. KGaA, Weinheim.) (b) Schematic representation of cleavage patterns in a pure calcite crystal, a calcite crystal with intercalated sea urchin proteins. The cleavage planes are always parallel to the (10·4) faces. The protein is occluded on the three symmetry-related sets of {11·0) planes parallel to the *c*-axis. (Reproduced with permission from ref 310. Copyright 1992 Wiley-VCH Verlag GmbH & Co. KGaA, Weinheim.)

crystals developed severe imperfections at their surfaces which looked like etch pits. Similar morphologies were obtained when the crystals were removed from the gel and placed in aqueous medium, while standard calcite was not etched significantly when placed in a solution of the gelator molecule. These results indicate that the occlusion of the gelator is responsible for the altered solubility of the calcite crystals, a phenomenon that may be related to the observed differences in solubility of different biogenic crystals.

Also in biological systems, calcium carbonate crystals grow inside a hydrogel matrix. This aspect is of great importance, as it strongly determines the diffusion of ions, and thereby the kinetics of crystal nucleation and growth. Accordingly, this topic has been investigated by several groups using hydrogels from biological as well as from synthetic origin.[270,325−329] Estrof and co-workers combined this aspect of biomimetic mineralization with the possibility to control the oriented nucleation of the crystals.[330] Crystals were grown inside an agarose-based hydrogel, in which a SAM of ω-mercapto hexadecanoic acid on gold was placed (Figure 62). The activity of the SAM resulted in the formation of crystals mostly on the SAM, rather than in the bulk of the gel. Moreover, the majority of the crystals had nucleated from the (01·2) plane, as was expected for this monolayer. The crystals developed with rhombohedral faces, as opposed to the starlike crystals that are observed without the presence of the SAM. Also in this case, the crystals developed etch pits upon prolonged presence in the hydrogel, indicating their dissolution due to the incorporation of the gel fibers. Importantly, the presence of the gel changes the aspect ratios of the crystals grown on the SAM.

As was discussed previously, crystals grown on SAMs in the absence of the gel have a higher aspect ratio (length/with), which has been attributed to a lattice match between calcite and the SAM in the [10·0] direction (length) but a mismatch in the [12.$\bar{1}$] direction (width).[331] This aspect ratio decreases to almost half for crystals grown in 3% w/v agarose (Figure 62). It is proposed that this observation may be related to the incorporation of gel fibers inside of the calcite crystals, which may change the kinetics of growth, and thus the morphology, by altering the interface energy of the crystals.

A more direct demonstration of the inclusion of organic polymers inside single crystals was given by the growth of calcium carbonate in the presence of sulfonated π-conjugate polymers.[186] In the presence of **47**, which only carries sulfonated side chains, fluorescent {10·4} oriented calcite crystals are formed (Figure 63). Dissolution of the crystal surface by etching with acid affects the shape but not the fluorescence of the crystals, confirming that the polymers are not just adsorbed to the surface of the crystals but actually occluded in the crystal. Through the addition of Mg^{2+}, both fluorescent aragonite spherulites and fluorescent amorphous films could be obtained for both **47** and **48**.

Depending on the process used, the inclusion of acidic macromolecules in ACC may be regarded as a rather obvious consequence of their interaction with the constituting inorganic ions in solution prior to their coprecipitation. Cölfen and co-workers reported that the ACC stabilized by phytic acid contained ~5 wt % of the stabilizer. Similarly, Groves et al. determined the amount of PAA in the amorphous film to be approximately 7%.[282] Nevertheless, after transformation of the poly(aspartic acid)-stabilized amorphous phase, Gower et al. were not able to detect any organic polymer in the crystalline film using X-ray microanalysis.[332] In this study, the analysis of some parts of the films was indicative of the presence of calcium carbonate hexahydrate, an unstable crystalline phase that has been reported to be stabilized by, e.g., polyaspartate, which suggests that some polymer must have been present also in the crystalline state.

An interesting case in this respect is formed by the polymer brushes of Volkmer and Klok.[296] Although no direct evidence was provided, the brushes must be occluded within the ACC formed. Furthermore, as the thickness of the mineral layer is similar to the height of the brush, it suggests that the polymer must be included also in the calcitic film.

6.4. When Is Organic Material Really Included in the Crystal?

Considering the fact that even single crystals of calcite are not necessarily a continuous inorganic phase, the assignment of materials as either intercrystalline or intracrystalline is not always straightforward. Aizenberg et al. have shown that the aqueous phase and associated impurities can be pushed out of the mineral film upon crystallization.[299] It may therefore be expected that during the crystallization of ACC also a part of the stabilizing macromolecules become excluded from the crystal to form intercrystalline material or even may be completely excluded from the mineral phase. Based on their observations in the formation of mesocrystals, Cölfen et al. propose a model in which the additive (PSS)

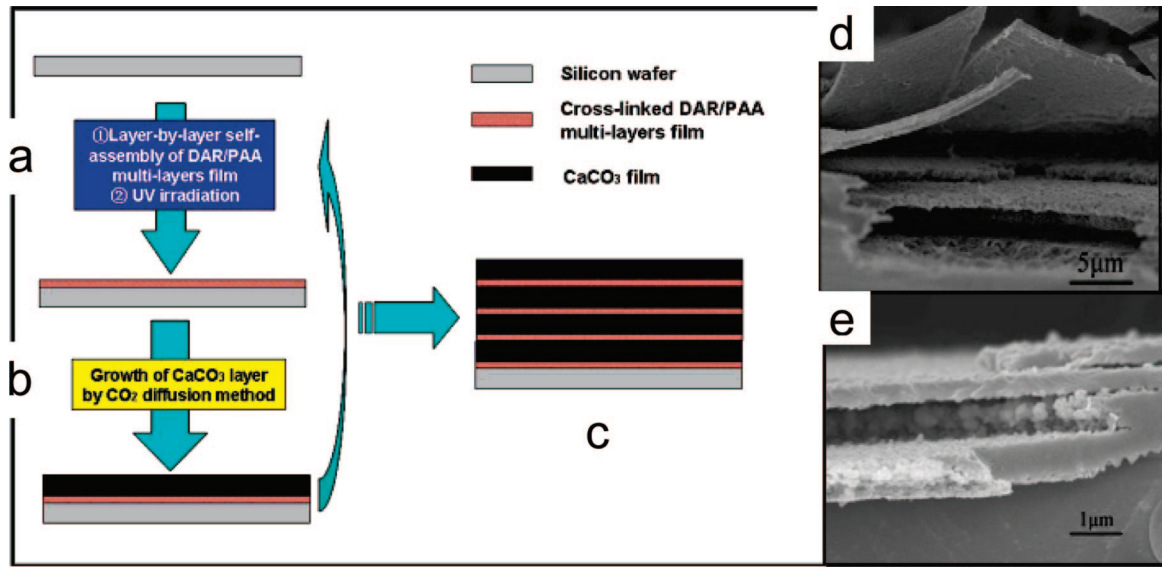

Figure 60. (a−c): Schematic illustration for the fabrication of artifical nacre: preparation of the multilayer organic/inorganic hybrid composite by alternately repeating steps (a) and (b). (d, e) SEM images of the cross section of the artificial nacres with different layers prepared by cyclic fabrication of DAR/PAA multilayered films and $CaCO_3$ layers. (Reprinted with permission from ref 321. Copyright 2007 American Chemical Society.)

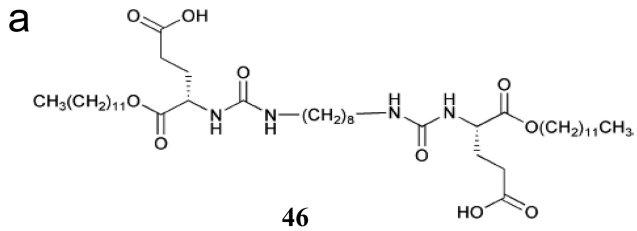

46

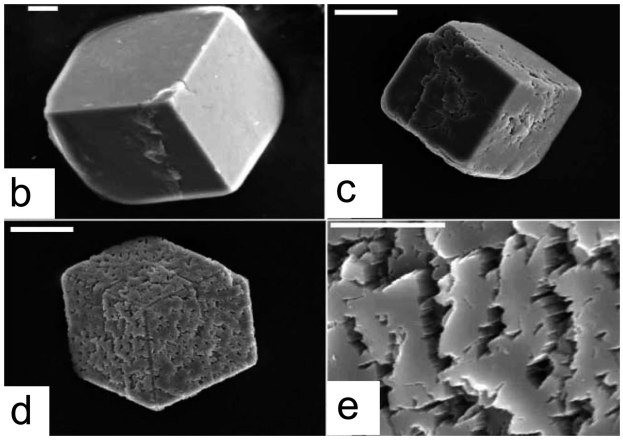

Figure 61. (a) Molecular structure of **46**. (b−e) Changes in calcite surface texture as a function of time. Crystals removed from a gel of **1** after (b) 3.5 h [scale bar: 5 μm], (c) 10.5 h [scale bar: 20 μm], and (d) 24 h [scale bar: 20 μm]. (e) A magnified view of the surface texture of the 24 h crystal shown in part (d) [scale bar: 5 μm]. (From ref 324 (http://dx.doi.org/10.1039/b309731e). Copyright 2004. Reproduced by permission of The Royal Society of Chemistry.)

nucleates amorphous precursor particles (nucleation clusters) which subsequently transform into primary nanoparticles with surface-associated PSS molecules.[236] Further development of the mesocrystals occurs by the oriented association of these building blocks, which leads to clearly segmented shapes. Also, this model implicates the exclusion of the polymeric additive from the primary crystallites and their subsequent entrapment as "intercrystalline material inside a mesocrystal".

Similarly, in the stabilization of vaterite, it has been frequently proposed that the additive is adhered to the surface of the constituting nanoparticles. For example, Naka and coworkers have reported the vaterite they produced to contain 27 and 39 wt % of the carboxy-terminated PAMAM dendrimer of generation 1.5 and 3.5, respectively.[199] Tremel et al. reported an organic content of 5% for vaterite spheres grown on OH-terminated SAMs in the presence of PAA.[333] Here we may expect the organic to be present at the surface of the nanoparticles but also included in the vaterite crystals.

7. What's Next in Biomimetic Mineralization?

In this review we have been discussing the interaction of templates and additives with calcium carbonate, trying to establish a model for the action of the organic molecules based on their molecular structure. In the preceding sections, we have concluded that epitaxial relations are certainly not required for the controlled nucleation of the nonequilibrium faces of calcium carbonate on an organic surface. Nevertheless, it is remarkable to see the many accounts in which a match exits between the geometric placement or the orientation of the ions in the crystal and the functional groups at the template surface. Moreover, for several systems, it was shown that they adapt in such a way that the match between template and crystal surface is optimized. On the other hand, examples are present in which no such relation is likely to be present and where control on the basis of surface charges has been suggested. Both experimental data and molecular dynamics simulations indicate that, in many cases, the system itself is trying to optimize the match between template and developing mineral phase and particular attention has been given to the adaptability of surfaces. We would like to emphasize that further development of this type of modeling would yield an extremely strong tool in the understanding and eventually the prediction of the effects of additives and surfaces on the development of inorganic materials.

For the control of crystal growth in solution, we have seen that there are several modes of control that can be exerted by organic molecules. Little is known about the precise nature of the processes, although a few main mechanisms

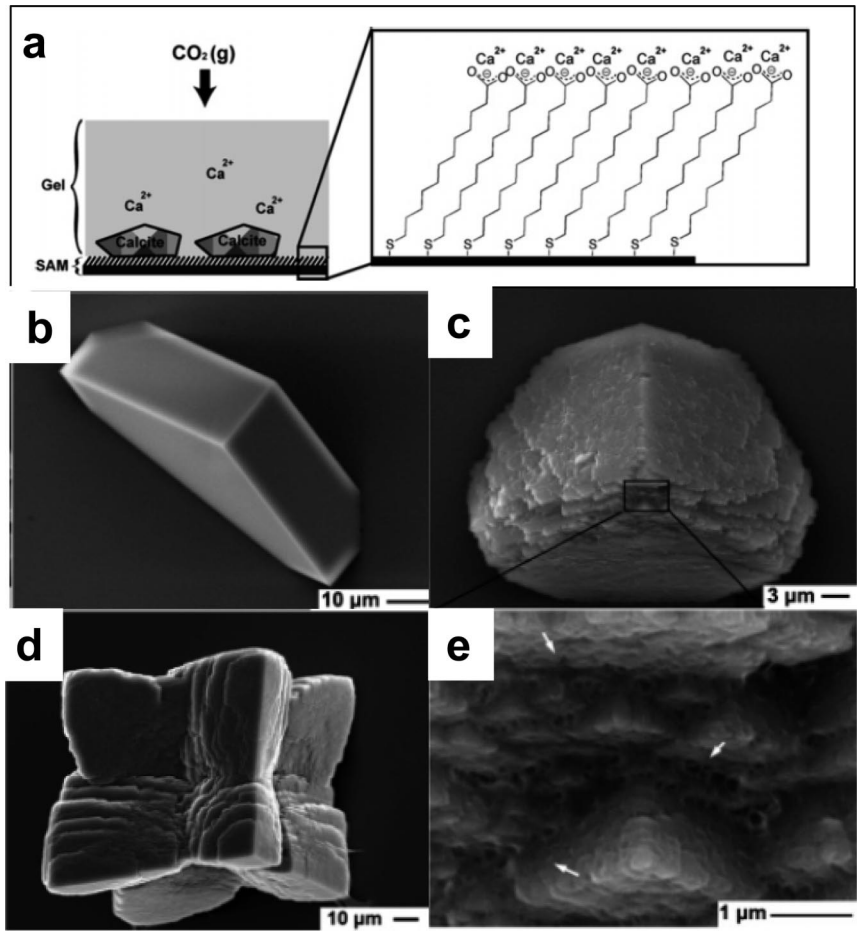

Figure 62. (a) Schematic representation of an agarose gel containing $CaCl_2$ on top of a carboxylate-terminated SAM on a gold-coated silicon wafer. The slow diffusion of CO_2(g) into the gel results in the precipitation of calcite crystals. (b−e) SEM images of calcite crystals grown (b) in solution or (c, e) in the systems depicted in parts (a) and (d) in bulk agarose gel. Part (e) is an enlargement of part (c). (Reprinted with permission from ref 330). Copyright 2007 American Chemical Society.)

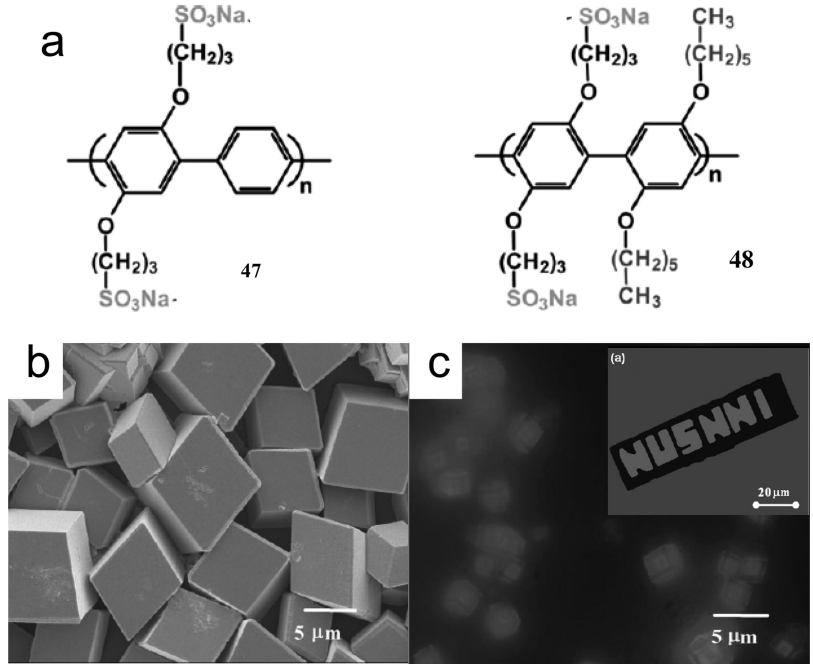

Figure 63. (a) Molecular structure of the sulfonated poly(*p*-phenylenes) **47** and **48**. (b) SEM and (c) CLSM images of the $CaCO_3$ crystals grown in the presence of **47**. Inset: fluorescence image of a patterned-polymer containing amorphous calcium carbonate film. (Reproduced with permission from ref 186). Copyright 2007 Wiley-VCH Verlag GmbH & Co. KGaA, Weinheim.)

can be distinguished. The interaction of the organic molecules can lead to the stabilization of primary particles in the early stages of mineral formation, generally leading to the expression of thermodynamically less stable phases. The interaction

with particles that have already crystallized to form the most stable polymorph calcite can lead either to the complete inhibition of growth, thereby favoring the formation of the less stable phases, or to the inhibition of growth only in a specific direction, leading to crystals with nonequilibrium morphology. The route an additive will take strongly depends on the kinetics of the mineralization system. Nevertheless, it has been demonstrated that cooperativity and preorganization of functional groups play a major role in the strength of the interactions and hence in the expression of the effects in polymorph selection and morphological appearance.

In addition, calculations have indicated that the observed activity of some molecules is directly related to their ability to displace water molecules at the crystal surface.[252] For example, Magdans and co-workers used GXRD and molecular dynamics simulations to investigate the interactions between glycine and the (10.4) calcite surface.[334] It was found that the glycine molecules did not interact through a direct charge matching fit but that they replaced the water molecules in the ordered second hydration layer on the mineral surface. Furthermore, it has been shown that such molecules can switch between limiting and stimulating crystal growth, depending on their concentration in solution. Moreover, most biomimetic systems use water as the mineralization medium, while, in biology, generally a hydrogel-like environment is present. It is well-known that this affects that way the crystals develop, and here we have also seen that this can be used to enhance the control over crystal nucleation and growth. These will be important issues to take into account in the design and analysis of future biomimetic experiments.

In the recent past, it has been demonstrated that the formation of calcium carbonate crystals does not necessarily proceed via the straightforward assembly of inorganic ions on the surface of a template.[54] In fact, it has been shown that, in many cases, the formation of calcite and aragonite in biological systems occurs through the formation and conversion of ACC.[335] Furthermore, also in laboratory experiments, it has been demonstrated that calcite and aragonite can form via an amorphous precursor phase. Nevertheless, there have been only a few cases in which it was demonstrated that the amorphous phase could be transformed into a crystalline phase with a preferred orientation.[336] Although the use of amorphous precursor phases has been well established for the synthesis of films and complex 3D structures, still little is known about the mechanism involved in their transformation and the differences between stable and transient ACC. Recently, it has been demonstrated that time-resolved cryoTEM experiments can play an important role in studying the early stages of mineralization experiments, in particular in the detection of transient phases.[49]

Biomimetic mineralization experiments can be divided into two categories: the first category comprises those that aim at resolving mechanisms by creating experimental setups mimicking nature and comparing the outcome with data from biological studies. It is this type of experiments that will finally provide the insight allowing us to transcribe nature's strategy to synthetic methods for advanced materials. This brings us to the other category: the experiments that are aiming at producing materials with methods that in one or more aspects resemble the strategies used in biologival systems. The biggest challenge here still remains the construction of materials using biomimetic methods that resemble natural materials not only in their structure but also in their properties. For this we need to fully understand and control the interplay between the organic and inorganic phases during the mineralization reaction. This can only be achieved through the preparation and use of well-defined systems that allow one to construct a model of their structure and monitor the changes during the mineral formation at both the molecular and morphological levels. In particular, the use of *in situ* characterization techniques, where possible in combination with computer modeling, can be expected to improve our insight in the processes involved in biomimetic mineralization. However, such systems cannot be designed without a detailed understanding of the biological systems. It is therefore imperative that we keep a focus on resolving strategies and mechanisms in biomineralization, both by direct studies and by biomimetic experiments, before rushing into biomimetic materials synthesis.

8. Acknowledgments

The authors would like to thank Jarno van Roosmalen, Eric J. Creusen, Frits L. Boogaard, and Pim Moeskops for their help in preparing the manuscript and the reviewers for their useful remarks.

9. References

(1) Lowenstam, H. A.; Weiner, S. *On Biomineralization*; Oxford University Press: 1989.
(2) Stupp, S. I.; Mejicano, G. C.; Hanson, J. A. *J. Biomed. Mater. Res.* **1993**, *27*, 289.
(3) Mann, S. *Angew. Chem., Int. Ed.* **2000**, *39*, 3392.
(4) Smith, B. L.; Schäffer, T. E.; Viani, M.; Thombson, J. B.; Frederick, N. A.; Kindt, J.; Belcher, A.; Stucky, G. D.; Morse, D. E.; Hansma, P. K. *Nature* **1999**, *399*, 761.
(5) Kato, T. *Adv. Mater.* **2000**, *12*, 1543.
(6) Falini, G.; Fermani, S.; Gazzano, M.; Ripamonti, A. *Chem.—Eur. J.* **1998**, *4*, 1048.
(7) Cölfen, H.; Antonietti, M. *Langmuir* **1998**, *14*, 582.
(8) Addadi, L.; Weiner, S. *Angew. Chem., Int. Ed.* **1992**, *31*, 153.
(9) Landau, E. M.; Levanon, M.; Leiserowitz, L.; Lahav, M.; Sagiv, J. *Nature* **1985**, *318*, 353.
(10) Mann, S.; Heywood, B. R.; Rajam, S.; Birchal, J. D. *Nature* **1988**, *334*, 692.
(11) Aizenberg, J.; Black, A. J.; Whitesides, G. M. *Nature* **1998**, *394*, 868.
(12) Cölfen, H.; Qi, L. *Chem.—Eur. J.* **2001**, *7*, 106.
(13) Yu, S.-H.; Cölfen, H. *J. Mater. Chem.* **2004**, *14*, 2124.
(14) Cölfen, H. *Macromol. Eng.* **2007**, *4*, 2597.
(15) Cölfen, H. *Top. Curr. Chem.* **2007**, *271* (Biomineralization II), 1.
(16) For the rhombohedral (hexagonal) system, conventionally four crystallographic indices are used, i.e. (*hkil*), for which it holds that $i = -(h + k)$. Therefore, this notation is often abbreviated to (*hk*·*l*), in which the dot represents the index *i*.
(17) Wullf, G. *Z. Krystallogr.* **1901**, *34*, 449.
(18) Deer, W. A.; Howie, R. A.; Zussman, J. *Introduction to rock forming minerals*; Longman: Harlow, U.K., 1992.
(19) Morse, J. W.; Arvidson, R. S.; Lüttge, A. *Chem. Rev.* **2007**, *107*, 342.
(20) Plummer, L. N.; Busenberg, E. *Geochim. Cosmochim. Acta* **1982**, *46*, 1011.
(21) Millero, F. J. *Chem. Rev.* **2007**, *107*, 308.
(22) De Leeuw, N. H.; Parker, S. C. *J. Phys. Chem. B* **1998**, *102*, 2914.
(23) The energy as measured with cleavage experiments is an intricate mixture between the thermodynamic surface energy and several dissipating factors, such as plasticity, roughness, secondary cracks, and crack tip rounding. Hence, their thermodynamic status has to be discussed in detail.
(24) Kerisit, S.; Parker, S. C. *Chem. Commun.* **2004**, 52.
(25) Kerisit, S.; Parker, S. C. *J. Am. Chem. Soc.* **2004**, *126*, 10152.
(26) Perry, T. D., IV; Cygan, R. T.; Mitchell, R. *Geochim. Cosmochim. Acta* **2007**, *71*, 5876.
(27) Nielsen, A. E. *Kinetics of precipitation*; Oxford, 1964.
(28) Liu, X. Y.; Lim, S. W. *J. Am. Chem. Soc.* **2003**, *125*, 888.
(29) Travaille, A. M.; Steijven, E. G. A.; Meekes, H.; van Kempen, H. *J. Phys. Chem. B* **2005**, *109*, 5618.

(30) Rieke, P. C. *J. Cryst. Growth* **1997**, *182*, 472.
(31) De Yoreo, J. J.; Vekilov, P. G. *Rev. Min. Geol.* **2003**, *54*, 57.
(32) It is important to notice that this calculation assumes classical nucleation from the direct assembly of calcium and cabonate ions.
(33) Dickinson, S. R.; Henderson, G. E.; McGrath, K. M. *J. Cryst. Growth* **2002**, *244*, 369.
(34) For an elaborate review of the VCG approach, see: Berg, J. C. In *Wetttability*; Berg, J. C., Ed.; Marcel Dekker, Inc.: New York, 1993; p 75.
(35) Nielsen, A. E. *Pure Appl. Chem.* **1981**, *53*, 2025.
(36) Aquilano, D.; Calleri, M.; Natoli, E.; Rubbo, M.; Sgualdino, G. *Mater. Chem. Phys.* **2000**, *669*, 159.
(37) Dalas, E.; Koutsokos, P. *J. Colloid Interface Sci.* **1989**, *127*, 273.
(38) Manoli, F.; Dalas, E. *J. Cryst. Growth* **2000**, *217*, 422.
(39) Malkaj, P.; Kanakis, J.; Dalas, E. *J. Cryst. Growth* **2004**, *266*, 533.
(40) Meldrum, F. C.; Hyde, S. T. *J. Cryst. Growth* **2001**, *231*, 544.
(41) Van der Leeden, M. C.; Van Rosmalen, G. M. *Desalination* **1987**, *66*, 185.
(42) Cody, R. D. *J. Sediment. Petrol.* **1991**, *61*, 704.
(43) Prieto, M.; Putnis, A.; Fernández-Díaz, L.; López-Andrés, S. *J. Cryst. Growth* **1994**, *142*, 225.
(44) Teng, H. H.; Dove, P. M.; Orme, C. A.; Deyoreo, J. J. *Science* **1998**, *282*, 724.
(45) Tang, R.; Darragh, M.; Orme, C. A.; Guan, X.; Hoyer, J. R.; Nancollas, G. H. *Angew. Chem., Int. Ed.* **2005**, *44*, 3698.
(46) Orme, C. A.; Noy, A.; Wirzbicki, A.; McBride, M. T.; Grantham, M.; Teng, H. H.; Dove, P. M.; De Yoreo, J. J. *Nature* **2001**, *411*, 775.
(47) Coveney, P. V.; Davey, R.; Griffin, J. L. W.; He, Y.; Hamlin, J. D.; Stackhouse, S.; Whiting, A. *J. Am. Chem. Soc.* **2000**, *122*, 11557.
(48) Yang, S.; Navrotsky, A. *Chem. Mater.* **2002**, *14*, 2803.
(49) Pichon, B. P.; Bomans, P. H. H.; Frederik, P. M.; Sommerdijk, N. A. J. M.; J. Am. Chem. Soc., accepted.
(50) For a brief review by one of the originators of this modelling, see: Van der Merwe, J. H. *Metall. Mater. Trans.* **2002**, *33A*, 2475.
(51) Duffy, D. M.; Harding, J. J. *J. Mater. Chem.* **2002**, *12*, 3419.
(52) Duffy, D. M.; Travaille, A. M.; van Kempen, H.; Harding, J. J. *J. Phys. Chem. B* **2005**, *109*, 5713.
(53) Cooper, S. J.; Sessions, R. B.; Lubetkin, S. D. *Langmuir* **1997**, *13*, 7165.
(54) Mann, S.; Cölfen, H. *Angew. Chem., Int. Ed.* **2003**, *42*, 2350.
(55) Zhang, T. H.; Liu, X. Y. *J. Am. Chem. Soc.* **2007**, *129*, 13520.
(56) Weiner, S.; Traub, W. *FEBS Lett.* **1980**, *111*, 311.
(57) Landau, E. M.; Levanon, M.; Leiserowitz, L.; Lahav, M.; Sagiv, J. *Nature* **1985**, *318*, 353.
(58) Addadi, L.; Weiner, S. *Proc. Natl. Acad. Sci. U.S.A.* **1985**, *82*, 4110.
(59) Addadi, L.; Moradian, J.; Shay, E.; Maroudas, N. G.; Weiner, S. *Proc. Natl. Acad. Sci. U.S.A.* **1987**, *84*, 2732.
(60) Walker, J. B. A.; Heywood, B. R.; Mann, S. J. *Chem. Mater.* **1991**, *1*, 889.
(61) Heywood, B. R.; Rajam, S.; Mann, S. *J. Chem. Soc., Faraday Trans.* **1991**, *87*, 727.
(62) Mann, S.; Heywood, B. R.; Rajam, S.; Birchall, J. D. *Proc. R. Soc. London* **1989**, *423*, 457.
(63) Didymus, J. M.; Oliver, P. M.; Mann, S.; De Vries, A. L.; Hauschka, P. V.; Westbroek, P. *J. Chem. Soc., Faraday Trans.* **1993**, *89*, 2891.
(64) For a recent review, see: Tremel, W.; Küther, J.; Balz, M.; Loges, N. Wolf, S. E.; Template surfaces for the formation of calcium carbonate. In *Handbook of Biomineralization: Biomimetic and Bioinspired Chemistry*; 2007; p *209*.
(65) Archibald, D. D.; Quadri, S. B.; Gaber, B. P. *Langmuir* **1996**, *12*, 538.
(66) Küther, J.; Seshadri, R.; Nelles, G.; Asschenmacher, W.; Butt, H.-J.; Mader, W.; Tremel, W. *Chem. Mater.* **1999**, *9*, 1317.
(67) Bartz, M.; Küther, J.; Nelles, G.; Weber, N.; Seshadri, R.; Tremel, W. *J. Mater. Chem.* **1999**, *9*, 1121.
(68) Küther, J.; Seshadri, R.; Tremel, W. *Angew. Chem.* **1998**, *37*, 3044.
(69) Rautaray, D.; Kumar, P. S.; Wadgaonkar, P. P.; Sastry, M. *Chem. Mater.* **2004**, *16*, 988.
(70) Mann, S.; Heywood, B. R.; Rajam, S.; Walker, J. B. A.; Davey, R. J.; Birchall, J. D. *Adv. Mater.* **1990**, *2*, 257.
(71) Heywood, B. R.; Mann, S. *Chem. Mater.* **1994**, *6*, 311.
(72) Champ, S.; Dickinson, J. A.; Fallon, P. S.; Heywood, B. R.; Mascal, M. *Angew. Chem., Int. Ed.* **2000**, *39*, 2716.
(73) Aizenberg, J.; Black, A. J.; Whitesides, G. M. *J. Am. Chem. Soc.* **1999**, *121*, 4500.
(74) Nuzzo, R. G.; Dubois, L. H.; Allara, D. L. *J. Am. Chem. Soc.* **1990**, *112*, 558.
(75) Laibinis, P. E.; Whitesides, G. M.; Allara, D. L.; Tao, Y.-T.; Parikh, A. N.; Nuzzo, R. G. *J. Am. Chem. Soc.* **1991**, *113*, 7152.
(76) Han, Y.-J.; Aizenberg, J. *Angew. Chem., Int. Ed.* **2003**, *42*, 3668.
(77) Heywood, B. R.; Rajam, S.; Mann, S. *J. Chem. Soc., Faraday Trans.* **1991**, *87*, 735.
(78) Dimasi, E.; Gower, L. B. *Mater. Res. Soc. Symp. Proc.* **2002**, *711*, 301.
(79) Dimasi, E.; Olszta, M. J.; Patel, V. M.; Gower, L. B. *CrystEngComm* **2003**, *5*, 346.
(80) Lahiri, J.; Xu, G.; Dabbs, D. M.; Yao, N.; Aksay, I. A.; Groves, J. T. *J. Am. Chem. Soc.* **1997**, *119*, 5449.
(81) Kim, I. W.; Robertson, R. E.; Zand, R. *Adv. Mater.* **2003**, *15*, 709.
(82) Pokroy, B.; Zolotoyabko, E. *Chem. Commun.* **2005**, 2140.
(83) Buijnsters, P. J. J. A.; Donners, J. J. J. M.; Hill, S. J.; Heywood, B. R.; Nolte, R. J. M.; Zwanenburg, B.; Sommerdijk, N. A. J. M. *Langmuir* **2001**, *17*, 3623.
(84) Donners, J. J. J. M.; Nolte, R. J. M.; Sommerdijk, N. A. J. M. *J. Am. Chem. Soc.* **2002**, *124*, 9700.
(85) Berman, A.; Ahn, D. J.; Lio, A.; Salmeron, M.; Reichert, A.; Charych, D. *Science* **1995**, *269*, 515.
(86) Sato, K.; Kumagai, Y.; Watari, K.; Tanaka, J. *Langmuir* **2004**, *20*, 2979.
(87) Travaille, A. M.; Donners, J. J. J. M.; Gerritsen, J. W.; Sommerdijk, N. A. J. M.; Nolte, R. J. M.; van Kempen, H. *Adv. Mater.* **2002**, *14*, 492–495.
(88) pH dependent differences in selectivity were also reported for fatty acid bilayer stacks:(a) Damle, C.; Kumar, A.; Sainkar, S. R.; Bhagawat, M.; Sastry, M. *Langmuir* **2002**, *18*, 6075–6080.
(89) Travaille, A. M.; Kaptijn, L.; Verwer, P.; Hulsken, B.; Elemans, J. A. A. W.; Nolte, R. J. M.; van Kempen, H. *J. Am. Chem. Soc.* **2003**, *125*, 11571.
(90) Han, Y. J.; Aizenberg, J. *J. Am. Chem. Soc.* **2003**, *I125*, 4032.
(91) Pokroy, B.; Aizenberg, J. *CrystEngComm* **2007**, *9*, 1219.
(92) Kwak, S.-Y.; Dimasi, E.; Han, Y.-J.; Aizenberg, J.; Kuzmenko, I. *Cryst. Growth Des.* **2005**, *5*, 2139.
(93) Li, J.; Liang, K. S.; Scoles, G.; Ulman, A. *Langmuir* **1995**, *11*, 4418.
(94) Volkmer, D.; Fricke, M.; Vollhardt, D.; Siegel, S. *J. Chem. Soc., Dalton Trans.* **2002**, 4547.
(95) Volkmer, D.; Fricke, M.; Agena, C.; Mattay, J. *CrystEngComm* **2002**, *4*, 288.
(96) Volkmer, D.; Fricke, M.; Agena, C.; Mattay, J. *J. Mater. Chem.* **2004**, *14*, 2249.
(97) Volkmer, D.; Fricke, M.; Gleiche, M.; Chi, L. *Mater. Sci. Eng., C* **2005**, *25*, 161.
(98) Calvert, P.; Rieke, P. *Chem. Mater.* **1996**, *8*, 1715.
(99) Volkmer, D.; Fricke, M. *Z. Anorg. Allg. Chem.* **2003**, *629*, 2381.
(100) Loste, E.; Díaz-Martý, E.; Zarbakhsh, A.; Meldrum, F. C. *Langmuir* **2003**, *19*, 2830.
(101) The longer fatty acids ($>C_{20}$) exclusively give rise to the formation of oriented calcite, whereas the lower acids (palmitic and stearic acid) give rise to mixtures containing, in addition to oriented calcite, also aragonite, vaterite, as well as unmodified calcite. This observation has been explained by considering that in the experimental setup used the monolayer acts as a diffusion barrier for the outgassing of the CO_2.The length of the fatty acids will determine the diffusion rate and thereby the kinetics of the mineralization reaction, which depends on the rate of CO_2 outgassing and thereby on the thickness of the monolayer.
(102) Aizenberg, J.; Black, A. J.; Whitesides, G. M. *Nature* **1999**, *398*, 495.
(103) Aizenberg, J. *J. Chem. Soc., Dalton Trans.* **2000**, 3963.
(104) Lee, J. R. I.; Han, Y.-J.; Willey, T. M.; Wang, D.; Meulenberg, R. W.; Nilsson, J.; Dove, P. M.; Terminello, L. J.; van Buuren, T.; DeYoreo, J. J. *J. Am. Chem. Soc.* **2007**, *129*, 10370.
(105) In both cases, it should be noted that these measurements were made on dried samples, of which the structure not necessarily represents the situation under mineralization conditions.
(106) Ahn, D. J.; Berman, A.; Charych, D. *J. Phys. Chem.* **1996**, *100*, 12455.
(107) The $(01\cdot0)$ plane belongs to the symmetry related family of $\{1\bar{1}\cdot0\}$ planes, consistent with previous reports; see refs 72 and 101.
(108) Popescu, D. C.; Smulders, M. M. J.; Pichon, B. P.; Chebotareva, N.; Kwak, S.-Y.; van Asselen, O. L. J.; Sijbesma, R. P.; DiMasi, E.; Sommerdijk, N. A. J. M. *J. Am. Chem. Soc.* **2007**, *129*, 14058.
(109) DiMasi, E.; Kwak, S.-Y.; Pichon, B. P.; Sommerdijk, N. A. J. M. *CrystEngComm* **2007**, *9*, 1192.
(110) Cavalli, S.; Popescu, D. C.; Tellers, E. E.; Vos, M. R. J.; Pichon, B. P.; Overhand, M.; Rapaport, H.; Sommerdijk, N. A. J. M.; Kros, A. *Angew. Chem., Int. Ed.* **2006**, *45*, 739.
(111) Sommerdijk, N. A. J. M.; Popescu, D. C.; Cavalli, S.; Kros, A. On the role of Template Adaptability in the Biomimetic Formation of $CaCO_3$. Self-organizing Monolayers of β sheet forming Peptides. In *Biomineralization: from Paleontology to Materials Science. Proceedings of the 9th International Symposium on Biomineralization*; Arias, J. L., Fernández, M. S., Eds.; 2007; pp 495−508.
(112) Addadi, L.; Joester, D.; Nudelman, F.; Weiner, S. *Chem.—Eur. J.* **2006**, *12*, 980.
(113) Falini, G.; Albeck, S.; Weiner, S.; Addadi, L. *Science* **1996**, *271*, 67.

(114) Marxen, J. C.; Becker, W.; Finke, D.; Hasse, B.; Epple, M. *J. Molluscan Stud.* **2003**, *69*, 113.
(115) Beniash, E.; Aizenberg, J.; Addadi, L.; Weiner, S. *Proc. R. Soc. London, Ser. B* **1997**, *264*, 461.
(116) Dillaman, R.; Hequembourg, S.; Gay, M. *J. Morph.* **2005**, *263*, 356.
(117) Weiss, I. M.; Tuross, N.; Addadi, L.; Weiner, S. *J. Exp. Zool.* **2002**, *293*, 478.
(118) Sugawara, A.; Nishimura, T.; Yamamoto, Y.; Inoue, H.; Nagasawa, H.; Kato, T. *Angew. Chem., Int. Ed.* **2006**, *45*, 2876.
(119) Weiner, S.; Sagi, I.; Addadi, L. *Science* **2005**, *309*, 1027.
(120) Addadi, L.; Raz, S.; Weiner, S. *Adv. Mater.* **2003**, *15*, 959.
(121) Politi, Y.; Mahamid, J.; Goldberg, H.; Weiner, S.; Addadi, L. *CrystEngComm.* **2007**, *9*, 1171.
(122) Politi, Y.; Levi-Kalisman, Y.; Raz, S.; Wilt, F.; Addadi, L.; Weiner, S.; Sagi, I. *Adv. Funct. Mater.* **2006**, *16*, 1289.
(123) Hasse, B.; Ehrenberg, H.; Marxen, J. C.; Becker, W.; Epple, M. *Chem.−Eur. J.* **2000**, *6*, 3679.
(124) Demadis, K. D.; Katarachia, S. D. *Phosphorus, Sulfur Silicon* **2004**, *179*, 627.
(125) Addadi, L.; Moradian, J.; Shay, E.; Maroudas, N. G.; Weiner, S. *Proc. Natl. Acad. Sci. U.S.A.* **1987**, *84*, 2732.
(126) Kitano, Y.; Wood, D. W. *Geochim. Cosmochim. Acta* **1965**, *29*, 29.
(127) Abdel-Aal, N.; Sawada, K. *J. Cryst. Growth* **2003**, *256*, 188.
(128) Sikiriæ, M. D.; Füredi-Milhofer, H. *Adv. Colloid Interface Sci.* **2006**, *128−130*, 135.
(129) Very recently the selective stabilization of all three anhydrous crystalline polymorphs was demonstrated using a single additive: poly(sodium 4-styrene sulfonate)-*co*-*N*-isoporpylacylamide). Xu, A.-W.; Dong, W.-F.; Antonietti, M.; Cölfen, H. *Adv. Funct. Mater* **2008**, *18*, 1307.
(130) Dorfmüller, G. *Deutsch. Zuckerind.* **1938**, *63*, 1217.
(131) Matsushita, I.; Hamada, Y.; Moriga, T.; Ashida, T.; Nakabayashi, I. *J. Ceram. Soc. Jpn.* **1996**, *104*, 1081.
(132) Günther, C.; Becker, A.; Wolf, G.; Epple, M. *Anorg. Allg. Chem.* **2005**, *631*, 2830.
(133) Johnston, J.; Merwin, H. E.; Williamson, E. D. *Am. J. Sci.* **1916**, *41*, 473.
(134) Breèeviæ, L.; Nielsen, A. E. *J. Cryst. Growth* **1989**, *98*, 504.
(135) Sawada, K. *Pure Appl. Chem.* **1997**, *69*, 921.
(136) Koga, N.; Nakagoe, Y.; Tanaka, H. *Thermochim. Acta* **1998**, *318*, 239.
(137) Faatz, M.; Gröhn, F.; Wegner, G. *Adv. Mater.* **2004**, *16*, 996.
(138) Loste, E.; Meldrum, F. C. *Chem. Commun.* **2001**, 901.
(139) Lee, H. So.; Ha, T. H.; Kim, K. *Mater. Chem. Phys.* **2005**, *93*, 376.
(140) Xu, X.; Han, J. T.; Cho, K. *Chem. Mater.* **2004**, *16*, 1740.
(141) Xu, X.; Han, J. T.; Cho, K. *Langmuir* **2005**, *21*, 4801.
(142) Han, T. Y.-J.; Aizenberg, J. *Chem. Mater.* **2008**, *20*, 1064.
(143) Sawada, K. *Pure Appl. Chem.* **1997**, *69*, 921.
(144) Raz, S.; Weiner, S.; Addadi, L. *Adv. Mater.* **2000**, *12*, 38.
(145) Sommerdijk, N. A. J. M.; van Leeuwen, E. N. M.; Vos, M. R. J.; Jansen, J. A. *CrystEngComm* **2007**, 1209.
(146) See Gower et al. in this issue.
(147) MacAdam, J.; Parsons, S. A. *Rev. Environ. Sci. Biotechnol. 3* **2004**, 159.
(148) Ogino, T.; Tsunashima, N.; Suzuki, T.; Sakaguchi, M.; Sawada, K. *Nippon Kagaku Kaishi* **1988**, *6*, 899.
(149) Donners, J. J. J. M.; Heywood, B. R.; Meijer, E. W.; Nolte, R. J. M.; Roman, C.; Schenning, A. P. H. J.; Sommerdijk, N. A. J. M. *Chem. Commun.* **2000**, 1937.
(150) Donners, J. J. J. M.; Heywood, B. R.; Meijer, E. W.; Nolte, R. J. M.; Sommerdijk, N. A. J. M. *Chem.−Eur. J.* **2002**, *8*, 2561.
(151) Xu, A.-W.; Yu, Q.; Dong, W.-F.; Antonietti, M.; Cölfen, H. *Adv. Mater.* **2005**, *17*, 2217.
(152) Nassif, N.; Gehrke, N.; Pinna, N.; Shirshova, N.; Tauer, K.; Antonietti, M.; Cölfen, H. *Angew. Chem., Int. Ed.* **2005**, *44*, 6004.
(153) Hosoda, N.; Sugawara, A.; Kato, T. *Macromolecules* **2003**, *36*, 6449.
(154) Kato, T.; Suzuki, T.; Amamiya, T.; Irie, T.; Komiyama, M.; Yui, H. *Supramol. Sci.* **1998**, *5*, 411.
(155) Falini, G. *Int. J. Inorg. Mater.* **2000**, *2*, 455.
(156) Gower, L. A.; Tirrell, D. A. *J. Cryst. Growth* **1998**, *191*, 153.
(157) Gao, Y. X.; Yu, S. H.; Guo, X. H. *Langmuir* **2006**, *22*, 6125.
(158) In particular, the use of hydrophilic block copolymers has yielded several examples of very effective stabilization of vaterite; see, for example, refs 8 and 13−16. This topic is, however, outside the scope of this review.
(159) Hou, W.; Feng, Q. *J. Cryst. Growth* **2005**, *282*, 214.
(160) Park, H. K.; Lee, I.; Kim, K. *Chem. Commun.* **2004**, 24.
(161) Kai, A.; Fuijikawa, K.; Miki, T. *Jpn. J. Appl. Phys.* **2002**, *41*, 439.
(162) Manoli, F.; Kanakis, J.; Malkaj, P.; Dalas, E. *J. Cryst. Growth* **2002**, *236*, 363.
(163) Shivkumara, C.; Singh, P.; Gupta, A.; Hegde, M. S. *Mater. Res. Bull.* **2006**, *41*, 1455.
(164) Orme, C. A.; Noy, A.; Wierzbicki, A.; McBride, M. T.; Grantham, M.; Teng, H. H.; Dove, P. M.; DeYoreo, J. J. *Nature* **2001**, *411*, 775.
(165) Wolf, S. E.; Loger, N.; Mathiasch, B.; Panthoefer, M.; Mey, I.; Janshoff, A.; Tremel, W. *Angew. Chem., Int. Ed.* **2007**, *46*, 5618.
(166) Malkaj, P.; Kanakis, J.; Dalas, E. *J. Cryst. Growth* **2004**, *266*, 533.
(167) Manoli, F.; Dalas, E. *J. Cryst. Growth* **2001**, *222*, 293.
(168) Kitamura, M. *J. Cryst. Growth* **2002**, *237−239*, 2205.
(169) Xie, A.-J.; Shen, Y.-H.; Zhang, C.-Y.; Yuan, Z.-W.; Zhu, X.-M.; Yan, Y.-M. *J. Cryst. Growth* **2001**, *285*, 436.
(170) Tong, H.; Ma, W.; Wang, L.; Wan, P.; Hu, J.; Cao, L. *Biomaterials* **2004**, *25*, 3923.
(171) Malkaj, P.; Kanakis, J.; Dalas, E. *Cryst. Growth Des.* **2004**, *4*, 721.
(172) Suhara, T.; Esumi, K.; Meguro, K. *Bull. Chem. Soc. Jpn.* **1983**, *56*, 2932.
(173) Wei, H.; Shen, Q.; Zhao, Y.; Zhou, Y.; Wang, D.; Xu, D. *J. Cryst. Growth* **2005**, *279*, 439.
(174) Wei, H.; Shen, Q.; Zhao, Y.; Zhou, Y.; Wang, D.; Xu, D. *J. Cryst. Growth* **2004**, *264*, 424.
(175) Szczes, A.; Chibowski, E.; Hołysz, L. *Colloid Surf., A* **2007**, *297*, 14.
(176) Liu, D.; Yates, M. Z. *Langmuir* **2006**, *22*, 5566.
(177) Wei, H.; Shen, Q.; Zhao, Y.; Wang, D.; Xu, D. *J. Cryst. Growth* **2004**, *260*, 545.
(178) Chibowski, E.; Szczes, A.; Holysz, L. *Langmuir* **2005**, *21*, 8114.
(179) Shen, Q.; Wang, L.; Huang, Y.; Sun, J.; Wang, H.; Zhou, Y.; Wang, D. *J. Phys. Chem. B* **2006**, *110*, 23148.
(180) Manoli, F.; Dalas, E. *J. Cryst. Growth* **2000**, *218*, 359.
(181) Anderson, R. E.; Barron, A. R. *Main Group Chem.* **2005**, *4*, 279.
(182) Xie, A.-J.; Yuan, Z.-W.; Shen, Y.-H. *J. Cryst. Growth* **2005**, *276*, 265.
(183) Li, W.; Gao, C. *Langmuir* **2007**, *23*, 4575.
(184) Meng, Q.; Chen, D.; Yue, L.; Fang, J.; Zhao, H.; Wang, L. *Macromol. Chem. Phys.* **2007**, *208*, 474.
(185) Xyla, A. G.; Giannimaras, E. K.; Koutsoukos, P. G. *Colloids Surf.* **1991**, *53*, 241.
(186) Sindhu, S.; Jegadesan, S.; Hairong, L.; Ajikumar, P. K.; Vetrichelvan, M.; Valiyaveettil, S. *Adv. Funct. Mater.* **2007**, *17*, 1698.
(187) Huang, J. H.; Mao, Z. F.; Luo, M. F. *Mater. Res. Bull.* **2007**, *42*, 2184.
(188) Sugawara, T.; Suwa, Y.; Ohkawa, K.; Yamamoto, H. *Macromol. Rapid Commun.* **2003**, *24*, 847.
(189) Xu, A. W.; Antonietti, M.; Cölfen, H.; Fang, Y.-P. *Adv. Funct. Mater.* **2006**, *16*, 903.
(190) Wada, N.; Yamashita, K.; Umegaki, T. *J. Colloid Interface Sci.* **1999**, *212*, 357.
(191) Westin, K.-J.; Rasmuson, Å. C. *J. Colloid Interface Sci.* **2005**, *282*, 370.
(192) Westin, K.-J.; Rasmuson, Å. C. *J. Colloid Interface Sci.* **2005**, *282*, 359.
(193) Naka, K.; Keum, D.-K.; Tanaka, Y.; Chujo, Y. *Bull. Chem. Soc. Jpn.* **2004**, *77*, 827.
(194) Naka, K.; Keum, D.-K.; Tanaka, Y.; Chujo, Y. *Chem. Commun.* **2000**, 1537.
(195) Keum, D.; Naka, K.; Tanaka, Y.; Chujo, Y. *Bull. Chem. Soc. Jpn.* **2004**, *77*, 827.
(196) A similar experiment was described in:(a) Gou, Y.; Yang, X.; Zhang, X.; Jiang, K. *Macromol. Biosci.* **2003**, *3*, 163.
(197) Keum, D.-K.; Naka, K.; Chujo, Y. *Bull. Chem. Soc. Jpn.* **2003**, *76*, 1687.
(198) Naka, K. *Top. Curr. Chem.* **2007**, *271*, 119.
(199) Naka, K.; Tanaka, Y.; Chujo, Y. *Langmuir* **2002**, *18*, 3655.
(200) Naka, K.; Tanaka, Y.; Chujo, Y.; Ito, Y. *Chem. Commun.* **1999**, 1931.
(201) Fricke, M.; Volkmer, D.; Krill, C. E., III; Kellermann, M.; Hirsch, A. *Cryst. Growth Des.* **2006**, *6*, 1120.
(202) Litvin, A. L.; Samuelson, L. A.; Charych, D. H.; Spevak, W.; Kaplan, D. L. *J. Phys. Chem.* **1995**, *99*, 12065.
(203) Küther, J.; Seshadri, R.; Knoll, W.; Tremel, W. *J. Mater. Chem.* **1998**, *8*, 641.
(204) Lee, I.; Han, S. W.; Choi, H. J.; Kim, K. *Adv. Mater.* **2001**, *13*, 1617.
(205) Aizenberg, J.; Black, A. J.; Whitesides, G. M. *J. Am. Chem. Soc.* **1999**, *121*, 4500.
(206) Küther, J.; Tremel, W. *Chem. Commun.* **1997**, 2029.
(207) Küther, J.; Tremel, W. *Thin Solid Films* **1998**, *327−329*, 554.
(208) Küther, J.; Seshadri, R.; Neles, G.; Butt, H. J.; Knoll, W.; Tremel, W. *Adv. Mater.* **1998**, *5*, 401.
(209) Balz, M.; Barriau, E.; Istratov, V.; Frey, H.; Tremel, W. *Langmuir* **2005**, *21*, 3987.
(210) Balz, M.; Therese, H. A.; Li, J.; Gutmann, J. S.; Kappl, M.; Nasdala, L.; Hofmeister, W.; Butt, H.-J.; Tremel, W. *Adv. Funct. Mater.* **2005**, *15*, 683.
(211) Litvin, A. L.; Valiyaveettil, S.; Kaplan, D. L.; Mann, S. *Adv. Mater.* **1997**, *9*, 124.

(212) Küther, J.; Nelles, G.; Seshadri, R.; Schaub, M.; Butt, H.-J.; Tremel, W. *Chem.—Eur. J.* **1998**, *4*, 1834.
(213) Didymus, J. M.; Mann, S.; Benton, W. J.; Collins, I. R. *Langmuir* **1995**, *11*, 3130.
(214) Pichon, B. P.; Cantin, S.; Smulders, M. M. J.; Vos, M. R. J.; Chebotareva, N.; Popescu, D. C.; van Asselen, O.; Perrot, F.; Sijbesma, R.; Sommerdijk, N. A. J. M. *Langmuir* **2007**, *23*, 12655.
(215) Fricke, M.; Volkmer, D. *Top. Curr. Chem.* **2007**, *270*, 1.
(216) Walsh, D.; Lebeau, B.; Mann, S. *Adv. Mater.* **1999**, *11*, 324.
(217) Kang, S. H.; Hirasawa, I.; Kim, W.-S.; Choi, C. K. *J. Colloid Interface Sci.* **2005**, *288*, 496.
(218) Liu, D.; Yates, M. Z. *Langmuir* **2006**, *22*, 5566.
(219) Tang, Y.; Du, B.; Li, L.; Yang, J.; Zhang, Y. *Chin. Sci. Bull.* **2007**, *52*, 78.
(220) Kandori, K.; Shizuka, N.; Kon-no, K.; Kitahara, A. *J. Dispersion Sci. Technol.* **1987**, *8*, 477.
(221) Nakahara, Y.; Mizuguchi, M.; Miyata, K. *J. Colloid Interface Sci.* **1979**, *68*, 401.
(222) A similar system producing vaterite is described in:(a) Hirai, T.; Hariguchi, S.; Komasawa, I.; Davey, R. J. *Langmuir* **1997**, *13*, 6650.
(223) Li, M.; Mann, S. *Adv. Funct. Mater.* **2002**, *12*, 773.
(224) Politi, Y.; Levi-Kalisman, Y.; Raz, S.; Wilt, F.; Addadi, L.; Weiner, S.; Sagi, I. *Adv. Funct. Mater.* **2006**, *16*, 1289.
(225) Li, M.; Lebeau, B.; Mann, S. *Adv. Mater.* **2003**, *15*, 2032.
(226) Aragonite was also observed in a reverse micellar sytem described in:(a) Ganguli, A. K.; Ahmed, J.; Vaidya, S.; Ahmad, T. *J. Nanosci. Nanotechnol.* **2007**, *7*, 1760.
(227) Thachepan, S.; Li, M.; Davis, S. A.; Mann, S. *Chem. Mater.* **2006**, *18*, 3557.
(228) Shen, Y.; Xie, A.; Chen, Z.; Xu, W.; Yao, H.; Li, S.; Huang, L.; Wu, Z.; Kong, X. *Mater. Sci. Eng., A* **2007**, *443*, 95.
(229) Young, J. R.; Davis, S. A.; Bown, P. R.; Mann, S. *J. Struct. Biol.* **1999**, *126*, 195.
(230) Didymus, J. M.; Oliver, P.; Mann, S.; DeVries, A. L.; Hauschka, P. V.; Westbroek, P. *J. Chem. Soc., Faraday Trans.* **1993**, *89*, 2891.
(231) Jackson, T. A.; Bischoff, J. L. *J. Geol.* **1971**, *79*, 493.
(232) Guo, Y.; Yang, L.; Yang, X.; Zhang, X.; Zhu, S.; Jiang, K. *Macromol. Biosci.* **2003**, *3*, 163.
(233) Mukkamala, S. B.; Anson, C. E.; Powell, A. K. *J. Inorg. Biochem.* **2006**, *100*, 1128.
(234) Estroff, L. A.; Incarvito, C. D.; Hamilton, A. D. *J. Am. Chem. Soc.* **2004**, *126*, 2.
(235) Imai, H.; Terada, T.; Yamabi, S. *Chem. Commun.* **2003**, 484.
(236) Wang, T.; Antonietti, M.; Cölfen, H. *Chem.—Eur. J.* **2006**, *12*, 5722.
(237) Volkmer, D.; Fricke, M.; Huber, T.; Sewald, N. *Chem. Commun.* **2004**, 1872.
(238) DeOliveira, D. B.; Laursen, R. A. *J. Am. Chem. Soc.* **1997**, *119*, 10627.
(239) Cornelissen, J. J. L. M.; Donners, J. J. J. M.; de Gelder, R.; Graswinckel, W. S.; Metselaar, G. A.; Rowan, A. E.; Sommerdijk, N. A. J. M.; Nolte, R. J. M. *Science* **2001**, *293*, 676.
(240) The role of calcium ion binding in the structuring of macromolecules was demonstrated by Brack et al., who showed that for $(Glu\text{-}Leu)_{\sim 55}$ the binding of divalent ions lead to β-sheet formation preceding the adsorption of the polymer to the mineral surface. See:(a) Bertrand, M.; Brack, A. *Origins of Life and Evolution of the Biosphere* **1997**, *27*, 585. (b) Bertrand, M.; Brack, A. *Chem.—Eur. J.* **2000**, *6*, 3452.
(241) Rapaport, H.; Kjaer, K.; Jensen, T. R.; Leiserowitz, L.; Tirrell, D. A. *J. Am. Chem. Soc.* **2000**, *122*, 12523.
(242) Cavalli, S.; Handgraaf, J.-W.; Tellers, E. E.; Popescu, D. C.; Overhand, M.; Kjaer, K.; Vaiser, V.; Sommerdijk, N. A. J. M.; Rapaport, H.; Kros, A. *J. Am. Chem. Soc.* **2006**, *128*, 13959.
(243) Kim, I. W.; Morse, D. E.; Evans, J. S. *Langmuir* **2004**, *20*, 11664.
(244) Kim, I. W.; Darragh, M. R.; Orme, C.; Evans, J. S. *Cryst. Growth Des.* **2006**, *6*, 5.
(245) Collino, S.; Evans, J. S. *Biomacromolecules* **2007**, *8*, 1686.
(246) Delak, K.; Collino, S.; Evans, J. S. *Langmuir* **2007**, *23*, 11951.
(247) Ajikumar, P. K.; Vivekanandan, S.; Lakshminarayanan, R.; Jois, S. D. S.; Kini, R. M.; Valiyaveettil, S. *Angew. Chem., Int. Ed.* **2005**, *44*, 5476.
(248) The $\{4\bar{4}\cdot 0\}$ faces make an angle of 3.6° with the $\{1\bar{1}\cdot 0\}$ faces; see ref 230.
(249) Mann, S.; Didymus, J. M.; Sanderson, N. P.; Heywood, B. R.; Samper, E. J. *J. Chem Soc., Faraday Trans.* **1990**, *86*, 1873.
(250) Jones, F.; Mocerino, M.; Ogden, M. I.; Oliveira, A.; Parkinson, G. M. *Cryst. Growth Des.* **2005**, *5*, 2336.
(251) Davis, K. J.; Dove, P. M.; De Yoreo, J. J. *Science* **2000**, *290*, 1134.
(252) Elhadj, S.; Salter, E. A.; Wierzbicki, A.; De Yoreo, J. J.; Han, N.; Dove, P. M. *Cryst. Growth Des.* **2006**, *6*, 197.
(253) Fu, G.; Qiu, S. R.; Orme, C. A.; Morse, D. E.; De Yoreo, J. J. *Adv. Mater.* **2005**, *17*, 2678.
(254) Elhadj, S.; De Yoreo, J. J.; Hoyer, J. R.; Dove, P. M. *Proc. Natl. Acad. Sci.* **2006**, *103*, 19237.
(255) Cölfen, H.; Meldrum, F. C. Chem. Rev., this issue.
(256) Mann, S.; Cölfen, H. *Angew. Chem., Int. Ed.* **2003**, *42*, 2350.
(257) Chen, S.-F.; Yu, S.-H.; Wang, T.-X.; Jian, J.; Cölfen, H.; Hu, B.; Yu, B. *Adv. Mater.* **2005**, *17*, 1461.
(258) Mukkamala, S. B.; Powell, A. K. *Chem. Commun.* **2004**, 918.
(259) Yu, S.-H.; Cölfen, H.; Antonietti, M. *Chem.—Eur. J.* **2002**, *8*, 2937.
(260) Wada, K.; Yamashita, K.; Umegakim, T. *J. Colloid Interface Sci.* **1999**, *212*, 357.
(261) Stupp, S. I.; Braun, P. V. *Science* **1997**, *277*, 1242.
(262) Förster, S.; Antonietti, M. *Adv. Mater.* **1998**, *10*, 195.
(263) Douglas, T.; Young, M. *Adv. Mater.* **1999**, *11*, 679.
(264) Tricot, Y.-M.; Fendler, J. H. *J. Am. Chem. Soc.* **1984**, *106*, 7359.
(265) Oliver, S.; Kuperman, A.; Coombs, N.; Lough, A.; Ozin, G. A. *Nature* **1995**, *378*, 47.
(266) Loste, E.; Meldrum, F. C. *Chem. Commun.* **2001**, *10*, 901.
(267) Walsh, D.; Hopwood, J. D.; Mann, S. *Science* **1994**, *254*, 1576.
(268) It should be noted that the use of ACC precursors is not a prerequisite for the generation of complex single crystalline structures. Polymeric inverse replicas of sea urchin spines have been invaded with calcium carbonate, thereby producing impressive single crystalline copies of the original spine, see: Park, R. J.; Meldrum, F. C. *J. Mater. Chem.* **2004**, *14*, 2291.
(269) Li, C.; Qi, L. *Angew. Chem., Int. Ed.* **2008**, *47*, 2388.
(270) Cheng, X.; Gower, L. B. *Biotechnol. Prog.* **2006**, *22*, 141.
(271) Monnier, A.; Schüth, F.; Huo, Q.; Kumar, D.; Margolese, D.; Maxwell, R. S.; Stucky, G. D.; Krishnamurty, M.; Petroff, P.; Fizouri, A.; Janicke, M.; Chmelka, B. F. *Science* **1993**, *261*, 1299.
(272) Hirai, T.; Hariguchi, S.; Komasawa, I.; Davey, R. J. *Langmuir* **1997**, *13*, 6650.
(273) Kang, S. H.; Hirasawa, I.; Kim, W.-S.; Choi, C. K. *J. Colloid Interface Sci.* **2005**, *288*, 496.
(274) Walsh, D.; Mann, S. *Nature* **1995**, *377*, 320.
(275) Aizenberg, J. *J. Chem. Soc., Dalton Trans.* **2000**, 3963.
(276) Aizenberg, J. *J. Cryst. Growth* **2000**, *211*, 143.
(277) Xu, X.; Han, J. T.; Cho, K. *Langmuir* **2005**, *21*, 4801.
(278) Volkmer, D.; Harms, M.; Gower, L. B.; Ziegler, A. *Angew. Chem., Int. Ed.* **2005**, *44*, 639.
(279) Han, J. T.; Xu, X.; Kim, D. H.; Cho, K. *Adv. Funct. Mater.* **2005**, *15*, 475.
(280) DiMasi, E.; Patel, V. M.; Sivakumar, M.; Olszta, M. J.; Yang, Y. P.; Gower, L. B. *Langmuir* **2002**, *18*, 8902.
(281) Gower, L. B.; Odom, D. J. *J. Cryst. Growth* **2000**, *210*, 719.
(282) Xu, G.; Yao, N.; Aksay, I. A.; Groves, J. T. *J. Am. Chem. Soc.* **1998**, *120*, 11977.
(283) Sugawara, A.; Ishii, T.; Kato, T. *Angew. Chem., Int. Ed.* **2003**, *42*, 5299.
(284) Kotachi, A.; Miura, T.; Imai, H. *Chem. Mater.* **2004**, *16*, 3191.
(285) Ajikumar, P. K.; Lakshminarayanan, R.; Valiyaveettil, S. *Cryst. Growth Des.* **2004**, *4*, 331.
(286) Wakayama, H.; Hall, S. R.; Mann, S. *J. Mater. Chem.* **2005**, *15*, 1134.
(287) Zhang, S.; Gonsalves, K. E. *Langmuir* **1998**, *14*, 6761.
(288) Hosoda, N.; Kato, T. *Chem. Mater.* **2001**, *13*, 688.
(289) Hosoda, N.; Sugawara, A.; Kato, T. *Macromolecules* **2003**, *36*, 6449.
(290) Kato, T.; Sugawara, A.; Hosoda, N. *Adv. Mater.* **2002**, *14*, 869.
(291) Gower, L. A.; Tirrell, D. A. *J. Cryst. Growth* **1998**, *191*, 153.
(292) Tanaka, Y. i.; Nemoto, T.; Naka, K.; Chujo, Y. *Polym. Bull.* **2000**, *45*, 447.
(293) Amos, F. F.; Sharbaugh, D. M.; Talham, D. R.; Gower, L. B. *Langmuir* **2007**, *23*, 1988.
(294) Müller, H.; Zentel, R.; Janshoff, A.; Jank, M. *Langmuir* **2006**, *22*, 11034.
(295) Popescu, D. C.; van Leeuwen, E. N. M.; Rossi, N. A. A.; Holder, S. J.; Jansen, J. A.; Sommerdijk, N. A. J. M. *Angew. Chem., Int. Ed.* **2006**, *45*, 1762.
(296) Tugulu, S.; Harms, M.; Fricke, M.; Volkmer, D.; Klok, H.-A. *Angew. Chem., Int. Ed.* **2006**, *45*, 7458.
(297) Lu, C.; Qi, L.; Ma, J.; Cheng, H.; Zhang, M.; Cao, W. *Langmuir* **2004**, *20*, 7378.
(298) Kim, Y.-Y.; Douglas, E. P.; Gower, L. B. *Langmuir* **2007**, *23*, 4862.
(299) Aizenberg, J.; Muller, D. A.; Grazul, J. L.; Haman, D. R. *Science* **2003**, *299*, 1205.
(300) See also: Xu, X.; Han, J. T.; Kim, D. H.; Cho, K. *J. Phys. Chem. B* **2006**, *110*, 2764.
(301) Marin, F.; Pokroy, B.; Luquet, G.; Layrolle, P.; de Groot, K. *Biomaterials* **2007**, *28*, 2368.
(302) Pokroy, B.; Fitch, A. N.; Marin, F.; Kapon, M.; Adir, N.; Zolotoyabko, E. *J. Struct. Biol.* **2006**, *155*, 96.
(303) Imai, H.; Terada, T.; Yamabi, S. *Chem. Commun.* **2003**, 484.
(304) Kulak, A. N.; Iddon, P.; Li, Y.; Armes, S. P.; Cölfen, H.; Paris, O.; Wilson, R. M.; Meldrum, F. C. *J. Am. Chem. Soc.* **2007**, *129*, 3729.
(305) Cölfen, H.; Antonietti, M. *Angew. Chem., Int. Ed.* **2005**, *44*, 5576.
(306) Niederberger, M.; Cölfen, H. *Phys. Chem. Chem. Phys.* **2006**, *8*, 3271.

(307) Oaki, Y.; Kotachi, A.; Miura, T.; Imai, H. *Adv. Funct. Mater.* **2006**, *16*, 1633.
(308) Oaki, Y.; Imai, H. *Small* **2006**, *2*, 66.
(309) Smith, B.; Schäffer, T. E.; Viani, M.; Thompson, J. B.; Frederick, N. A.; Kindt, J.; Belcher, A.; Stucky, G. D.; Morse, D. E.; Hansma, P. K. *Nature* **1999**, *399*, 761.
(310) Addadi, L.; Weiner, S. *Angew. Chem., Int. Ed. Engl.* **1992**, *31*, 153.
(311) Berman, A.; Addadi, L.; Weiner, S. *Nature* **1988**, *331*, 546.
(312) Berman, A.; Addadi, L.; Kvick, A.; Leiserowitz, L.; Nelson, M.; Weiner, S. *Science* **1990**, *250*, 664.
(313) Nudelman, F.; Chen, H. H.; Goldberg, H. A.; Weiner, S.; Addadi, L. *Faraday Discuss.* **2007**, *136*, 9.
(314) Berman, A.; Hanson, J.; Leiserowitz, L.; Koetzle, T. F.; Weiner, S.; Addadi, L. *J. Phys. Chem.* **1993**, *97*, 5162.
(315) Pokroy, B.; Fitch, A.; Lee, P.; Quintana, J. P.; Caspi, E. N.; Zolotoyabko, E. *J. Struct. Biol.* **2006**, *153*, 145.
(316) Pokroy, B.; Quintana, J. P.; Caspi, E. N.; Berner, A.; Zolotoyabko, E. *Nat. Mater.* **2004**, *3*, 900.
(317) Pokroy, B.; Fitch, A. N.; Marin, F.; Kapon, M.; Adir, N.; Zolotoyabko, E. *J. Struct. Biol.* **2006**, *155*, 96.
(318) Pokroy, B.; Fitch, A. N.; Zolotoyabko, E. *Adv. Mater.* **2006**, *18*, 2363.
(319) Gehrke, N.; Nassif, N.; Pinna, N.; Antonietti, M.; Gupta, H. S.; Cölfen, H. *Chem. Mater.* **2005**, *17*, 6514.
(320) The mean value for these materials was 16.1 GPa; for nacre this value is 53.6 GPa.
(321) Wei, H.; Ma, N.; Shi, F.; Wang, Z.; Zhang, X. *Chem. Mater.* **2007**, *19*, 19748.
(322) Amos, F. F.; Sharbaugh, D. M.; Talham, D. R.; Gower, L. B.; Fricke, M.; Volkmer, D. *Langmuir* **2007**, *23*, 1988.
(323) It should be noted here that, although the incorporation of Mg^{2+} ions normally is not observed for aragonite, this may also affect the observed lattice parameters.
(324) Estroff, L. A.; Addadi, L.; Weiner, S.; Hamilton, A. D. *Org. Biomol. Chem.* **2004**, *2*, 137.
(325) Grassmann, O.; Neder, R. B.; Putnis, A.; Lobmann, P. *Am. Mineral.* **2003**, *88*, 647.
(326) Kuang, M.; Wang, D.; Gao, M.; Hartmann, J.; Moehwald, H. *Chem. Mater.* **2005**, *17*, 656.
(327) Kuang, M.; Wang, D.; Moehwald, H. *Chem. Mater.* **2006**, *18*, 1073.
(328) Zhao, J.; Li, Y.-J.; Cheng, G.-X. *Chin. Sci. Bull.* **2007**, *52*, 1796.
(329) Oaki, Y.; Hayashi, S.; Imai, H. *Chem. Commun.* **2007**, *27*, 2841.
(330) Li, H.; Estroff, L. A. *J. Am. Chem. Soc.* **2007**, *129*, 5480.
(331) Travaille, A. M.; Kaptijn, L.; Verwer, P.; Hulsken, B.; Elemans, J. A. A. W.; Nolte, R. J. M.; van Kempen, H. *J. Am. Chem. Soc.* **2003**, *125*, 11571.
(332) Gower, L. A.; Tirrell, D. A. *J. Cryst. Growth* **1998**, *191*, 153.
(333) Loges, N.; Graf, K.; Nasdala, X.; Tremel, W. *Langmuir* **2006**, *22*, 3073.
(334) Magdans, U.; Torrelles, X.; Angermund, K.; Gies, H.; Rius, J. *Langmuir* **2007**, *23*, 4999.
(335) Politi, Y.; Arad, T.; Klein, E.; Weiner, S.; Addadi, L. *Science* **2004**, *306*, 1161.
(336) Politi, Y.; Levi-Kalisman, Y.; Raz, S.; Wilt, F.; Addadi, L.; Weiner, S.; Sagi, I. *Adv. Funct. Mater.* **2006**, *16*, 1289.

CR078259O